Experimental and Modelling Study of Ionic Conductivity in Lithium Phosphate and Silicate Glasses

Matteo P. Hogan

September 2014

A thesis submitted to the University of Kent

In the subject of Physics

For the Degree of Master of Science

Abstract

This study is an attempt to investigate ionic conductivity and structural components of lithium containing glasses for their use as possible electrolytes in solid state Li-ion batteries.

$33.3Li_2O$-$66.7SiO_2$, Li_2O-P_2O_5 (multiple compositions) and $Li_3Fe_2(PO_4)_3$ glasses were synthesised using conventional melt quenching and were characterised using various techniques including XRD, DSC, TGA, pycnometry and ^{31}P MAS-NMR. It was found a small (5mol%) addition of Nb_2O_5 to the $Li_3Fe_2(PO_4)_3$ glass was necessary for the formation of a glass $37.5Li_2O$-$20Fe_2O_3$-$5Nb_2O_5$-$37.5P_2O_5$.

The glasses conductivity was then measured using impedance spectroscopy over a frequency range of 200kHz – 100Hz and a temperature range of 300K – 525K. It was observed that an increasing temperature corresponded to an increasing conductivity, as expected from the Arrhenious equation: $\sigma = \sigma_0 \exp\left(-\frac{E_a}{k_B T}\right)$. Conductivity values were compared to published values and the first reported conductivity values for $37.5Li_2O$-$20Fe_2O_3$-$5Nb_2O_5$-$37.5P_2O_5$ glass were obtained. Activation energies were also calculated and compared to published data.

MD models of lithium disilicate, lithium metaphosphate and $37.5Li_2O$-$20Fe_2O_3$-$5Nb_2O_5$-$37.5P_2O_5$ were made. These models were then analysed and compared to experimental diffraction results. It was found that the lithium disilicate and the lithium metaphosphate model structures compare well to experimental data (X-ray and Neutron diffraction). Conductivity was estimated from mean squared displacement. All models gave an overestimation of conductivity compared to experimental data, due to limitations of the simulation method. However, MD did predict that lithium disilicate and lithium metaphosphate glasses have a similar conductivity as observed experimentally.

It was found that whilst the addition of Fe (and Nb) to the lithium phosphate glass improved chemical durability, its conductivity was reduced. In addition to this the conductivity for the $37.5Li_2O$-$20Fe_2O_3$-$5Nb_2O_5$-$37.5P_2O_5$ glass was found to be significantly lower than its crystalline counterpart which will be a disadvantage for its use as a solid electrolyte.

Acknowledgements

I would firstly like to thank my supervisor, Dr. Gavin Mountjoy. For his constant support, guidance and expert knowledge throughout this project. It has been a pleasure working with him.

Next I would like to thank the University of Kent. For the opportunity to conduct this research and the use of their facilities, in particular the Functional Materials Group from the School of Physical Sciences.

Thanks should also be given to Dr. Alex Hannon at ISIS. For the use of their facilities and equipment.

Thanks should also be given to Queen Mary University of London and Dr. Nasima Kanwal for the use of their equipment and data analysis.

Finally to my girlfriend Sian, and my Family. For constant support, love and understanding without which, this project would not have been possible.

Contents

Chapter 1: Introduction

1.1 Lithium Ion Batteries

Batteries have played a part in our lives for many years. There have been findings suggesting that batteries were in use thousands of years ago in the form of the Parthian battery [1] though these designs are very primitive and unable to produce a large current or voltage. The first "modern" battery was invented in 1800 AD by an Italian scientist named Alessandro Volta who piled up layers of copper and zinc electrodes separated by layers of cloth soaked in sulphuric acid which acted as what we now call the electrolyte. This battery became known as the "voltaic cell". [2] The main problem with this type of battery is the fact that the battery is non-rechargeable which today is classed as a "primary" battery.

A French scientist named Gaston Planté invented the rechargeable "secondary" battery in 1859 which was lead acid based, similar to lead acid systems used today in a number of applications including in vehicles. There are both advantages and disadvantages to "primary" and "secondary" type batteries, a few of which are listed in table 1.1 below.

Table 1.1:Advantages and Disadvantages of Primary and Secondary Batteries

	Advantages	**Disadvantages**
Primary	Low initial cost of materials High capacity High initial voltage Low self-discharge rate	More expensive long term High waste when disposing Not suitable for "high drain" applications
Secondary	Low cost over long periods Long life Suitable for "high drain" applications	High initial cost High self-discharge rate May require maintenance

The importance of the "secondary" battery is huge as it made the invention of portable electronic devices possible. It would now be almost unthinkable to introduce a portable electronic device without a secondary battery powering it due to our demand for convenience and due to the huge long term cost of powering these devices with primary

batteries. As our demand for electricity and portability increases so does the need for better performing batteries. This has led to a vast number of battery types being invented. At present, the front runner of these batteries is the lithium ion battery. The reason lithium ion batteries dominate this sector is in part due to their high specific energy (energy density Wh/kg), low maintenance and high specific power (W/kg). Figure 1.1 below shows the specific power and specific energy of different types of batteries showing lithium ion as a strong option with lithium polymer in direct competition and only lithium metal outperforming it. However, there are numerous concerns with lithium metal batteries because after multiple cycles lithium dendrites are formed on the lithium metal surface, which in turn could cause short circuits to occur within the battery, and this could cause the battery to combust making them unsafe for use in standard battery compositions.

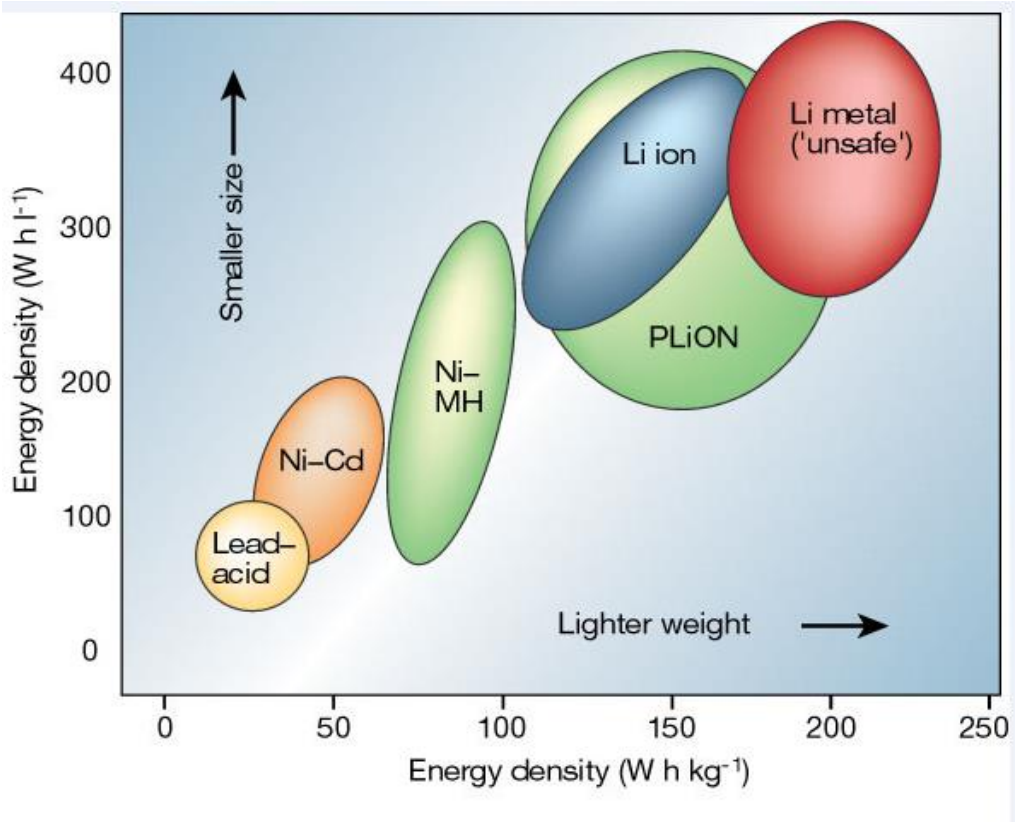

Figure 1.1: A diagram showing Specific energy vs Specific power of different types of batteries [20]

Lithium ion batteries are used across the world and in a wide range of applications from mobile electronic devices to hybrid and electric vehicles. They hold a large share of overall battery sales which led to the Lithium ion battery market being worth $11.7 billion in 2012 and this is expected to double by 2016 [3]. Lithium ion batteries have no obvious imminent threats to their dominance in the secondary battery market where their largest growth is expected to be in the automotive industry with an estimated 25% share of the total lithium ion battery market by 2016 (compared to 14% in 2012) [4].

There are three main parts to a lithium ion battery. The basic set up can be seen in figure 1.2 below. In this diagram there are two electrodes, a positive cathode and a negative anode, with an electrolyte in the middle. The cathode of a Lithium ion battery is formed of a lithium containing metal oxide such as lithium cobalt oxide ($LiCoO_2$). The anode is typically formed of graphite whilst the electrolyte is formed of a lithium ion conducting material to allow efficient transport of the Li^+ ions. A battery generates electrical energy through repeated redox reactions. Oxidation is when the oxidation state of an ion is increased by the removal of an electron whereas reduction is when it is decreased by the addition of an electron. When the battery is being charged the Li^+ ions are moved from the cathode through the electrolyte transport medium to the graphite anode which has a layered structure for efficient storage. During this time electrons flow through the wire from the cathode to the anode. This means that in the cathode material the metal ion has gone through an oxidation reaction e.g. $Fe^{2+} - e^- = Fe^{3+}$. Now this energy is stored to be used when needed. As annotated in the diagram below when the battery is being discharged the Li^+ ions are reverted back to the lithium containing metal oxide cathode releasing the energy that was originally stored. This means that in the cathode the metal ion has gone through a reduction reaction: $Fe^{3+} + e^- = Fe^{2+}$. These two processes can be repeated and therefore the battery can be used multiple times.

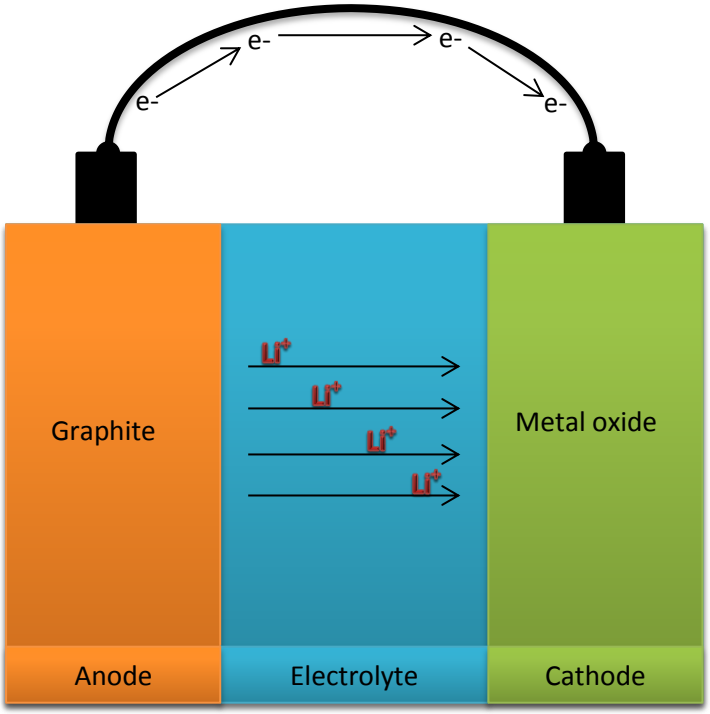

Figure 1.2: A diagram showing the basic setup of a lithium ion battery in a state of discharge

1.2 Electrolytes for Lithium Ion Batteries

Materials used for electrolytes are usually a non-aqueous liquid, consisting of lithium salts, typically $LiPF_6$ or $LiBF_4$, dissolved in an organic solvent. [5] These are used as electrolytes due do their high ionic conductivities of $\approx 10^{-2} S/cm$. [6] However there are some fundamental disadvantages of traditional liquid electrolytes used in that because they are in liquid form they can leak from the battery housing and many are flammable and therefore have a possibility to cause battery fires and explosions. Considering lithium ion batteries are used in consumer electronics this creates a possible safety hazard. This is where solid electrolytes come in to play. Whilst they typically have lower conductivities than their liquid counterparts they would bring multiple advantages over liquid electrolytes. These include: removal of the leakage problem, good performance over a broad temperature range, a range of synthesis methods, flexibility which allows for multiple applications from bulk to thin film batteries, and they will also avoid the issue of flammability.

Solid electrolytes, similar to liquid electrolytes, are substances which exhibit high ionic conductivity and low electronic conductivity. They are also often referred to by the name of super ionic conductors which can be defined as materials which at temperatures below their melting point have conductivity values $\sigma > 10^{-4} Scm^{-1}$ and negligible conductivity contribution from electrons. There are several factors which affect ionic conductivity in a solid, these include:

- Charge carrier density, that is to say the more charge carriers in a given space the higher the conductivity will typically be.
- Charge carrier mobility or diffusivity, that is to say that the ions have the ability to move freely within the system due to low activation energies.
- Temperature, this affects the energy and hence the mobility of the charge carriers and typically results in increased conductivity with increased temperature.

Crystalline substances such as $Li_{3.25}Ge_{0.25}P_{0.75}S_4$ and $(La,Li)TiO_3$ are most commonly used for solid electrolytes. [7] [8] However, a few studies have been carried out with regards to the use of glasses as a solid electrolyte in lithium ion batteries. [9] [10] [11] There are multiple reasons as to why a glass would be preferable over a crystalline solid electrolyte. Unlike crystalline solids, glasses have no grain boundaries which means this does not contribute to a glass' internal resistance. Glasses also have a very disordered structure meaning that ions are located randomly which is preferable for high conductivity. Glass also has a poor electronic conductivity contribution. [12]

1.3 Glasses

Glass has been around for thousands of years and used for many applications, but it is not known how glass first originated. It has been suggested that glass was first discovered by accident. A possible scenario is on the coast of a saltwater sea on the sands of the beaches during a large fire in an ancient settlement. The combination of ingredients could have formed the first man made glass: bones left in the fire contain calcium oxide (CaO), the sea salt has a composition of sodium chloride (NaCl), and the sand is composed of silicon dioxide (SiO_2). [13] It is likely that the first uses for glass were decorative objects such as beads or for tools requiring sharp edges such as spear points. This then developed over time improving on the glass' quality and techniques for synthesising glass. Today glass has a vast portfolio of applications ranging from windows and construction to optics, and including biomedical applications, seals on fuel cells, and battery materials.

Currently silica containing glasses are the most common glasses for domestic use. This is due to silica being not only abundant but also a very good glass former based on tetrahedral SiO_4 units. A glass former is a molecule which contributes to a glass network and its resistance to crystallisation means it readily forms a glass when cooled. Another example of a glass former is phosphorus oxide, again with its structure based on tetrahedral PO_4 units. Both of these glass formers will be used in this study of different lithium containing glasses. Along with glass formers other elements may be added to a glass' batch which can alter the resultant glass' properties. If for example a glass for decorative purposes is made a colorant might be added. Similarly if other properties are required such as improved chemical stability, improved mechanical durability, decreased melting temperature, refinement of the melt or increased forming flexibility, a glass modifier with the desired effect may be added. Some common examples of this would be CaO (commonly referred to as lime) and Na_2O (commonly referred to as soda). Whilst the addition of lime can improve the hardness and strength of a glass it will also reduce the "setting" rate. Alternatively the addition of soda will reduce the glass transition and melting temperature, however, it will reduce the glass' chemical durability and make it soluble in water. These two modifiers are commonly added to silica to form what is known as "soda-lime" glass which is used for windows.

A glass can be defined as an amorphous solid with no long range, periodic atomic arrangement that must also exhibit glass transition behaviour. [13] As an example figure 1.3 below illustrates the difference in structure between crystalline SiO_2 (left) and amorphous glass SiO_2 (right).

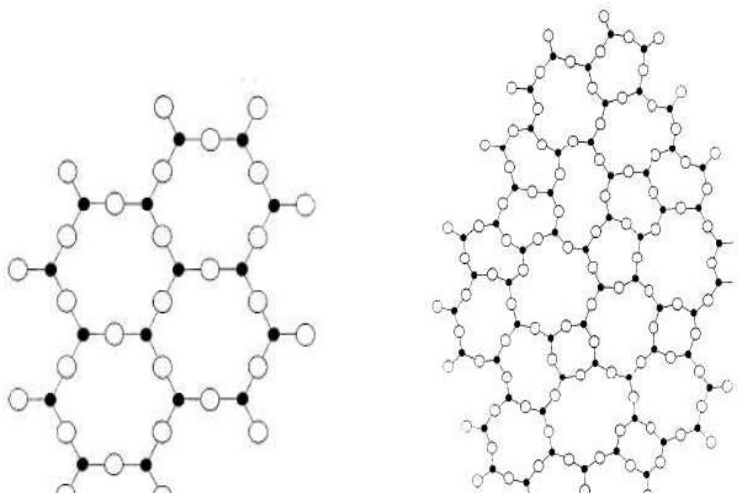

Figure 1.3: An illustration of crystalline (left) and glass (right) SiO_2 [14]

This alone does not make it a glass as not all amorphous solids are glasses. To be defined as a glass the amorphous solid must also exhibit glass transition behaviour. This is a time dependant process. When a liquid melt is cooled slowly the atoms begin to arrange themselves into the lowest energy structure (equilibrium structure). If the liquid cools to the point of the melting temperature T_m and then solidifies a sharp decrease in enthalpy will be observed as crystallisation occurs. The crystalline solid has long range, periodic atomic arrangement hence it is not a glass. If however the melt is cooled to a temperature below T_m, without solidifying, it can be thought of as a super cooled liquid. If this liquid then continues to cool without rearranging the atoms into a crystal structure, due to the time constraints imposed by the glass forming technique used (typically rapid melt quenching), then it will form a glass. This can be thought of as essentially freezing the liquid structure in place making it into a solid. The point at which the two equilibrium enthalpy lines (the glass and the liquid lines) meet is known as the glass transition temperature T_g (T_f as shown in figure 1.4).

This is illustrated in figure 1.4 below.

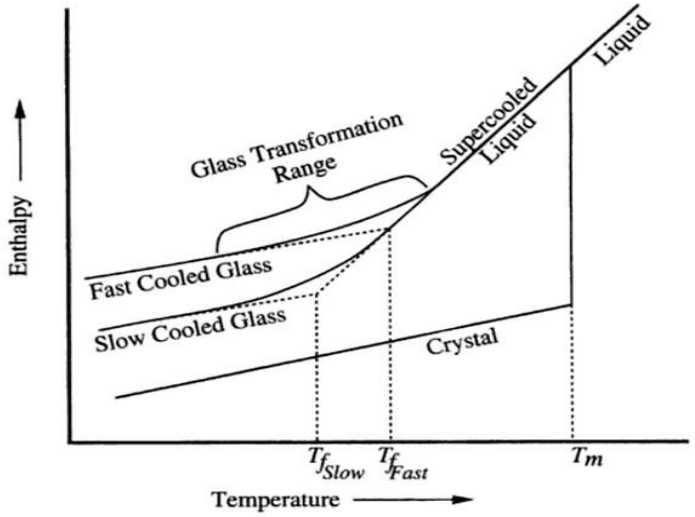

Figure 1.4: A graph to show the effect of Temperature on the Enthalpy of a glass forming melt [13]

Another way of thinking about this process is in terms of volume rather than enthalpy as the same relationship is observed.

Of course not all rapidly cooled liquids will form a glass. Some will crystallise regardless of cooling rate as there are certain parameters which are considered important in order to form a glass. Note that parameters 1-3 definitely apply to SiO_4 and PO_4 tetrahedra.

These parameters were derived by Zachariasen [14]:

(1) An oxygen atom is linked to not more than two glass former atoms.
(2) The number of oxygen atoms surrounding glass former atoms must be small.
(3) The glass former oxygen polyhedra share corners with each other, not edges or faces.
(4) At least three corners in each glass former oxygen polyhedron must be shared.

1.4 Ionic Conductivity of Glasses

In electronic conductivity it is the movement of charge carriers called electrons which creates the current. However, in glass it is the ions (an atom or molecule with a net electric charge due to the loss or gain of electrons) that are the charge carriers. There are two types of ions: anions which are negatively charged ions and cations which are positively charged ions. The basic principle behind ionic conductivity in glasses is that in order for ions to contribute to conductivity they must move in the desired direction, however, there are certain barriers which must be overcome. The first is the binding energy E_b which is the energy required for the cation to remove itself from its current site near a non-bridging oxygen (NBO). Next is the strain energy E_s which is the energy associated with the ions motion as the ion must overcome the energy barrier created by the bridging oxygen (BO). Together these energies are referred to as the activation energy $E_A = E_b + E_s$. This barrier can be depicted using (a) the strong electrolyte model (Anderson – Stuart) and (b) the weak electrolyte model shown in figure 1.5 below. [15]

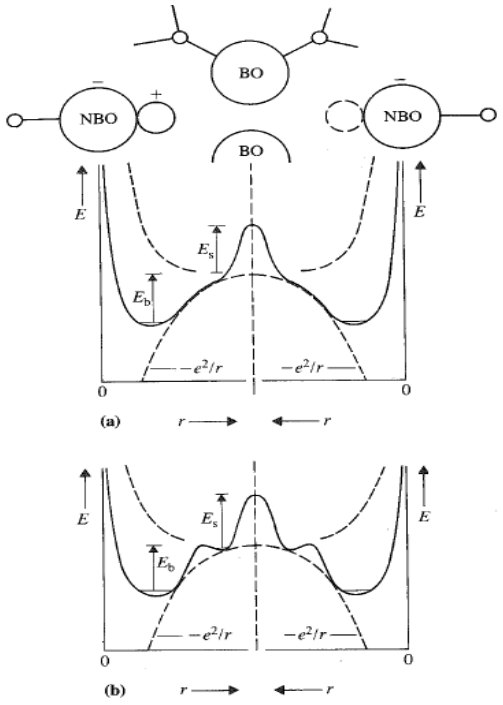

Figure 1.5: A representation of the cation conduction energetics using the strong electrolyte model (a) and the weak electrolyte model (b) [15]

The strong electrolyte model suggests that all cations are dissociated from their host anion (primary NBO site) and therefore all can contribute to conductivity equally, whereas the weak electrolyte model suggests that only a small fraction of cations are dissociated from their host anion meaning a limited number of carriers are available for conduction. Experimentally for temperatures below T_g, the ionic conductivity σ of all glasses appears to obey a perfect Arrhenius law: [12] [15] [16]

$$\boldsymbol{\sigma = \sigma_0 \exp\left(-\frac{E_A}{k_B T}\right)} \qquad \textbf{Equation 1.1}$$

This equation means that the higher the activation energy E_A the lower the conductivity, as the rate at which the ions can "hop" is determined by the energy barrier they experience. This may be due to more energy being needed to dissociate a cation from its NBO site before conductivity is initiated (increasing E_b) or that more energy is required to move the ion (increasing E_s). It also states that conductivity increases with temperature.

Glasses often have metal cations added such as sodium to impart certain properties into the resulting glass as stated earlier. This can also give the glass ionic conductivity properties such that they can be used in battery applications. Another example of a metal cation which might be added to a glass is lithium. Li^+ ions are smaller than sodium ions. They therefore have an increased conductivity compared with sodium as their reduced size allows the ions to move more freely through the conductive pathways.

Before considering the mechanisms of conductivity in glasses, let us first think about ionic conductivity in crystalline materials. Diffusion is the random movement of ions within the solid and forms a net contribution to conductivity. The transport mechanisms in crystal structures are normally governed by defects within the structure, often created intentionally, and include: interstitial movement and vacancy transport. An interstitial ion is an example of a defect within the crystalline structure, it can be thought of as an excess ion. Interstitial movement can be categorised into two types: direct interstitial movement, where the transport of ions is in-between "normal sites" (from one interstitial location to another interstitial location) and indirect interstitial movement, where an ion located in an interstitial forces an ion in a lattice out and takes its place. Vacancy transport is where an ion hops from its current site to a vacant site normally caused by a missing ion. This vacancy, often referred to as a "hole" is another example of a defect.

This would suggest it is preferable to have more vacant sites than charge carriers so as to allow easier movement of ions. [17] Figure 1.6 shows representations of vacancy transport, and direct and indirect interstitial movement.

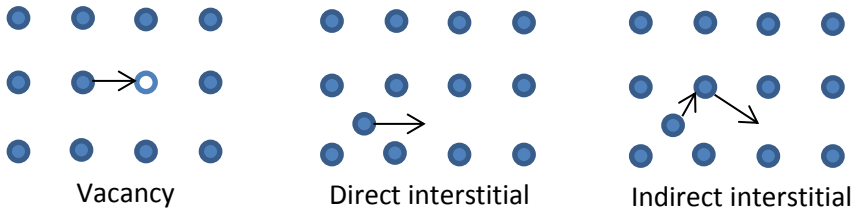

Figure 1.6: representations of various methods for conductivity

In glasses however, defects are less common because glasses do not have lattice structures like crystalline materials and so conductivity in glasses is largely attributed to ion 'migration'. [16] This is an ion having enough energy to overcome its binding energy and its strain energy, the ion replaces another ion which, in turn continues to move so whilst one ion has only moved from one cation site to another the effective charge movement is higher. The ratio between an ion 'jump' (tracer diffusion) and the effective movement of charge (charge diffusion) is called the Haven ratio, which, for oxide glasses is normally between 0.3 and 0.6. This ratio can be used to measure the directional correlations of ion movement. [18] As stated earlier in section 1.4 the higher the concentration of charge carriers i.e. Li^+ the higher the conductivity due to more charge carriers being available for conductivity. In addition, lithium breaks glass network tetrahedral chains which means more non-bridging oxygen.

This study will look at both Li phosphate and Li silicate glasses as studied by S.W. Martin and C.A. Angell [12] where it was found that silicates had higher conductivities than their phosphate counterparts and this was attributed to the higher concentration of non-bridging oxygen found in the silicate samples compared to phosphate samples. Another glass of interest has the same composition as the $Li_3Fe_2(PO_4)_3$ crystal. [19] The $Li_3Fe_2(PO_4)_3$ crystal has a NASICON (Sodium Super Ionic Conductor) type local structure which follows the structure template: $A_xB_y(PO_4)_3$ where A is an alkali metal ion (Li, Na) and B is a multivalent metal ion e.g. (Cr, Fe). This structure indicates high ionic conductivity and stability of phosphate units, both good attributes for the intended application. This is

another of the glasses that will be investigated in this study. It has the nominal composition $37.5Li_2O$-$25Fe_2O_3$-$37.5P_2O_5$. The goal is to measure the conductivity of this glass for the first time. The crystal structure of this composition is shown in figure 1.7 below [20] where lithium is shown in green, iron in yellow, phosphorus in pink and oxygen as red spheres. The goal is to measure the conductivity of this glass for the first time.

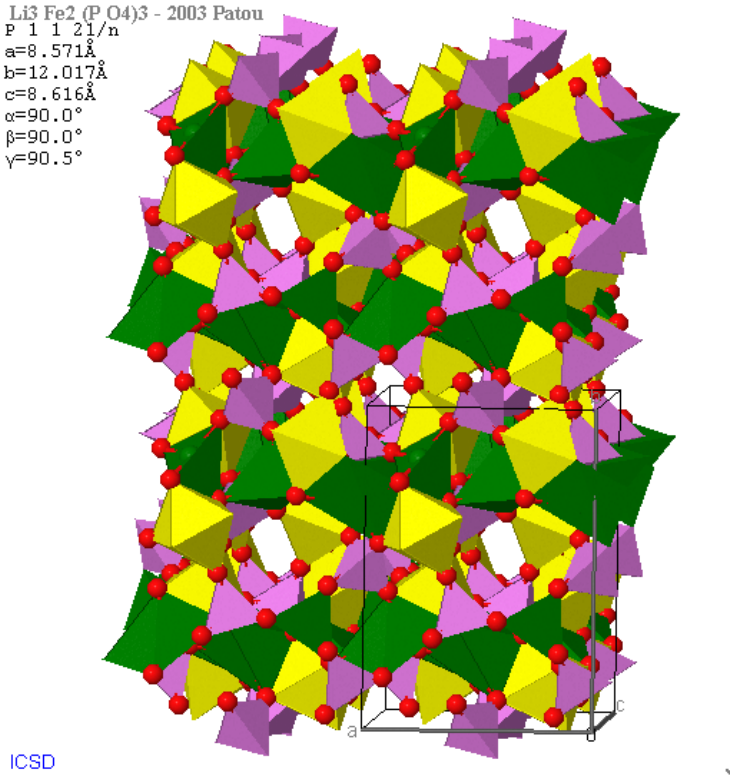

Figure 1.7: crystal structure of $37.5Li_2O$-$25Fe_2O_3$-$37.5P_2O_5$

[1] P. Keyser, “The Purpose of the Parthian Galvanic Cells: A First-Century A.D. Electric Battery Used for Analgesia,” *Journal of Near Eastern Studies,* vol. 52, pp. 81-89, 1993.

[2] P. Brenni, R. Galdi, F. Peitra and A. Savini, “From Volta onwards: a variety of electrical batteries in the Pavia Museum of Electrical Technology,” in *HISTory of ELectro-technology CONference (HISTELCON)*, 2012.

[3] Frost & Sullivan, “Global Lithium-ion Market to Double Despite Recent Issues,” Frost and Sullivan, London, 2013.

[4] National Alliance for Advanced Technology Batteries, “Lithium-Ion Battery Market on Verge of Dramatic Growth,” [Online]. Available: http://naatbatt.org/naatbatt-blog/lithium-ion-battery-market-on-verge-of-dramatic-growth/. [Accessed 08 August 2014].

[5] A. Hofmann, M. Schulz and T. Hanemann, “Effect of Conducting Salts in Ionic Liquid Based Electrolytes: Viscosity, Conductivity, and Li-Ion Cell Studies,” *International Journal of Electrochemical Science,* vol. 8, pp. 10170-10189, 2013.

[6] S. Zhang, K. Xu and T. Jow, “Study of LiBF4 as an electrolyte salt for a li-ion battery,” *Journal of the Electrochemical society,* vol. 149, pp. 586-590, 2002.

[7] J.Ahn and S. Yoon, “Characteristics of perovskite (Li0.5La0.5)TiO3 solid electrolyte thin films grown by pulsed laser deposition for rechargeable lithium microbattery,” *Electrochimica Acta,* vol. 50, no. 2-3, pp. 371-374, 2004.

[8] T. Kobayashi, “All solid-state batteries using super ionic conductor, thio-lisicon - Electrode/electrolyte interfacial design,” *Solid-State Ionics,* vol. 835, pp. 333-345, 2005.

[9] T. Katoh, Y. Inda, K. Nakajima, R. Ye and M. Baba, “Lithium/water battery with lithium ion conducting glass-ceramics electrolyte,” *Journal of Power Sources,* vol. 196, no. 16, pp. 6877-6880, 2011.

[10] B. Money and K. Hariharan, “Crystallization Kinetics and Phase Transformation in Superionic Lithium Metaphosphate (Li2O-P2O5) Glass System,” *Journal of Physics: Condensed Matter,* vol. 21, p. 115102, 2009.

[11] A. Hayashi, K. Noi, A. Sakuda and M. Tatsumisago, “Superionic glass-ceramic electrolytes for room temperature rechargeable sodium betteries,” *Nature Communications,* p. 3:856, 2012.

[12] S. Martin and C. Angell, “DC and AC Conductivity in Wide Composition range Li2O-P2O5 glasses,” *Journal of Non-Crystalline Solids,* vol. 83, pp. 185-207, 1986.

[13] J. Shelby, Introduction to Glass Science and Technology Second Edition, Royal Society of Chemistry, 2005.

[14] W. Zachariasen, “The Atomic Arrangement In Glass,” *Journal of the American Chemical*

Society, p. 3841–3851, 1932.

[15] S. Elliott, Physics of Amorphous Materials second edition, Longman Scientific and Technical, 1990.

[16] M. Nascimento, A. Rodrigues and J. Souquet, “Microscopic and thermodynamic interpretations of experimental data on ionic conductivity in lithium silicate glasses,” *European Journal of Glass Science and Technology,* vol. 51, pp. 69-77, 2009.

[17] L. Malavasi, C. Fisher and M. Islam, “Oxide-ion and proton conducting electrolyte materials for clean energy applications: structural mechanistic features,” *The Royal Society of Chemistry,* vol. 39, pp. 4370-4387, 2010.

[18] J. Dyre, P. Maass, B. Roling and D. Sidebottom, “Fundamental questions relating to ion conduction in disordered solids,” *Reports on Progress in Physics,* vol. 72, p. 046501, 2009.

[19] H. Karami and F. Taala, “Synthesis, characterization and application of Li3Fe2(PO4)3 nanoparticles as cathode of lithium-ion rechargeable batteries,” *Journal of Power Sources,* p. 6400–6411, 2011.

[20] S. Patoux, C. Wurm, M. Morcrette, G. Rousse and C. Masquelier, “A comparative structural and electrochemical study of monoclinic Li3 Fe2 (P O4)3 and Li3 V2 (P O4)3,” *Journal of Power Sources ,* vol. 119, pp. 278-284, 2003.

[21] J. M. Tarascon and M. Armand, “Issues and challenges facing rechargeable lithium batteries,” *Nature,* vol. 414, pp. 359-367, 2001.

Chapter 2: Glass Making and Characterisation

2.1 Melt Quenching

2.1.1 Method

The most commonly used method for synthesising a glass is the "melt quenching" technique. This technique involves heating up a crucible containing the ingredients of the glass (called a batch) in a furnace at a temperature high enough so that the ingredients have reacted and formed a liquid (called the melt). The melt is then poured onto a cold metal plate or mould and then immediately pressed on the top by another cold metal plate (this is called quenching). This process results in a glass whose atoms are arranged like a liquid which has been "frozen". As previously stated in chapter 1, the melt must not be cooled slowly otherwise the atoms would rearrange themselves into their lowest energy form which would be a crystal. Creating the batch involves calculating and weighing out specific amounts of the desired glass' constituent ingredients. Often the desired ingredients are not found in their simplest form, e.g. Li_2O, and therefore compounds containing the desired ingredient must be used, e.g. Li_2CO_3. The samples synthesised in this study are: $Li_2O–P_2O_5$ glasses of multiple compositions, $33.3Li_2O–66.7SiO_2$ glass and $37.5Li_2O$-$20Fe_2O_3$-$5Nb_2O_5$-$37.5P_2O_5$ glass. These glasses have been previously studied and therefore the ingredients and initial synthesis procedures used here matched the published articles. [1] [2] [3] [4] Figure 2.1 shows a $40Li_2O$-$60P_2O_5$ glass sample against a white and yellow background to emphasise its transparent nature.

Figure 2.1: Image of $40Li_2O$-$60P_2O_5$ glass

Table 2.1: Glass compositions used in this study and their respective yields and observations

Glass Composition	Yield (%)	Comments
$36.8Li_2O$-$63.2P_2O_5$	98.6	
$40Li_2O$-$60P_2O_5$	98.8	Small bubbles in sample
$45Li_2O$-$55P_2O_5$	99.5	
$50Li_2O$-$50P_2O_5$	99.0	Slightly grey in appearance
$55Li_2O$-$45P_2O_5$	Very low	Low yield due to overflow in furnace
$33.3Li_2O$-$66.7SiO_2$	99.9	
$37.5Li_2O$-$20Fe_2O_3$-$5Nb_2O_5$-$37.5P_2O_5$	97.5+	Some glass lost due to shattering on quench

All glass compositions, their respective yield and quality are given in table 2.1 above. The yields of most samples are high which indicates that the correct composition has been achieved. However, the samples' composition will be compared later in this chapter using a characterisation technique called nuclear magnetic resonance (NMR). The ingredients and final furnace programs used in this study are shown in table 2.2 below.

Table 2.2: a table to show glasses used within this study and their constituent ingredients along with furnace programs

Glass	**Ingredients**	**Furnace Program**
$Li_2O – P_2O_5$	Li_2CO_3, NH_6PO_4 [1]	Ramp at a rate of 10°C/minute up to 300°C, Dwell at 300°C for 1 hour, Ramp at a rate of 10°C/minute up to 950°C, Dwell at 950°C for 1 hour
$33.3Li_2O$ – $66.7SiO_2$	Li_2CO_3, SiO_2 [2]	Ramp at a rate of 10°C/minute up to 300°C, Dwell at 300°C for 30 minutes, Ramp at a rate of 10°C/minute up to 1275°C, Dwell at 1275°C for 1 hour
$37.5Li_2O$-$20Fe_2O_3$-$5Nb_2O_5$-$37.5P_2O_5$	Li_2CO_3, Fe_2O_3, NH_6PO_4, Nb_2O_5 [3] [4]	Ramp at a rate of 10°C/minute up to 300°C, Dwell at 300°C for 30 minutes, Ramp at a rate of 10°C/minute up to 1200°C, Dwell at 1200°C for 20 minutes

Some changes were made from the initial procedures to reduce time taken (reduced dwell times and quicker batch preparation) and reduce chances of overflow (additional

dwells at 300°C) without compromising results. It can be seen in the furnace program section of the table above there is a dwell at 300°C. This is there so that gases that are formed upon heating can be expelled safely and without any overflow occurring within the crucible which is a possibility if the ramping was simply continued straight to the final temperature. Gases released during this period include CO_2, NH_3 and H_2O. [1] The dwell at the final temperature is to ensure all reactants have reacted and formed a homogenous melt to remove inconsistencies in the sample created. As shown in table 2.2 above Nb_2O_5 has been added to the $Li_3Fe_2(PO_4)_3$ glass as without this small addition (5 mol% in the place of 5 mol% Fe_2O_3) the melt would not naturally form a glass as the compositions sits outside the glass forming region. [3] [5] [6] There were also discrepancies found between articles' final temperatures for $Li_3Fe_2(PO_4)_3$ glass which ranged from 950°C [4] to 1200°C. [3] The former was tested and proved unsuccessful as much of reactants remained unreacted (shown in figure 2.2 below) however the latter gave more satisfactory results shown in figure 2.3 below.

Figure 2.2: Showing a partially unreacted $37.5Li_2O$-$20Fe_2O_3$-$5Nb_2O_5$-$37.5P_2O_5$batch when heated to 950°C [4]

Figure 2.3: image of $37.5Li_2O$-$20Fe_2O_3$-$5Nb_2O_5$-$37.5P_2O_5$ glass

The equipment used for glass making in this study are: 95Pt – 5Au crucible, copper mould and plate and Lenton furnace. A typical amount of glass made per quench was between 7g and 10g depending on resultant glass viscosity. This is to ensure enough glass was obtained to fill the mould shown in figure 2.4 despite the residual glass remaining in the crucible.

Figure 2.4: Showing the copper mould used in this study

The mould has been designed in this way so that the sample forms a large uniformly shaped tablet for impedance spectroscopy and the remaining glass can be removed easily for other characterisation. In this study the characterisation techniques used include:

- XRD in order to determine whether the sample is amorphous or crystalline.
- Thermal Analysis to find glass transition T_g and crystallisation T_c temperatures.
- Micropycnometry to determine the samples volume and therefore density.
- NMR to determine Q^n connectivity of the glass network and therefore composition.

These techniques are widely used [1] [3] [7] and important as they allow us to define each sample as a glass (XRD), to better understand the samples network connectivity (NMR), obtain parameters such as density (micropycnometry) for use in molecular dynamics modelling, and deciding whether it is suitable for its intended applications i.e. possible operating temperatures via T_g and T_c determination (thermal analysis).

2.2 X-Ray Diffraction

2.2.1 Method

X-Ray diffraction (XRD) is one of the most useful and commonly used techniques for structural characterisation of crystalline solids. This technique works in principle by firing x-rays at a sample which has interatomic distances within the crystal lattice that are similar to the x-rays' wavelength. X-rays are generated by bombarding a target material (typically copper) with electrons which will give the desired wavelength of x-rays. [8]

Figure 2.5 below is a representation of a crystal lattice with interplanar spacing d_{hkl} where h,k,l are Miller indices of crystal planes (h,k,l). Two x-ray beams 1 and 2 are seen to be scattered from adjacent planes of atoms. The path difference between these two beams is equal to 2dsinθ which will constructively interfere if it is equal to n number of wavelengths where n is an integer. Therefore Bragg's law may be written: [8] [9]

$$n\lambda = 2d_{hkl}\, sin\theta. \qquad \textbf{Equation 2.1}$$

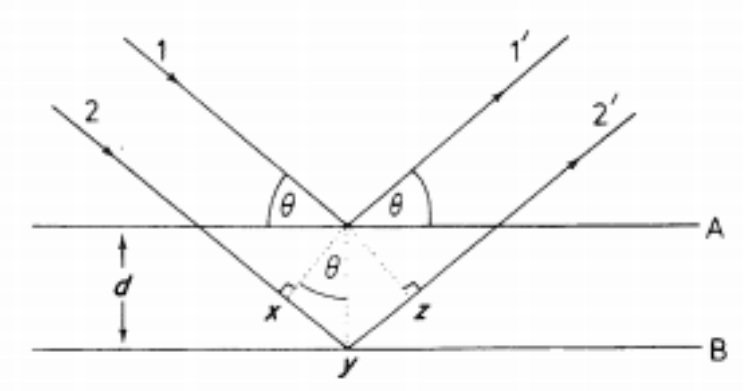

Figure 2.3: A figure showing the derivation of Bragg's law

In order to observe the diffraction constructive interference must occur. If the beam is reflected at a different angle to the Bragg angle then the beams will destructively interfere or cancel. A diffractometer such as the one used in this study is formed so that

x-rays are emmitted from an x-ray tube and directed at a target sample. The scattered x-rays are measured using a detector. The design of this arrangement is such that scattered intensities are measured over a range of scattered angles 2θ. This study uses X-ray powder diffraction technique which uses a powdered sample as the target. This is so that crystals are orientated in every direction which therefore means that lattice planes are also arranged in every direction. This means that for each set of planes at least some ought to be orientated at the Bragg diffraction angle. A graph is formed with peaks whose location on the graph corresponds to different interatomic spacings (d_{hkl}) and intensity which corresponds to the abundance of atoms located in that particular plane and is therefore governed by the structure of the crystal.

XRD has been discussed so far in relation to crystalline structures, however, this study focuses on glasses which scatter very differently to crystals when using XRD. Whilst with crystals XRD can identify the structure using Bragg peaks and their corresponding intensities, in amorphous materials like glasses there are no distinct Bragg peaks formed due to the disorder of atom arrangements in the sample. However it is this lack of Bragg peaks that can be used to define a sample as amorphous.

2.2.2 XRD of $50Li_2O$-$50P_2O_5$ glass

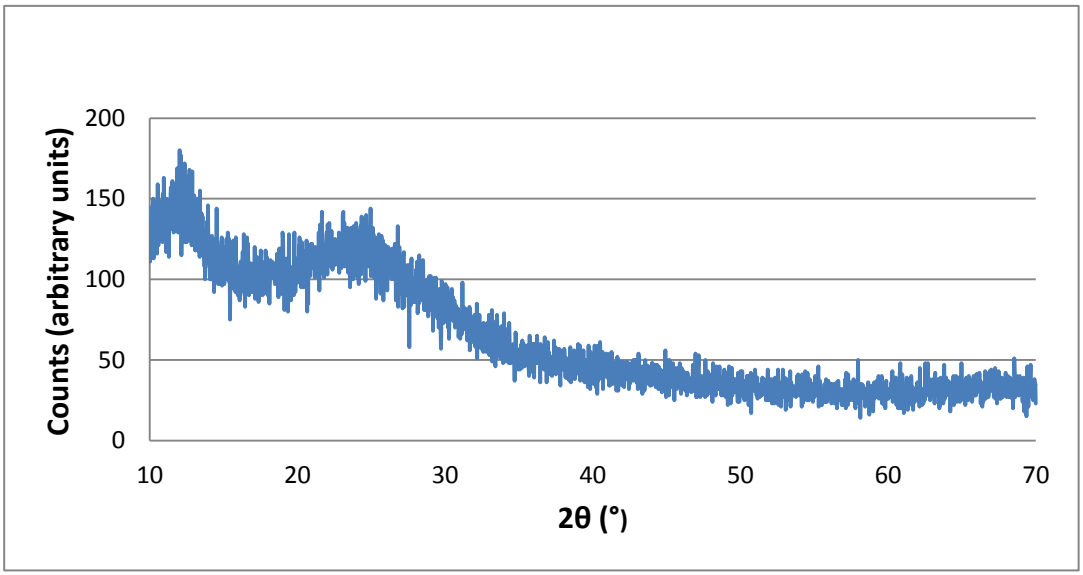

Figure 2.4: XRD results for amorphous $50Li_2O$-$50P_2O_5$

The diffractometer used for the XRD measurements in this study was a Bruker D8. Figure 2.6 above is an example of the XRD results for the $50Li_2O$-$50P_2O_5$ glass sample. It can be seen in the above graph that there are no distinct Bragg peaks, this indicates an amorphous sample. The sample was then heat treated in a furnace above its measured crystallisation temperature (T_c) and the XRD measurement was repeated. The resulting graph is shown below along with reference data. [10]

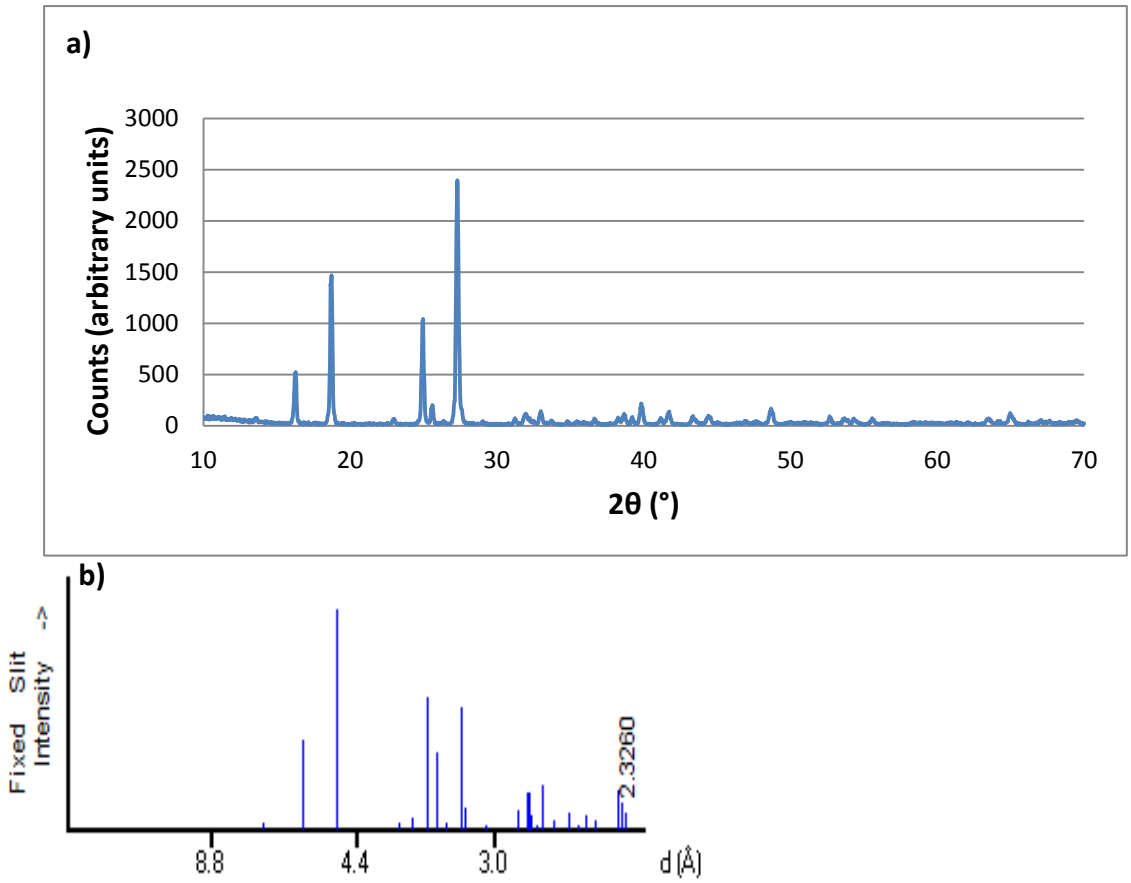

Figure 2.5: XRD results for a) crystalline $50Li_2O$-$50P_2O_5$ and b) JCPDS database reference sample 27-1177 [10]

In Figure 2.7 above, distinct Bragg peaks can be seen, the major peaks occur at angles 16.3°, 18.7°, 24.9°and 27.3° corresponding to crystalline $LiPO_3$ which is the resultant form expected from crystallising $50Li_2O$-$50P_2O_5$ glass. [11] [1]

2.3 Thermal Analysis

2.3.1 Method

Thermal analysis, as the name suggests involves measuring certain physical quantities such as enthalpy, heat capacity and change in mass as a function of temperature of a sample. [8] The techniques used to analyse the samples in this study are: Thermo Gravimetric Analysis (TGA) and Differential Scanning Calorimetry (DSC) both of which have been measured using a single instrument.

TGA is an experimental technique used to measure the change in a sample's mass as a function of either time or temperature. Mass changes are due to sample decomposition. Indicators such as the temperature at which decomposition begins can help in identifying the reason e.g. if a sample contained H_2O, then decomposition would be expected to begin at ≈ 100°C. This technique is useful as it can give information on whether samples contain moisture and how much, or at what temperature a sample decomposes.

DSC is an experimental technique that can quantitatively measure enthalpy changes of a sample when heated. The technique is similar to Differential Thermal Analysis (DTA) in that it uses an inert reference material alongside the measured sample in order to detect differences between the two materials. Figure 2.8 shows a system where both the reference material and sample are heated in unison and measured using thermocouples to create a voltage between the sample and the reference if a difference in temperature is observed. This eliminates the problem of fluctuations in heating rates as both materials will experience the same fluctuations. However when there is a difference in temperatures this is shown by either a peak (exothermic) or a trough (endothermic). Whilst DTA is effective in recognising thermal changes its peaks give only a qualitative indication of enthalpy changes. DSC however keeps both sample and reference at the same temperature and the extra thermal energy required to do so is measured, and therefore a quantitative result can be obtained. [8]

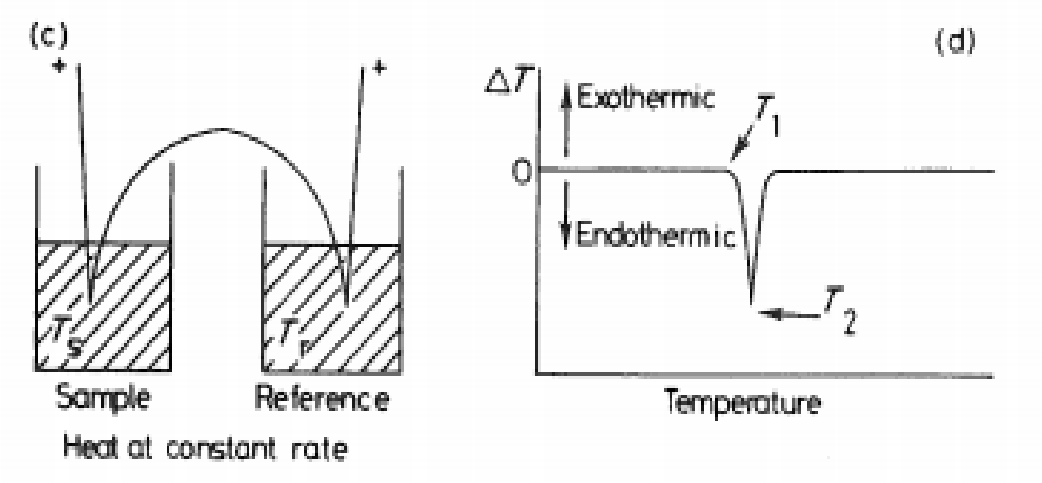

Figure 2.6: A figure to show the DTA method (c) and corresponding graph (d)

2.3.2 Crystallisation of $50Li_2O$-$50P_2O_5$ glass

Figure 2.9 below shows an example from a DSC and TGA analysis of $50Li_2O$-$50P_2O_5$ glass. Measurements were taken using a NETZSCH STA-409 instrument. The green line shows change in mass as a percentage of its initial mass. It can be seen that the change in mass of this sample was small (≈1%) which indicates that the sample has not decomposed and has not been significantly affected by moisture. The glass transition temperature T_g has been indicated and shows up on the graph as a small endothermic "dip" whilst the crystallisation temperature T_c which has also been indicated appears as a sharp exothermic peak.

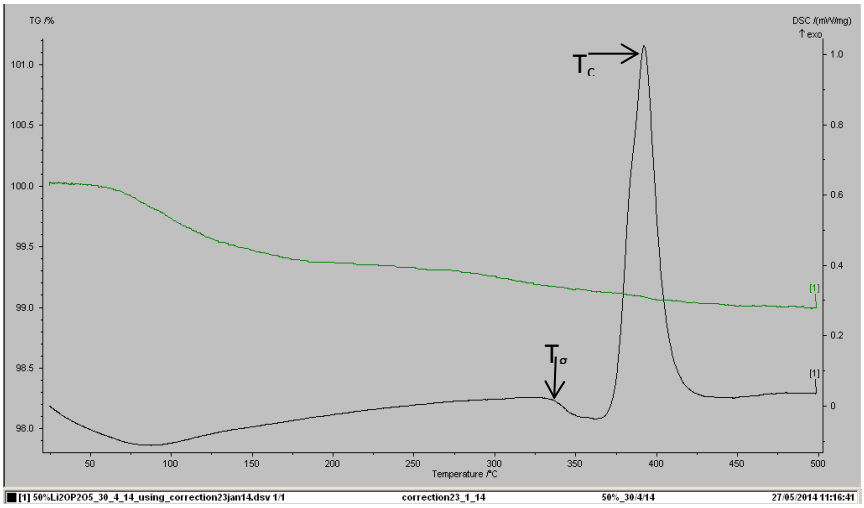

Figure 2.7: TGA and DSC results for $50Li_2O$-$50P_2O_5$ sample

The DSC measurement was repeated using a different sample of the same composition which has yielded a different result shown in figure 2.10 below.

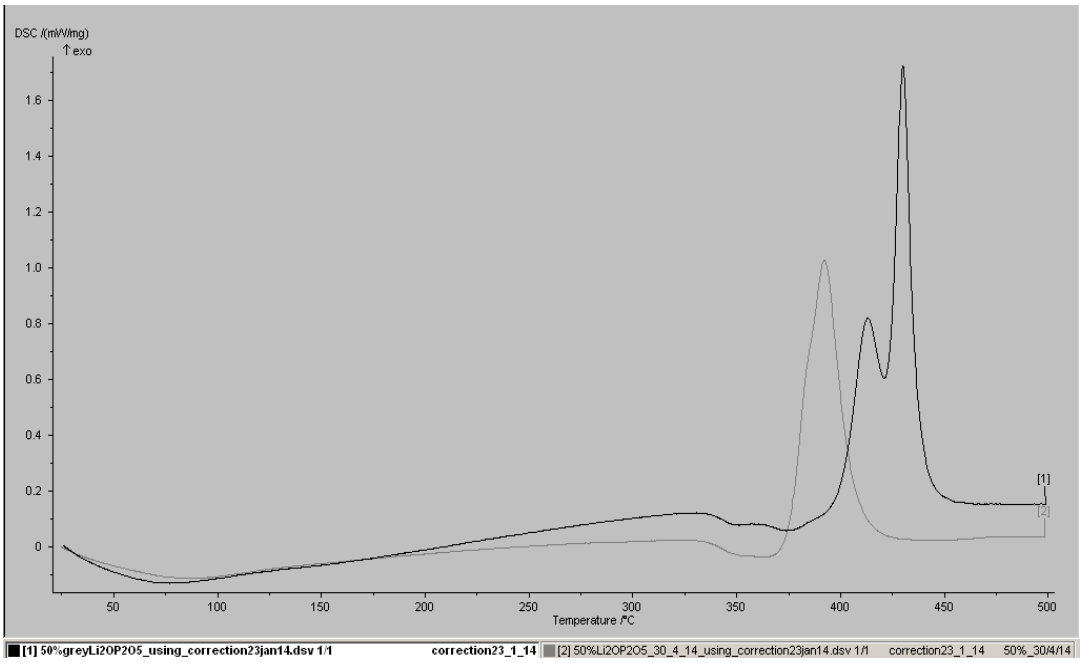

Figure 2.10: DSC curves for two different samples of $50Li_2O$-$50P_2O_5$ glass

Figure 2.10 shows that whilst the glass transition temperature has remained the same (due to consistent synthesis methods [12]), the crystallisation temperatures vary significantly (≈40°C). There are many factors which can affect a glass' crystallisation temperature including differences in the glass' thermal history, differences in heating rates during DSC measurements, and differences in synthesis methods. [12] [13] However, as these factors have remained constant with both samples, the most likely explanation is different particle sizes of glass powder when DSC measurements were taken as this can affect crystallization temperatures. [11] The graph also seems to indicate a single crystalline phase in one sample but two distinct crystalline phases in the other however upon close inspection it shows a merging of two peaks has occurred, as shown in the figure 2.11 below.

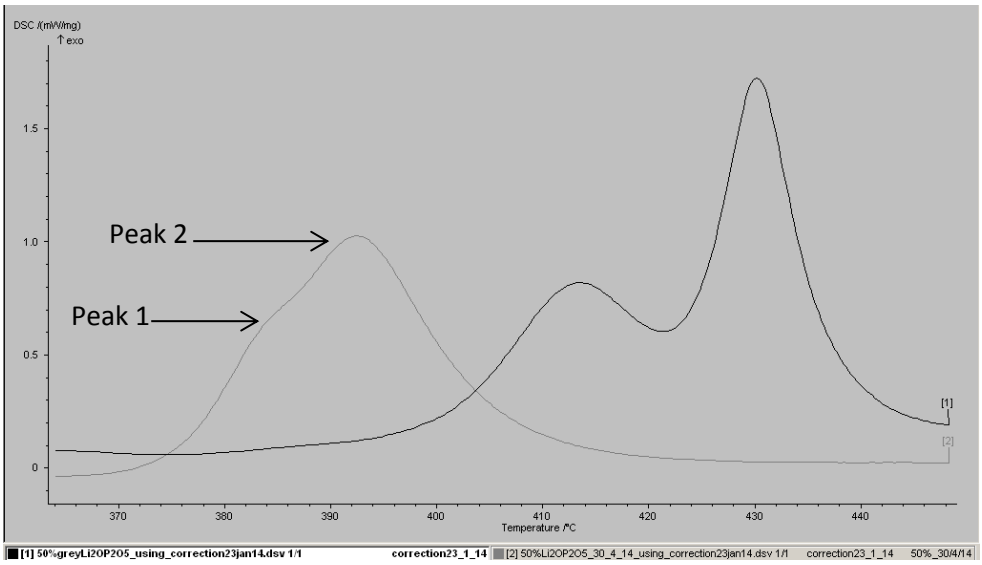

Figure 2.11:Enlarged DSC crystallization peaks for $50Li_2O$-$50P_2O_5$ glass

2.3.3 Glass transition of Li silicate and Li phosphate glasses

Using DSC curves which shows the samples undergo a glass transition, the samples can be determined to be glass. Table 2.3 below shows that higher lithium concentration samples (50-60 mol%) have higher glass transition temperatures compared to lower concentration samples (36.8-45 mol%), except 50 mol% which has the highest T_g of all phosphate samples tested. The trend seems to be the higher the lithium concentration the higher the transition temperature. This has been previously observed. [12] Glass transition temperatures are affected by how stable the structure of the glass is, which could explain why 50 mol% glass has the highest T_g. The $50Li_2O$-$50P_2O_5$ glass is also known as lithium metaphosphate which is a reference to its connectivity. Metaphosphate means that each phosphate tetrahedron is connected to two other tetrahedra which gives the glass stability, whereas the other samples have mixtures of 1, 2 and 3 connections. A diagram illustrating this is shown below in figure 2.12.

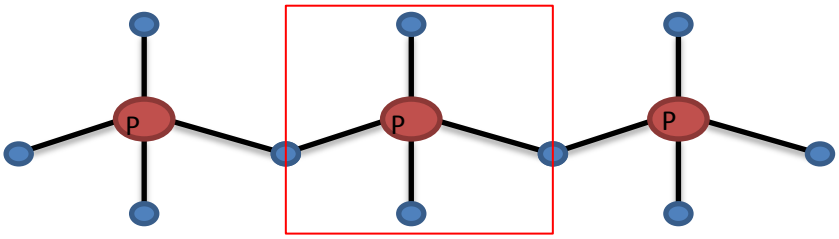

Figure 2.12: A representation of Q2 phosphate tetrahedra corresponding to lithium metaphosphate

It is also the higher concentration samples for which two different crystalline phases are observed after crystallisation. The two crystalline phases are attributed to $LiPO_3$ and $Li_6P_6O_{18}$. [11] Table 2.3 also shows that the silicate and lithium iron phosphate glasses have the highest glass transition temperatures of all tested samples. In the case of the lithium iron phosphate glass this is an indication that the glass' structure has gained stability from the addition of iron and a small amount of niobium within the phosphate system. It is believed that this is a first report of T_g for the $37.5Li_2O$-$20Fe_2O_3$-$5Nb_2O_5$-$37.5P_2O_5$ glass. This higher T_g is good in terms of the number of applications the glass can be used for in comparison with the binary lithium phosphate glasses which are less stable.

Table 2.3: A table to show glass transition temperature (T_g) and crystallisation temperatures (T_C)

Glass	T_g (°C)	T_{C1} (°C)	T_{C2} (°C)
$36.8Li_2O$ –$63.2P_2O_5$	202	237	N/A
$40Li_2O$ – $60P_2O_5$	210	275	N/A
$45Li_2O$ – $55P_2O_5$	290	399	N/A
$50Li_2O$ – $50P_2O_5$	335	385	392
$50Li_2O$ – $50P_2O_5$ grey	335	413	431
$55Li_2O$ – $45P_2O_5$	308	395	412
$60Li_2O$ – $40P_2O_5$	310	379	490
$33Li_2O$ – $66.7SiO_2$	460	623	N/A
$37.5Li_2O$-$20Fe_2O_3$-$5Nb_2O_5$-$37.5P_2O_5$	460	520	N/A

2.4 Micropycnometry

2.4.1 Method

A micropycnometer is an instrument that is used to determine a sample's volume, and from this volume it is then possible to determine the samples density which is a vital piece of information when modelling the material. The pycnometer measures the volume of a given sample by using a manometer and two chambers of different volume. Chamber one is an integral part of the equipment and cannot be accessed. Its volume is known as the reference volume V_R. Chamber two's volume is known as the cell volume V_C and this is where the sample is placed. The gas in the chambers must remain stable therefore helium is normally used due to its small size and inertness. Then helium is pumped into chamber one up to a pressure of ≈17 psi at which point the valve is closed. Once stabilised the reading is taken and denoted P_1. Once this reading has been taken the selector valve is switched to chamber 2 containing the sample. Once stabalised the pressure is written down as P_2 and then the helium is vented. This process is repeated multiple times until the P_1/P_2 ratio has stabilised. This data is then used along with the calibration data to determine the volume of the sample according to the following equation. [14]

$$\boldsymbol{V_P = V_C - V_R\left(\left(\frac{P_1}{P_2}\right) - 1\right)} \qquad \textbf{Equation 2.2}$$

Using this method it is possible to accurately determine the volume of bulk, porous and powdered samples with an error ≈0.005cm^3.

2.4.2 Density of Li phosphate glasses

Figure 2.13 below is an example of the readings taken using the pycnometer for the $55Li_2O - 45P_2O_5$ glass. The pycnometer used for this study was the Quantachrome MVP-6DC multipycnometer. Typically 2g or more of sample was used for each measurement. As you can see the results are stable with little fluctuation (the error bars show how much the result would change by if the last digit on the P_2 reading was increased or decreased by one).

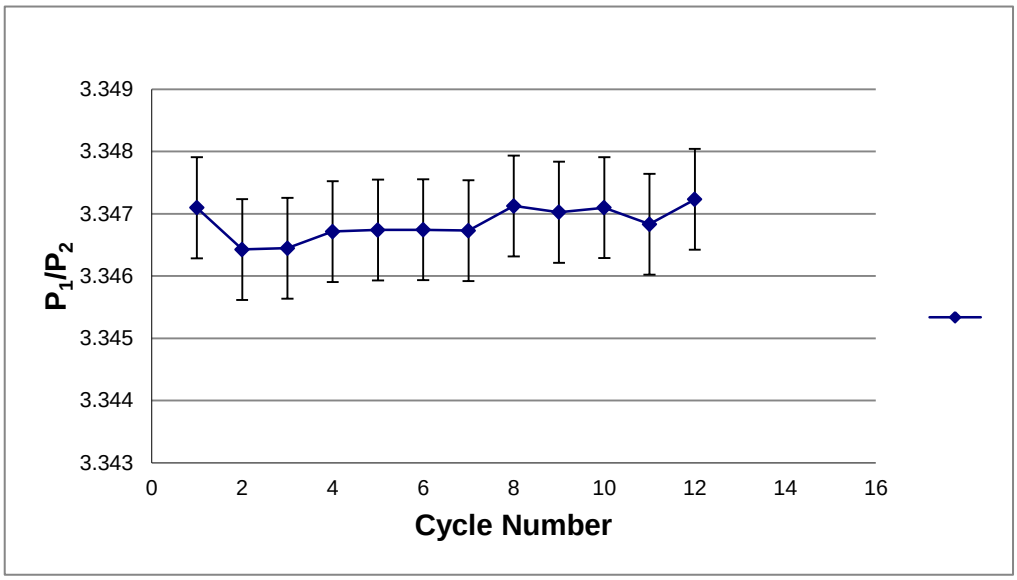

Figure 2.13: An example of results from the micropycnometer for $55Li_2O$-$45P_2O_5$ glass

Table 2.4: A table showing a glass' nominal composition and its measured density

mol% Li_2O - P_2O_5	Density (g/cm^3)
36.8	2.285 ±0.011
40.0	2.306 ±0.012
45.0	2.332 ±0.013
50.0	2.354 ±0.012
55.0	2.382 ±0.014

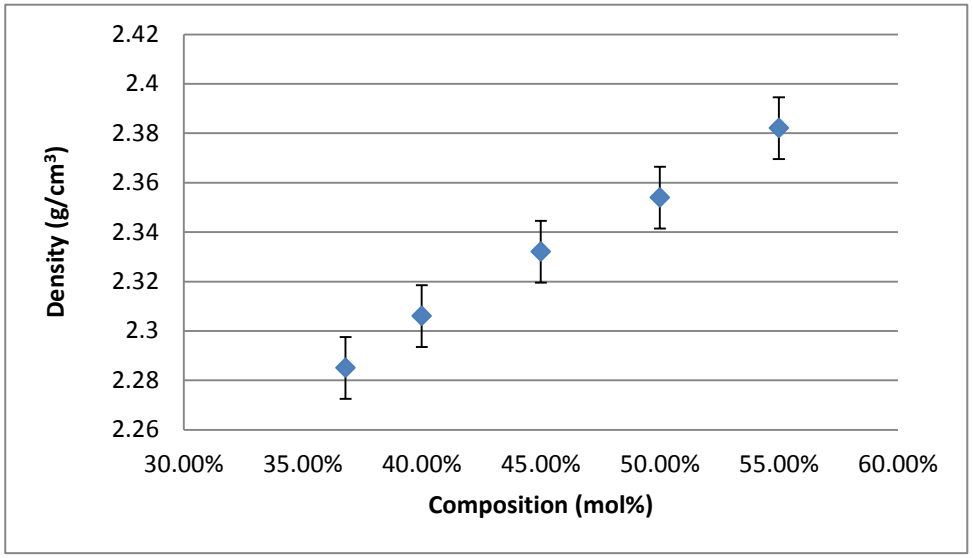

Figure 2.14: micropycnometry measurements of density from Kent instrument for $Li_2O - P_2O_5$ glasses

Table 2.4 above shows target composition and density. Figure 2.14 shows a linear relationship between composition and density where a higher lithium content corresponds to a higher density. This trend is expected as it follows findings from other experimental works in the SciGlass database. This is due to lithium being small so a larger amount can fit in a smaller space. However, there is quite a lot of variation in values given between this study's results and those published on SciGlass, mainly on values for 36.8 and 55 mol%. Figure 2.15 below shows the results of this study alongside results from Pronkin A.A. [15]and Kordes E. (from the SciGlass database reference unavailable).

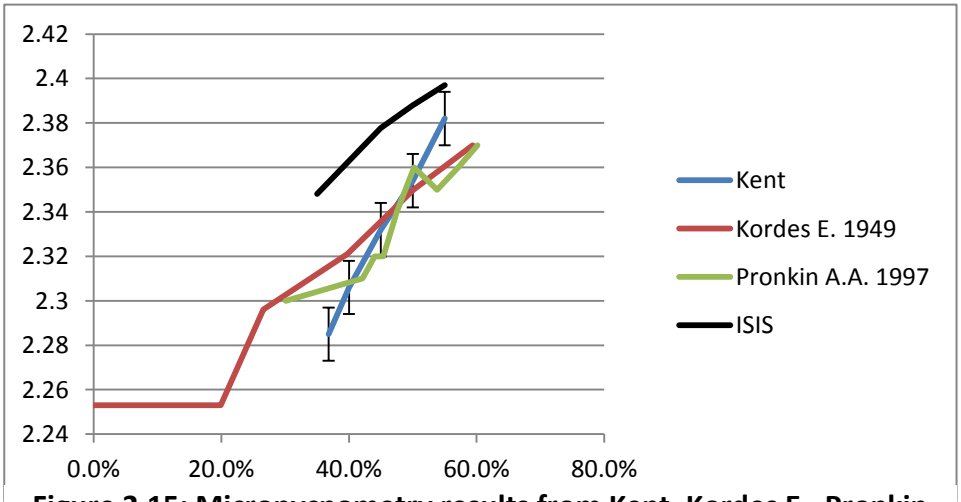

Figure 2.15: Micropycnometry results from Kent, Kordes E., Pronkin A.A. and ISIS for Li_2O-P_2O_5 glasses

There are multiple factors which could affect results and therefore explain the differences between studies. Compositions may be incorrect unless they have been verified using other characterisation methods (explored later on), samples may have contained bubbles (if using bulk samples for measurement), samples may have taken up moisture (phosphate glasses are known for their poor chemical durability [16]), or the researcher took pressure readings before they had fully stabilised. Another factor to consider is equipment. The results labelled "ISIS" in the above graph is from this study using a different pycnometer to the results labelled "Kent".

Figure 2.16: a powdered $40Li_2O$-$60P_2O_5$ glass after 2 months in air - affected by moisture

Figure 2.16 above shows the effect of moisture on a powdered lithium phosphate glass which has been left in an environment of air for an extended period of time. It can be seen in figure 2.16 that the sample has been badly affected by moisture which is an indicator of bad chemical durability. Whilst the powdered sample enhances the effect of moisture, the same phenomenon is observed with bulk samples which after time are found to be 'sticky' to touch. Because of this phosphate samples were always stored in a dessicator. This observation was not found in either the silicate or the $37.5Li_2O$-$20Fe_2O_3$-$5Nb_2O_5$-$37.5P_2O_5$ glass samples which can therefore be considered to have a much higher chemical durability. Density measurements for Li_2O-SiO_2 and $37.5Li_2O$-$20Fe_2O_3$-$5Nb_2O_5$-$37.5P_2O_5$ glasses are not reported here due to a fault occurring with the pycnometer at Kent, therefore the density measurement for the lithium silicate glass was obtained via the SciGlass database [17] and the density for the $37.5Li_2O$-$20Fe_2O_3$-$5Nb_2O_5$-$37.5P_2O_5$ glass was adjusted during molecular dynamics simulation of the glass (Chapter 4).

2.5 Nuclear Magnetic Resonance

2.5.1 Method

Atomic nuclei suitable for NMR spectroscopy have a non-zero nuclear spin which when placed in a magnetic field undergo nuclear spin transitions. The magnitudes of the energy change associated with these transitions are dependent upon the element and its local environment including bond lengths and binding partners. Magic Angle Spinning (MAS) NMR is a more recent technique which involves rotating a sample at high velocity at the critical angle of 54.74° to an applied magnetic field to generate a spectrum consisting of sharp peaks. The difference in nuclear magnetic resonance frequency between the tested sample and a reference standard is caused by variations in electron distribution due to bonds between different elements, and local structure, and is known as the 'chemical shift'. This is partly dependent upon the coordination numbers of an atom. For a phosphate sample it will also show whether the samples' phosphate tetrahedra are isolated or connected to other phosphate tetrahedra and how many. The amount of connections are noted down as Q^n numbers where n is the number of other tetrahedra it is linked to. From this, the composition of the sample can be determined. This is calculated firstly by comparing the ratio of phosphorus and oxygen. An example would be lithium metaphosphate, i.e. $LiPO_3$, where the ratio is 3. This ratio is how many equivalent oxygen a single phosphorus is connected to, where shared oxygen or bridging oxygen are counted as $\frac{1}{2}$. For lithium metaphosphate crystals it is known that each phosphate tetrahedra is attached to another two phosphate tetrahedra, i.e. Q^2. So an O:P ratio of 3 corresponds to a connectivity of 2, whereas an O:P ratio below 3 corresponds to a connectivity greater than 2 and vice versa.

2.5.2 ^{31}P MAS-NMR of Li phosphate glasses

(All NMR measurements and NMR spectra analysis was carried out by Dr. N. Kanwal at Queen Mary University of London). Solid state ^{31}P MAS–NMR experiments were carried out on Bruker Avance 600 MHz NMR instrument at resonance frequencies of 242.9 MHz. A 90° pulse (zg) with relaxation delays of 60 s were used to acquire ^{31}P spectra. Samples were contained in a 4 mm outer diameter zirconia rotor at spinning speeds of 12 kHz to acquire 4-16 ^{31}P. ^{31}P spectra were referenced to 85% phosphoric acid solution . Figure 2.17 shows a ^{31}P MAS-NMR spectrum for $50Li_2O$-$50P_2O_5$ glass. The NMR spectra are analysed by 'fitting' a spectrum calculated using variable parameters such as the chemical shift.

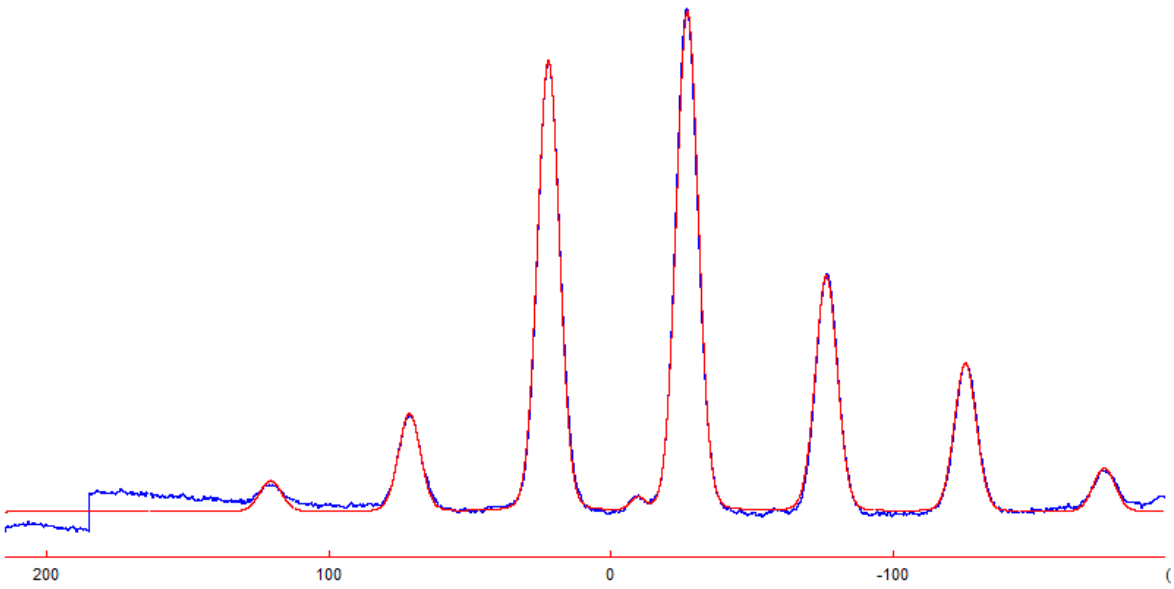

Figure 2.17: NMR spectra for $50Li_2O$-$50P_2O_5$ glass the blue line corresponds to the NMR spectra whilst the red line is the simulated spectra

Table 2.5: MAS-NMR results showing the glass' target composition and data

Target Composition	Chemical Shift, ppm	FWHM, ppm	Q^n	$\%Q^n$
$36.8Li_2O$-$63.2P_2O_5$	-44.87 -31.06	17.77 10.96	Q^3 Q^2	48.20 51.80
$40Li_2O$-$60P_2O_5$	-46.98 -32.46	15.12 11.67	Q^3 Q^2	44.45 55.55
$45Li_2O$-$55P_2O_5$	-41.36 -28.78	18.29 10.07	Q^3 Q^2	30.73 69.27
$50Li_2O$-$50P_2O_5$	-27.18 -9.47	9.12 5.79	Q^2 Q^1	99.59 0.41
$55Li_2O$-$45P_2O_5$	-26.38 -8.67	10.00 6.61	Q^2 Q^1	76.6 23.35
$60Li_2O$-$40P_2O_5$	-24.50 -8.13	9.57 6.35	Q^2 Q^1	48.97 51.03

Table 2.5 above shows the lithium phosphate glasses MAS-NMR results data that has been tabulated to include chemical shift and connectivity Q^n values. To confirm whether their stated compositions are as expected the glass composition can be estimated using the Q^n values. This is shown in table 2.6 below. The equation used to estimate the Q^n values is as follows.

If $y < 3$ then:

$$\boldsymbol{proportion\ of\ Q^3} = \left(\frac{\mathbf{3}-\boldsymbol{y}}{\mathbf{0.5}}\right) \times \mathbf{100}\% \qquad \textbf{Equation 2.3}$$

If $y > 3$ then:

$$\boldsymbol{proportion\ of\ Q^1} = \left(\frac{\boldsymbol{y}-\mathbf{3}}{\mathbf{0.5}}\right) \times \mathbf{100}\% \qquad \textbf{Equation 2.4}$$

Where y is the O:P ratio and the remaining proportion is assigned to Q^2.

Table 2.6: Target composition compared to composition estimated from Q^n values for Li_2O-P_2O_5 glasses

Target Composition (mol% Li_2O)	Expected (%Q^n)			Actual (%Q^n)			Estimated Composition (mol% Li_2O)
	Q^3	Q^2	Q^1	Q^3	Q^2	Q^1	
36.8%	41.77	58.23	0.00	48.2	51.8	0.00	34.12
40%	33.33	66.67	0.00	44.45	55.55	0.00	35.71
45%	18.18	81.82	0.00	30.73	69.27	0.00	40.92
50%	0.00	100.00	0.00	0.00	99.59	0.41	50.10
55%	0.00	77.78	22.22	0.00	76.6	23.35	55.23
60%	0.00	50.00	50.00	0.00	48.97	51.03	60.16

From this table it can be seen that whilst 50%, 55% and 60% compositions are as expected there is a discrepancy between target and estimated compositions for the 40% and 45% samples. This will affect the interpretation of results for micropycnometry and density calculations of 36.8% and 40% compositions. The adjustments have been made and are shown in the graph below. The data seems to fit more in agreement with other published results once the adjustments have taken place.

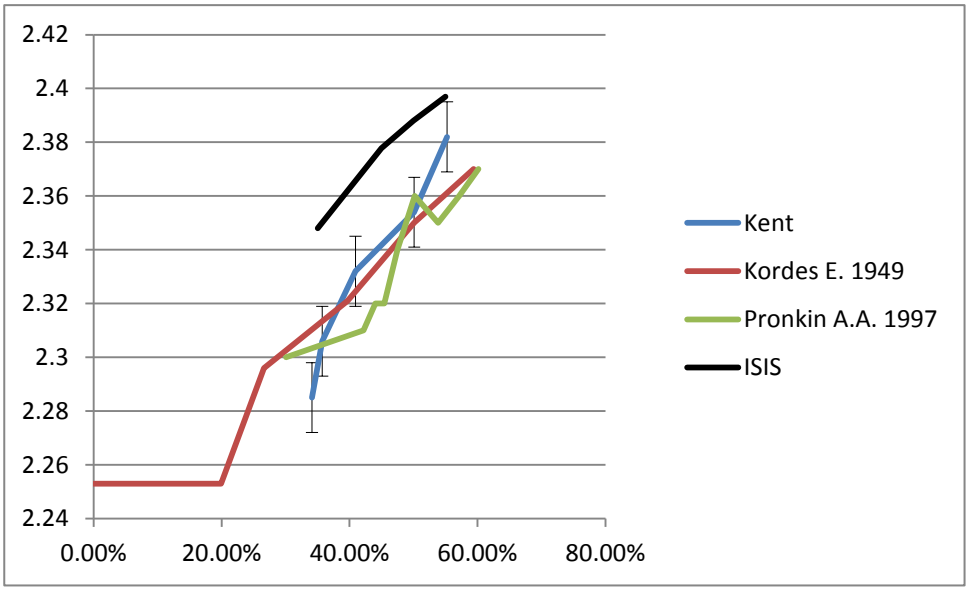

Figure 2.18: Micropycnometry results from Kent (using adjusted compositions), Kordes E, Pronkin A.A. and ISIS

[1] B. Money and K. Hariharan, “Lithium ion conduction in lithium metaphosphate based systems,” *Applied Physics A,* vol. 88, p. 647, 2007.

[2] B. Roy and H. Jain, “Phase Separation and Structural Differences between Alkali Silicate Glasses Prepared by the Sol-Gel and Melt-Quench Methods,” *Journal of the American Ceramic Society,* vol. 81, pp. 2360-70, 1998.

[3] K. Nagamine, K.Hirose, T. Honma and T. Komatsu, “Lithium ion conductive glass-ceramics with Li3Fe2(PO4)3 and YAG laser-induced local crystallization in lithium iron phosphate glasses,” *Solid State Ionics,* vol. 179, p. 508, 2008.

[4] A. A. Salah, P. Jowiak, J. Garbarczyk, K. Benkhouja, K. Zaghib, F. Gendron and C. Julien, “Local structure and redox energies of lithium phosphates with olivine- and Nasicon-like structures,” *Journal of Power Sources,* vol. 140, pp. 370-375, 2005.

[5] K.Hirose, T.Honma, Y.Benino and T.Komatsu, “Glass–ceramics with LiFePO4 crystals and crystal line patterning in glass by YAG laser irradiation,” *Solid State Ionics,* vol. 178, p. 801, 2007.

[6] R. Yang, Y. Wang, Y. Chen, X. Hao, J. Zhan and S. Liu, “Glass Formation Region of the Lithium Iron Phosphate Ternary System and the Properties of Obtained Glasses,” *Ceramics – Silikáty,* vol. 54, pp. 352 - 356, 2010.

[7] C. Gerbaldi, J. Nair, M. A. Kulandainathan, R. Kumar, C. Ferrara, P. Mustarelli and A. Stephan, “Innovative high performing metal organic framework (MOF)-laden nanocomposite polymer electrolytes for all-solid-state lithium batteries,” *Journal of Materials Chemistry A,* vol. 2, no. 26, pp. 9948-9954, 2014.

[8] A. R. West, Basic Solid State Chemistry second edition, Chichester: John Wiley and Sons, 2000.

[9] R. J. Tilley, Understanding Solids second edition, Chichester: John Wiley and Sons, 2013.

[10] J. Grenier and A. Durif, “CRYSTALLOGRAPHIC STUDY OF METAPHOSPHATES AND POLYPHOSPHATES OF LITHIUM,” *ZEITSCHRIFT FUR KRISTALLOGRAPHIE,* vol. 137, no. 1, pp. 10-16, 1973.

[11] K. Yukimitu, E. Araujo, J. Moraes, V. Reynoso and C. Carvalho, “Evidence of Distinc Phase transformations in Lithium Phosphate Glass Li2O-P2O5,” *Journal of Physics D,* vol. 35, pp. 3229-3232, 2002.

[12] S. Martin and C. Angell, “Dc and ac Conductivity in Wide Composition range Li2O-P2O5 glasses,” *Journal of Non-Crystalline Solids,* vol. 83, pp. 185-207, 1986.

[13] B. Money and K. Hariharan, “Crystallization Kinetics and Phase Transformation in Superionic Lithium Metaphosphate (Li2O-P2O5) Glass System,” *Journal of Physics: Condensed Matter,*

vol. 21, p. 115102, 2009.

[14] *Quantachrome multipycnometer user manual,* Quantachrome.

[15] A. Pronkin, “Physicochemical properties of glasses in the Li2O-P2O5 system,” *GLASS PHYSICS AND CHEMISTRY,* vol. 23, no. 5, pp. 383 -388, 1997.

[16] R. Brow, “Review: The structure of simple phosphate glasses,” *Journal of Non-Crystalline Solids,* vol. 263 & 264, pp. 1-28, 2000.

[17] G. El Damrawi, “Dependence of properties on structural units in Li2O-Al2O3-SiO2 glasses,” *Physics and Chemistry of glasses,* vol. 42, no. 2, pp. 116-120, 2001.

Chapter 3: Conductivity Measurements

3.1 Conductivity

Electrical conductivity is a materials ability to conduct an electric current. For example when an electrical potential difference is applied to a metal, the resulting electric field causes the movement of free electrons to move towards the positive terminal. This movement of electrons contributes to conductivity. This can be achieved by applying a d.c. voltage V across an electrically conducting material and measuring the current I. The resistance R is obtained by using the equation:

$$\boldsymbol{V = IR} \qquad \textbf{Equation 3.1}$$

A materials conductivity can be calculated from the materials resistivity (ρ), which is given by the following equation:

$$\boldsymbol{\rho = R\frac{A}{l}} \qquad \textbf{Equation 3.2}$$

Where l is the length and A is the cross-sectional area of the material. Conductivity is calculated as the inverse of resistivity:

$$\boldsymbol{\sigma = \frac{1}{\rho}} \qquad \textbf{Equation 3.3}$$

Therefore to calculate conductivity the materials resistance must be measured. However, with ionic conductivity this cannot be done as the material blocks the conduction of electrons and the electrodes placed at either side may block the transport of ions and would also result in the polarization affect taking place. Instead the approach of “impedance spectroscopy” can be used.

3.2 Impedance Spectroscopy

A.C. impedance spectroscopy is a useful and widely used method for measuring ionic conductivity of samples. [1] [2] [3] This technique involves the measurement of a samples' impedance (complex resistance) when applying an alternating voltage across two parallel electrodes of area A placed on either side of a sample of uniform thickness l. Electrodes can be either completely blocking (to ions), partially blocking, or non-blocking. For this study completely blocking electrodes were used on all samples so that no electrochemical reactions took place at the electrode/electrolyte interface. This was necessary as the sample should remain unchanged during testing. Electrodes can be applied to samples using multiple methods from conductive paints to sputtering and evaporation deposition. Sample preparation used in this study will be discussed later in this chapter. Complex impedance measurements can be carried out across a wide range of frequencies, typically from MHz down to fractions of Hz depending on the equipment available. The equipment used in this study has a range from 200 kHz to 100Hz. There are various ways in which impedance spectroscopy results may be represented. Conventionally two components of impedance Z are measured: the in-phase Z' (real) and out-of-phase Z'' (imaginary) components. The values of Z' and Z'' are then plotted and extrapolated to $\omega \to 0$ and $Z'' \to 0$ from which conductivity can be obtained from R=Z'. Plotting this allows for the identification of conduction processes present, including a sample's resistance caused by such things as bulk resistance or grain boundaries. [4] These conduction processes allow us to represent the samples conductivity as a circuit formed of resistors, capacitors and sometimes inductances. [5] This is to help better understand the processes taking place.

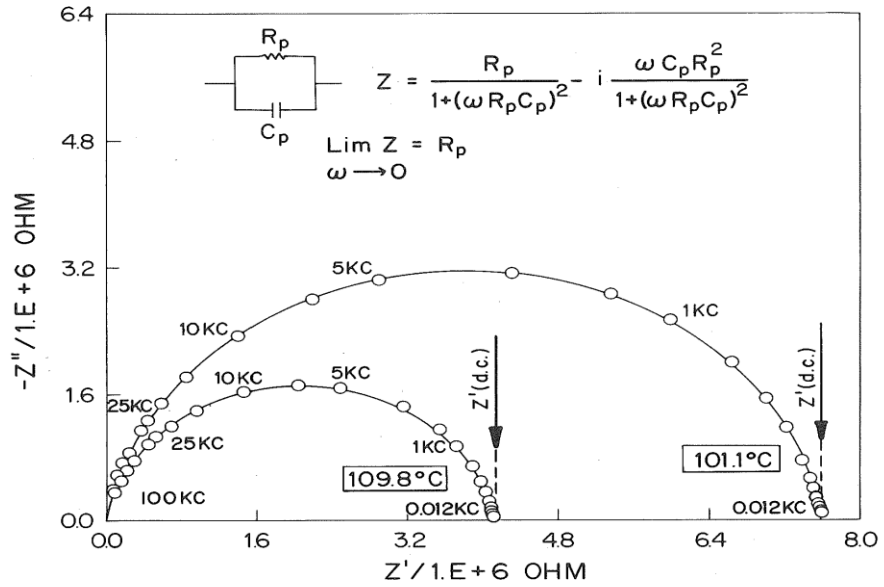

Figure 3.1: Complex Impedance plots for two temperatures and their equivalent circuit [6]

Figure 3.1 above shows examples of impedance plots and their equivalent circuit. [6] From the plot shown above, a samples resistance R is obtained from the intersection of the Z' axis and thus using aforementioned equations, the conductivity is calculated.

3.3 Equipment

Sample preparation is important as inconsistencies in a sample can affect impedance measurements and result in incorrect data being presented. In this study samples were formed using a mould as shown in chapter 2. This resulted in ≈2cm^2 samples with a thickness of ≈2mm. The samples cross sectional area (A) and thickness (l) respectively was measured afterwards using digital imaging measurement tool with an uncertainty of ±0.01mm^2 and a micrometer with an uncertainty of ±0.01mm. Ag electrodes were applied to each sample using a silver conductive paint. This ensured full coverage on each side of the sample. An example of a finished sample is shown in figure 3.2 below.

Figure 3.2: an example of a fully prepared sample

Samples were then placed in a rig attached to an impedance analyser both of these are shown in figures 3.3 and 3.4 below.

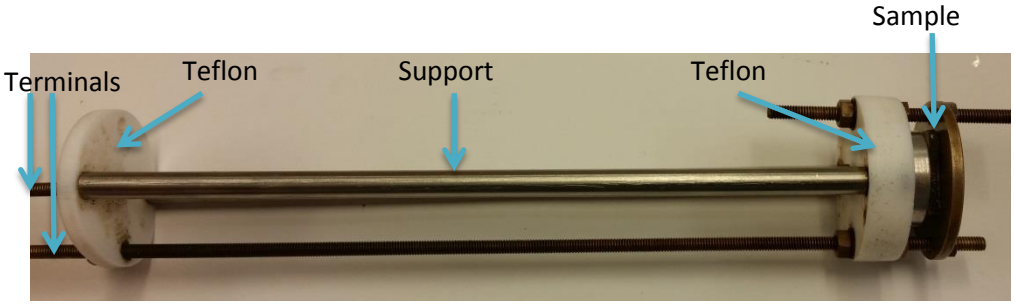

Figure 3.3: Rig used for impedance measurements (sample holder)

Figure 3.4: Wayne Kerr 4230 impedance analyser

As well as investigating how different glass types and compositions affect conductivity, how temperature affects conductivity was also investigated. This was done by placing the rig into a tube furnace as shown in figure 3.5 below.

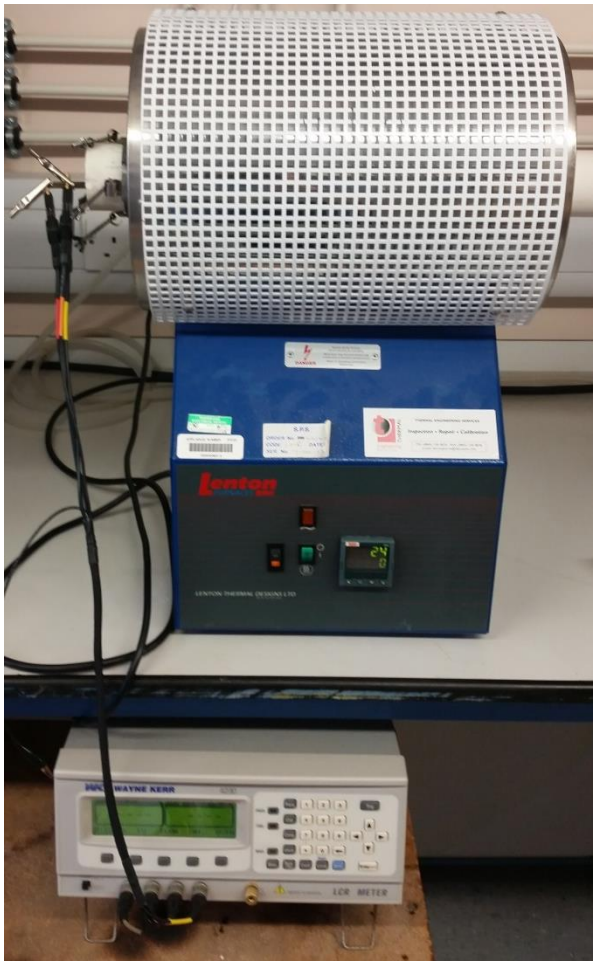

Figure 3.5: Full impedance spectroscopy set up

All impedance measurements were conducted in air. During temperature dependant measurements it was necessary to wait for impedance measurements to settle at each temperature stage before recording data. Typically this took approximately 1hr. At each stage readings were taken from 200KHz to 0.1KHz. At low temperatures an arc is the expected form an impedance plot should take which is due to the resistance of the sample. An example of an impedance plot from this study is shown in figure 3.6 below.

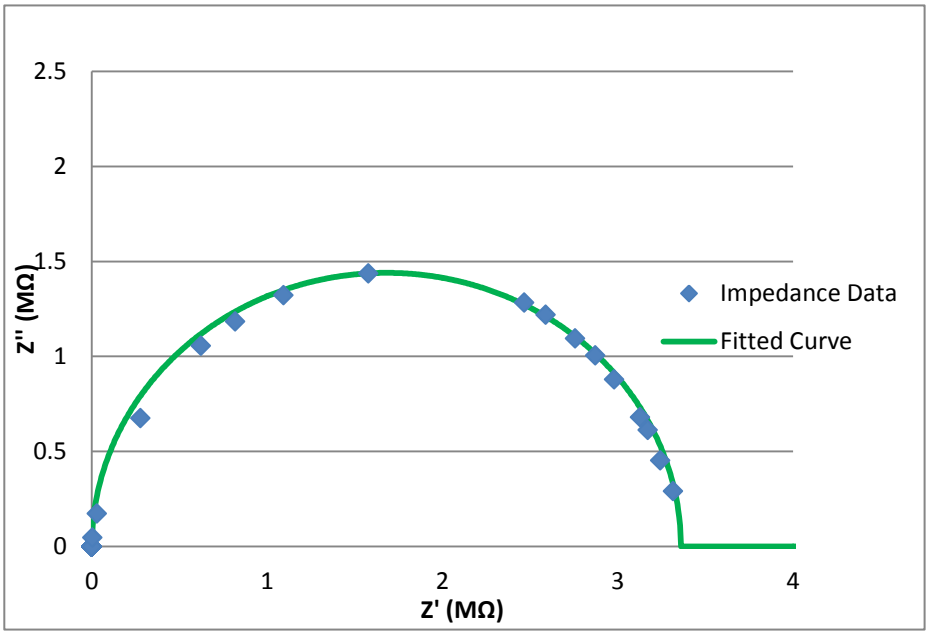

Figure 3.6: Impedance plot for $50Li_2O$-$50P_2O_5$ glass at 50°C

The important information to be taken from this is where the curve crosses the x-axis. This gives us the real part of the complex resistance Z' where the imaginary part Z'' = 0. From this conductivity is calculated. However, at higher temperatures the impedance plots look different. Rather than a curve which begins at the origin and ends with real resistance, a "spur" beginning at the real resistance and going outwards is observed as shown in figure 3.7 below.

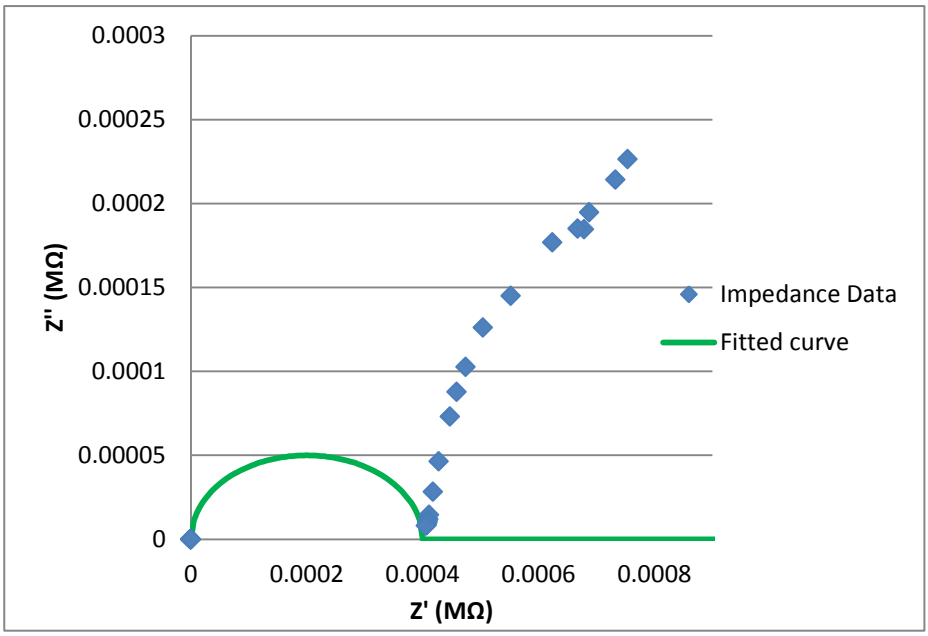

Figure 3.7: Impedance plot for $50Li_2O$-$50P_2O_5$ glass at 250°C

The reason this "spur" occurs is due to the polarisation effect taking place. This refers to the polarisation of the electrodes due to the highly mobile lithium ions. [6] The polarisation of the electrodes confirms the completely blocking nature of the Ag electrodes and the ionic nature of the samples conductivity. The higher the temperature the more dominant this feature becomes and the less dominant the bulk glass impedance feature becomes. As these features occur due to the mobility of ions (which is dependent on temperature) at high temperatures (typically 250°C) the arc feature is absent from the impedance plot. At mid-range temperatures a mixture of both of these features can be seen and at low temperatures only an arc is observed.

3.4 Conductivity of $33.3Li_2O$-$66.7SiO_2$ Glass

For silicate glasses only one sample was made and tested, $33.3Li_2O$-$66.7SiO_2$, whose conductivity measurements have been previously reported [7] [6] and can therefore be compared to this study's experimental findings. The reason more compositions for silicate glasses were not studied is due to the high temperatures (up to an extra 200°C) needed to synthesise higher lithium content silicate glasses. The results from this study have been graphed and tabulated in table 3.1 and figure 3.8 below.

Table 3.1: Conductivity results for $33.3Li_2O$-$66.7SiO_2$ glass

Temperature (K)	1000/T	Conductivity σ (S/cm)	$Log_{10}(\sigma)$
300	3.333	9.18×10^{-8}	-7.037
350	2.857	1.48×10^{-7}	-6.831
425	2.353	4.21×10^{-6}	-5.376
475	2.105	2.47×10^{-5}	-4.607
525	1.905	1.02×10^{-4}	-3.989

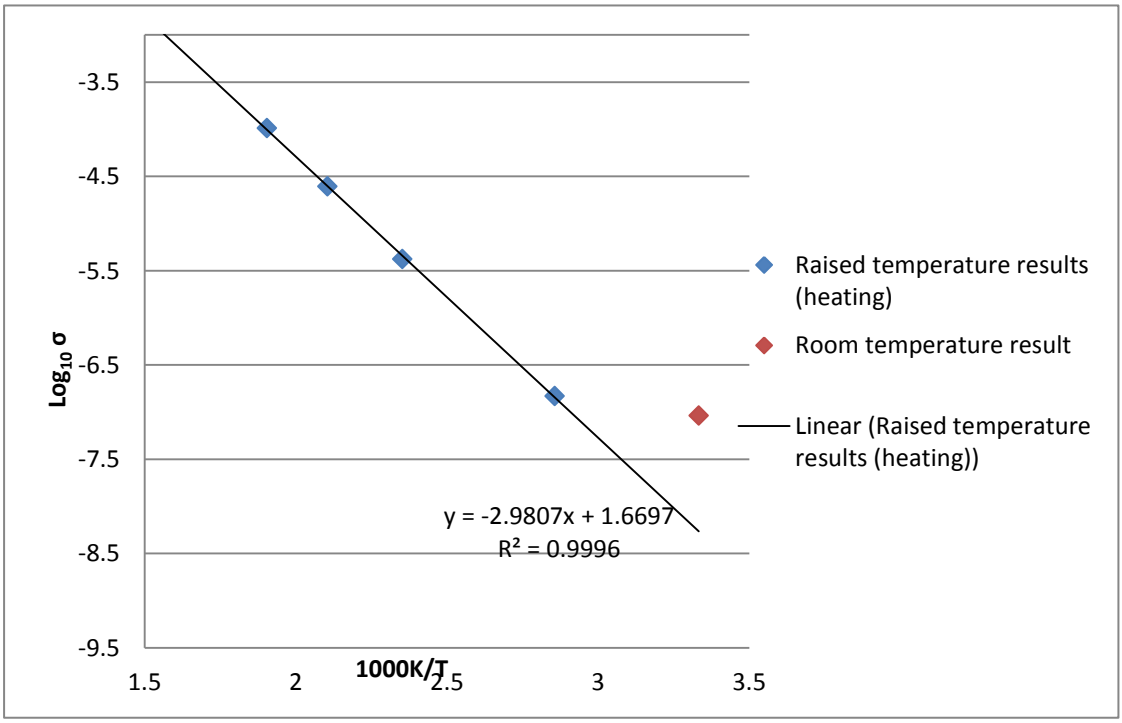

Figure 3.8: Conductivity plots for 33.3Li2O-66.7SiO2 glass

The graph above shows that $Log_{10}\sigma$ against 1000K/T forms a linear plot as expected according to the Arrhenius equation previously mentioned in chapter 1. However it can also be seen that the room temperature value does not sit on the line as expected. There are multiple reasons why this may occur, the most likely however is remnant moisture content on the sample which would have the effect of increased conductivity. However this effect would be removed upon heating of the sample due to moisture evaporation. Below is a graph showing results from this study in comparison with results from published data.

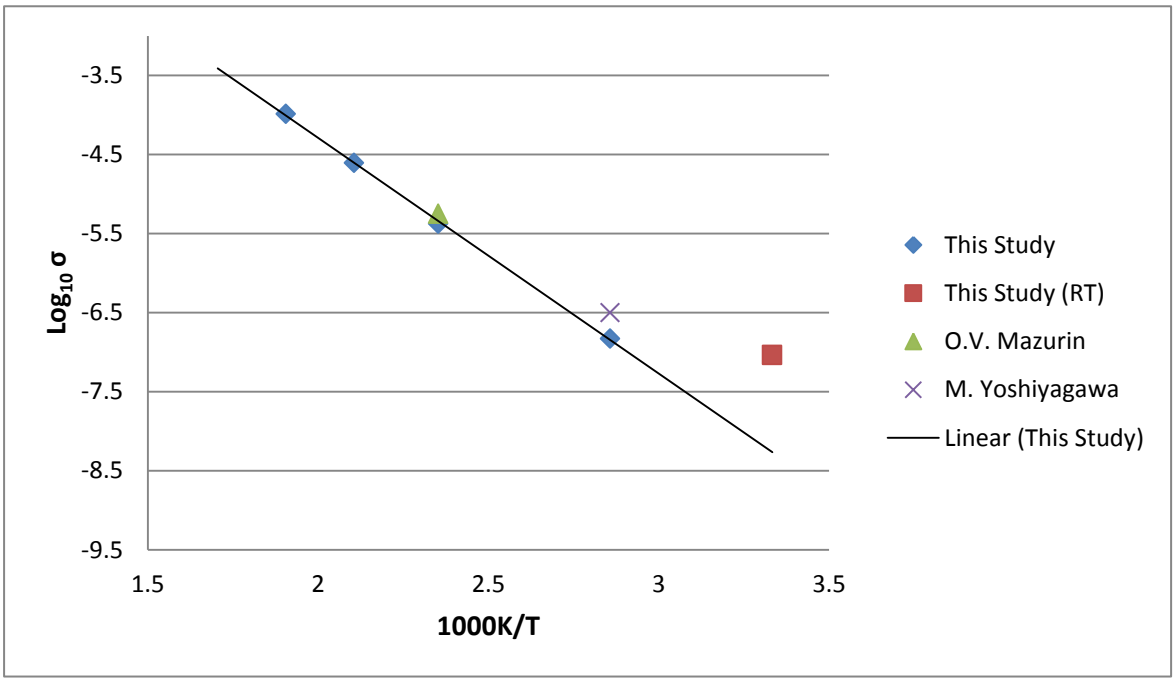

Figure 3.9: Comparison of conductivities between This Study, O.V. Mazurin [8] and M.Yoshiyagawa [7]

Figure 3.9 shows that the results from this study are in stong agreement with the results from Mazurin (1957) [8] study, however, results from this study show lower conductivities than expected in comparison with M. Yoshiyagawa (1982). [7] Reasons for this could be due to equipment accuracy or environment when readings were taken since M. Yoshiyagawa's experiments were conducted in a "dry Ar" atmosphere whereas this study's measurements were taken in air. Activation energies E_a were also calculated using the gradient of the graph, a value of 53.98 $kJmol^{-1}$ was obtained for the lithium disilicate sample. This compares well to the published figures of 54.03 $kJmol^{-1}$. [9] Due to the strong linear correlation in conductivity the errors for experimental values of E_a are considered very small.

3.5 Conductivity of Li Phosphate Glasses

For phosphate glasses, samples of multiple compositions were synthesised and room temperature impedance measurements were taken, the results from these measurements are shown in figure 3.10 below.

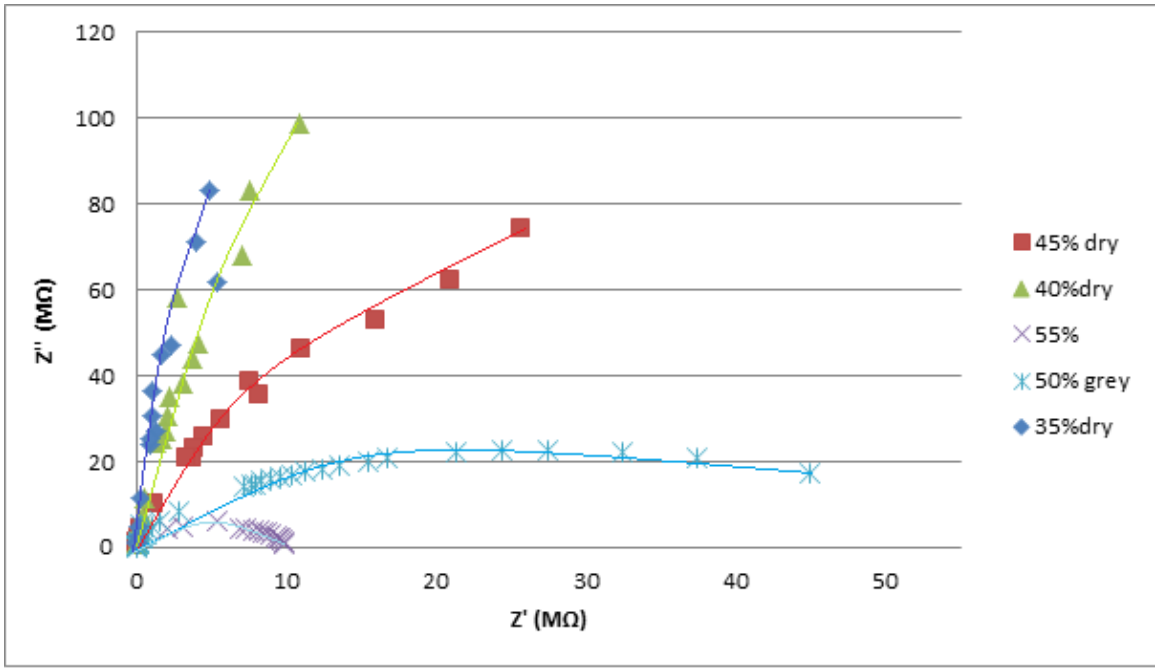

Figure 3.10: Room temperature conductivities for multiple glass compositions in the binary Li_2O-P_2O_5 system

The graph above shows that as lithium content increases, the size of the impedance arc decreases corresponding to a lower real resistance which, in turn, corresponds to a higher conductivity. This trend is as expected due to a higher charge carrier density with increased lithium content. This data also fits well with published results by S.W. Martin and C.A. Angell. [6] From this graph only 50% and 55% impedance curves could be accurately extrapolated to Z''=0 and so conductivities for these two glasses and, for comparison, the equivalent data from S.W. Martin and C.A. Angell are as follows.

Table 3.2: Room temperature conductivity comparison between This Study and S.W. Martin and C.A. Angell study [6]

Glass	Reference	$Log_{10}(\sigma)$
$50Li_2O$-$50P_2O_5$	This Study	-8.635
	[6]	-8.619
$55Li_2O$-$45P_2O_5$	This Study	-7.899
	[6]	-7.966

The table shows that for 50% both studies show similar results. Alternatively, for 55% results from 'This Study' show a higher conductivity than the Martin and Angell study. However, differences in experimental conductivity values are common as shown further in this section.

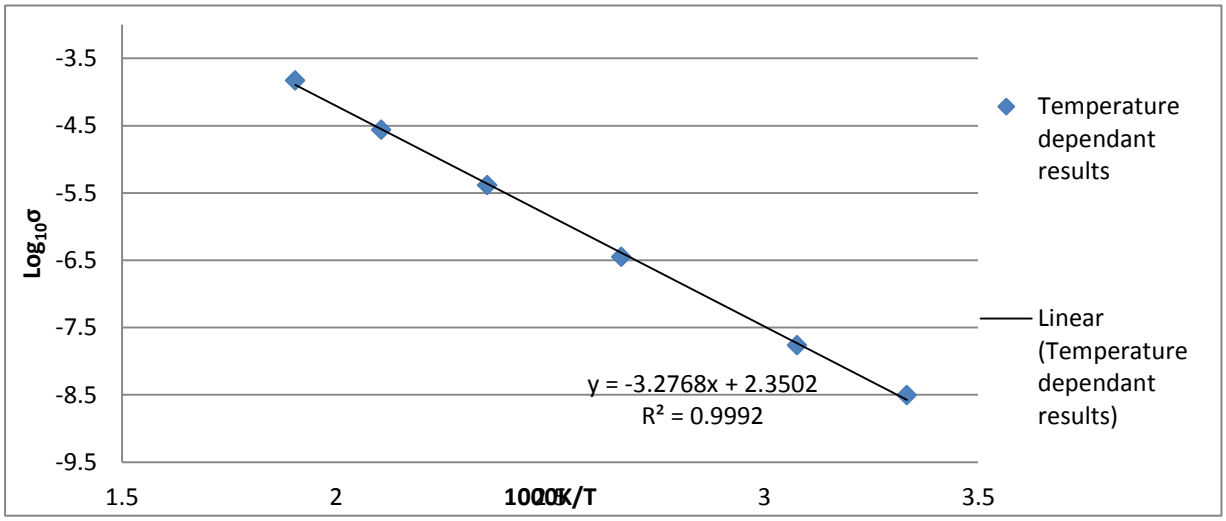

Figure 3.11: Conductivity plots for $50Li_2O$-$50P_2O_5$ glass

Figure 3.11 above shows the temperature dependency of conductivity in the lithium metaphosphate sample. The graph above shows a strong linear relationship between temperature and conductivity as expected. The sample was pre-dried immediately before conducting impedance measurements to ensure that room temperature results were less affected by moisture.

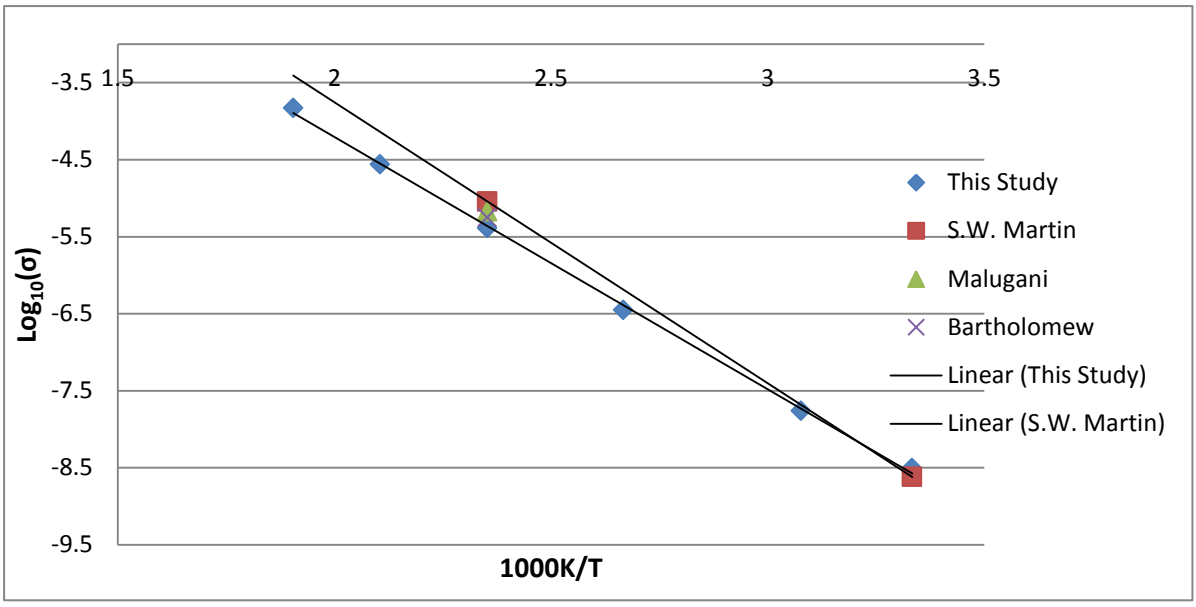

Figure 3.12: Comparison of conductivities between This Study, Martin and Angell, [6] Malugani [13] and Bartholomew [12]

Results were compared to Martin and Angell's study along with two other studies. Figure 3.12 above shows that whilst results from this study and the Martin and Angell study differ considerably at elevated temperatures, it is common to have discrepancies in these values. Reasons for this again could be equipment accuracy, sample synthesis and characterisation procedure or even the environment in which measurements were taken. However due to the strong linear trend shown in this study's results and due to the sample being characterised and found to be of the correct composition, these results can be taken with confidence for an atmosphere of air. Activation energy was calculated from the slope of the graph and a value of 62.75 $kJmol^{-1}$ was obtained. The published value is 68.99 $kJmol^{-1}$. Whilst not as close as with the lithium disilicate glass these values are within 10% of each other. Activation energy was recalculated excluding the room temperature (which may have been affected by residual surface moisture) and a value of 64.10$kJmol^{-1}$ was obtained, which is yet closer to the published value.

3.6 Conductivity of $37.5Li_2O$-$20Fe_2O_3$-$5Nb_2O_5$-$37.5P_2O_5$ glass

There was only one $37.5Li_2O$-$20Fe_2O_3$-$5Nb_2O_5$-$37.5P_2O_5$ glass synthesised, of which it is believed conductivity measurements have not yet been published. However, the equivalent glass-ceramic and ceramic conductivities have been reported [10] [11] and are compared to those measured in this study. The impedance results from this study have been tabulated and graphed in table 3.3 and figure 3.13 below.

Table 3.3: Conductivity results for $37.5Li_2O$-$20Fe_2O_3$-$5Nb_2O_5$-$37.5P_2O_5$ glass

Temperature (K)	1000/T	Conductivity σ (S/cm)	$Log_{10}(\sigma)$
300	3.333	9.895×10^{-10}	-9.005
350	2.857	3.192×10^{-8}	-7.496
375	2.667	1.199×10^{-7}	-6.921
400	2.500	4.378×10^{-7}	-6.359
425	2.353	1.477×10^{-6}	-5.831
450	2.222	4.398×10^{-6}	-5.360
475	2.105	1.164×10^{-5}	-4.930
500	2.000	2.954×10^{-5}	-4.530
525	1.905	6.510×10^{-6}	-4.186

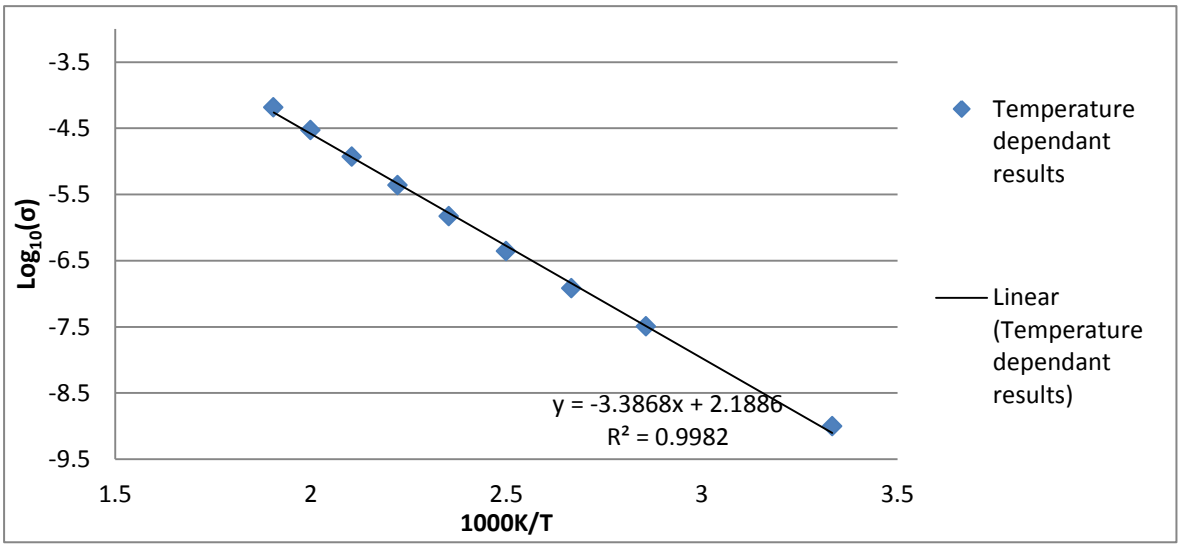

Figure 3.13: Conductivity results for $37.5Li_2O$-$20Fe_2O_3$-$5Nb_2O_5$-$37.5P_2O_5$ glass

The results shown in figure 3.13 above again show a strong linear relationship as expected. Figure 3.14 below shows how the glass compares to its published ceramic and glass-ceramic counterparts. It can be seen that, of the three studies, the glass (this study) is the lowest performing in terms of conductivity. The ceramic prepared by ultrasonic spray pyrolysis (USP) (Schitz) [11] has a conductivity ≈ 1 order of magnitude greater than the glass sample at room temperature. However, the strongest performer (at room temperature) is the glass-ceramic prepared by melt quenching and then heat treating above the crystallisation temperature (Nagamine), [10] with a conductivity over 3 orders of magnitude higher than the glass from this study. This is interesting as it suggests that a material which shares different properties of both its glass and crystalline counterparts exhibits higher conductivity values than either the glass or ceramic alone.

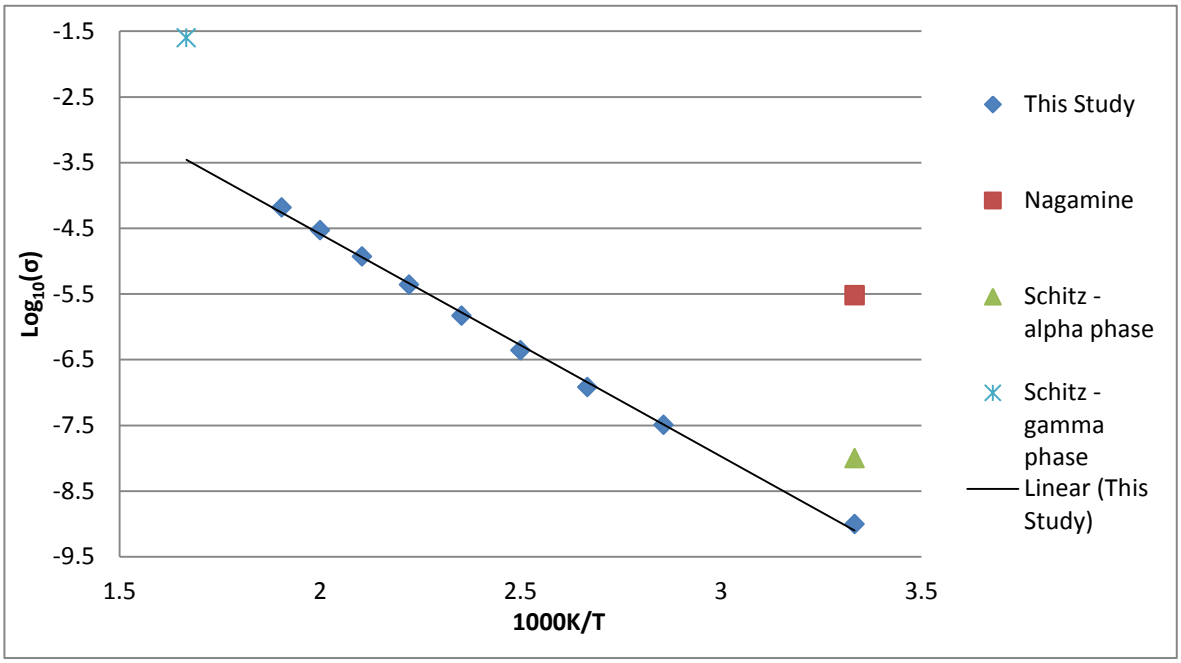

Figure 3.14: Comparison of conductivities of $Li_3Fe_2(PO_4)_3$ materials from This Study, Nagamine, [10] and Schitz. [11]

Activation energy was calculated to be 64.8571 $kJmol^{-1}$. As reports on this glass do not contain activation energies this has not been compared to another glass. Instead it can be compared to the glass-ceramic [10] which measured a value of 46.31 $kJmol^{-1}$ which is significantly lower than the value for the glass. A lower activation energy means less

energy is required to commence conductivity and the glass-ceramic reports a higher conductivity than the glass therefore a lower activation energy is expected. Activation energy was recalculated without the room temperature plot as the reading may have been affected by surface moisture, a value of 67.25 $kJmol^{-1}$ was obtained. There are multiple activation energy values reported in the Schitz study [11]. One for each phase (α, β and γ) of the material, which are defined by temperature boundaries as follows: α < 150°C < β < 260°C < γ. The points in figure 3.14 correspond to α and γ phases which have activation energies 71.40 $kJmol^{-1}$ and 46.31 $kJmol^{-1}$ respectively.

3.7 Comparison of Different Glass Compositions

The graph below compares the results for the $37.5Li_2O$-$20Fe_2O_3$-$5Nb_2O_5$-$37.5P_2O_5$, the 33.3% Li Silicate and the 50% Li phosphates glasses from this study.

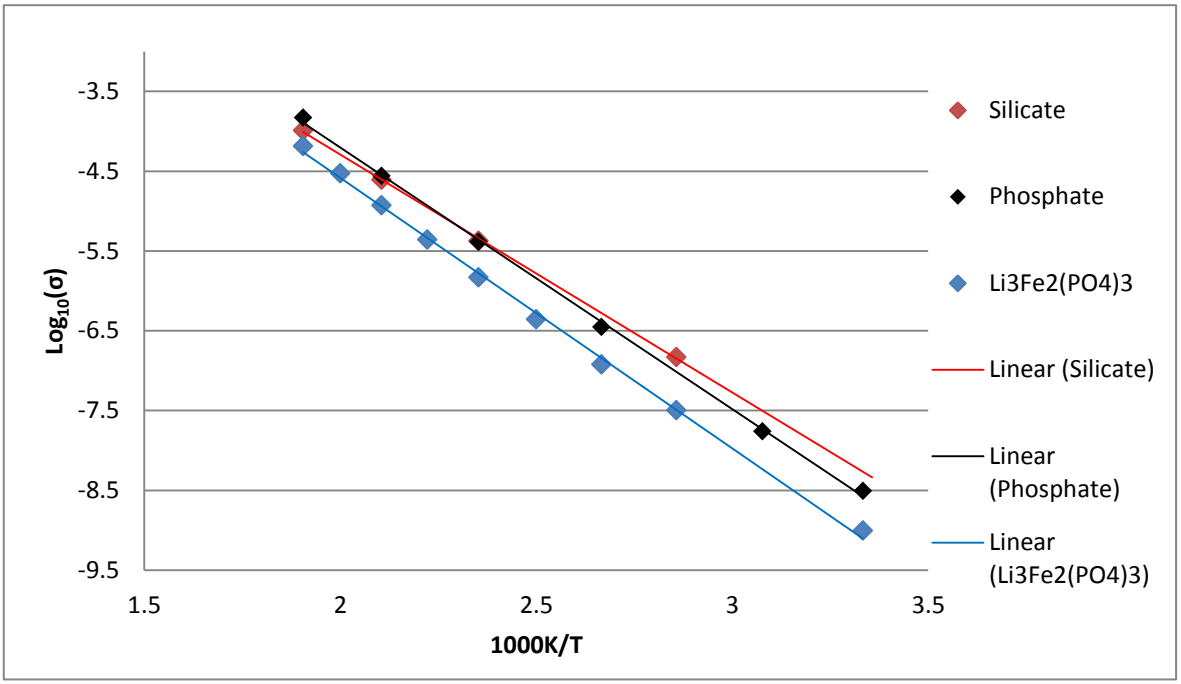

Figure 3.15: Comparison of conductivities between $33.3Li_2O$-$66.7SiO_2$, $50Li_2O$-$50P_2O_5$ and $37.5Li_2O$-$20Fe_2O_3$-$5Nb_2O_5$-$37.5P_2O_5$ glasses used within this study

The graph shows that whilst the $33.3Li_2O$-$66.7SiO_2$ glass compares well with the $50Li_2O$-$50P_2O_5$ glass the $37.5Li_2O$-$20Fe_2O_3$-$5Nb_2O_5$-$37.5P_2O_5$ glass has the lowest conductivity value throughout the temperature range. When comparing the conductivity values from the results in this study alone, it was found that when extrapolated to room temperature the $33.3Li_2O$-$66.7SiO_2$ glass had the highest conductivity value of $\approx 1 \times 10^{-8} S/cm$, however, at an elevated temperature of 525K the 50% phosphate sample surpassed the silicate conductivity with a value of $1.45 \times 10^{-4} S/cm$ compared to $1.02 \times 10^{-4} S/cm$. The reason the silicate glass (with a lower lithium content than the phosphate glass) performed so well was put down to a higher concentration of non-bridging oxygens as reported in the Martin and Angell study. [6] Throughout the entire temperature range the lowest performing sample was that of the $37.5Li_2O$-$20Fe_2O_3$-$5Nb_2O_5$-$37.5P_2O_5$ glass. As previously stated non-bridging oxygens are the sites where ions 'migrate' from and to

when contributing to ionic conductivity. So a higher concentration of charged non-bridging oxygens means more sites available for conduction. [6] The reason for the addition of iron and niobium to the lithium phosphate glass was to improve chemical durability (a known problem with phosphate glasses). Whilst the additions have shown improved chemical durability, the conductivity values are lower than the lithium metaphosphate glass.

[1] S. Shawuti and M. Gulgun, “Solid oxide-molten carbonate nano-composite fuel cells: Particle size effect,” *Journal of Power Sources,* vol. 267, pp. 128-135, 2014.

[2] N. D. Akmeida and G. Goward, “Proton dynamics in sulfonated ionic salt composites: Alternative membrane materials for proton exchange membrane fuel cells,” *Journal of Power Sources,* vol. 268, pp. 853-860, 2014.

[3] Q. Xiao, H.Y.Liu and Q. L. Xia, “A Nanocomposite Polymer Electrolyte with High-Temperature Stability for Rechargeable Lithium Batteries,” *Arabian Journal for Science and Engineering,* vol. 39, no. 9, pp. 6651-6657, 2014.

[4] Macdonald and J. Ross, “Impedance Spectroscopy,” *Annals of Biomedical Engineering,* vol. 20, pp. 289-305, 1992.

[5] Macdonald and J.Ross, Impedance Spctroscopy, New York: John Wiley & Sons, 1987.

[6] S. Martin and C. Angell, “Dc and ac Conductivity in Wide Composition range Li2O-P2O5 glasses,” *Journal of Non-Crystalline Solids,* vol. 83, pp. 185-207, 1986.

[7] M. Yoshiyagawa and M.Tomozawa, “Electrical properties of rapidly quenched lithium-silicate glasses,” *Journal De Physique,* vol. 43, pp. c9-411, 1982.

[8] O. V. Mazurin and E. S. Borisovskii, *Soviet Phys. Tech. Phys.,* vol. 27, p. 243, 1957.

[9] F. Ali, A. Chadwick, G. Greaves, M. Jermy, K. Ngai and M. Smith, “Examination of the mixed-alkali effect in (Li,Na) disilicate glasses by nuclear magnetic resonance and conductivity measurements,” *Solid State Nuclear Magnetic Resonance,* vol. 5, pp. 133-143, 1995.

[10] K. Nagamine, K.Hirose, T. Honma and T. Komatsu, “Lithium ion conductive glass-ceramics with Li3Fe2(PO4)3 and YAG laser-induced local crystallization in lithium iron phosphate glasses,” *Solid State Ionics,* vol. 179, p. 508, 2008.

[11] A. Ivanov-Schitz, A. Nistuk and N. Chaban, “Li3Fe2(PO4)3 solid electrolyte prepared by ultrasonic spray pyrolosis,” *Solid State Ionics,* vol. 139, pp. 153-157, 2001.

[12] R. Bartholomew, *Journal of Non-Crystalline Solids,* vol. 12, p. 321, 1973.

[13] G. Robert, J. Malugani and A. Saida, *Solid State Ionics,* vol. 3&4, p. 311, 1981.

Chapter 4: Molecular Dynamics Modelling

4.1 Molecular Dynamics Method

There are several reasons to include molecular dynamics (MD) modelling in this study. It allows us to simulate the glasses used within this study, gain information used in the characterisation of the samples and compare these with experimental data. It also enables us to create a visual representation of the structures under study. Classical molecular dynamics modelling is a computational simulation which involves the study of a system of particles representing atoms. The study runs over a given time period and computes the equilibrium and transport properties of the system. Classical MD modelling interactions obey Newtonian mechanics and attempt to simulate how a system would react experimentally under specific conditions by controlling parameters such as temperature and density. As MD modelling uses classical mechanics it does not take the effects of quantum mechanics into consideration which means that it does not correctly compute the translational and rotational motion of light atoms such as hydrogen and helium. [1]

As previously stated MD modelling obeys Newtonian mechanics and therefore follow Newton's laws of motion. When an atom becomes close enough to another so that they are considered to be interacting the effect of this interaction is calculated using Newton's second law:

$$\boldsymbol{f_x = ma} \qquad \textbf{Equation 4.1}$$

Where f is the force and x denotes the x direction and where m and a are the particles mass and acceleration respectively. This force may be derived in terms of potential energy as follows:

$$\boldsymbol{f_x(r) = -\frac{\delta u(r)}{\delta x}} \qquad \textbf{Equation 4.2}$$

Once all forces have been calculated Newton's laws of motion must be integrated in order to determine the atoms positions and velocities. This can be calculated using Verlet's algorithm. [2] This is based on a Taylor series expansion of a particles position r at a time t which can be written as:

$$\boldsymbol{r(t+\Delta t) = r(t) + v(t)\Delta t + \frac{f(t)\Delta t^2}{2m} + \cdots}$$ **Equation 4.3**

And

$$\boldsymbol{r(t-\Delta t) = r(t) - v(t)\Delta t + \frac{f(t)\Delta t^2}{2m} - \cdots}$$ **Equation 4.4**

From which can be obtained:

$$\boldsymbol{r(t+\Delta t) \approx 2r(t) - r(t-\Delta t) + \frac{f(t)\Delta t^2}{m}}$$ **Equation 4.5**

This equation however, gives an error proportional to Δt^4 where Δt is the time step used in the simulation. This issue can be avoided by instead using an algorithm based on Verlet's 'leapfrog' method, [3] [4] which calculates velocities at half integer time steps.

$$\boldsymbol{v\left(t+\frac{\Delta t}{2}\right) = v\left(t-\frac{\Delta t}{2}\right) + \frac{f(t)}{m}\Delta t}$$ **Equation 4.6**

These velocities are then used to calculate the atoms new position as follows:

$$\boldsymbol{r(t+\Delta t) = r(t) + v\left(t+\frac{\Delta t}{2}\right)\Delta t}$$ **Equation 4.7**

The velocity at time t is calculated using the equation:

$$\boldsymbol{v(t) = \frac{v\left(t+\frac{\Delta t}{2}\right)+v\left(t-\frac{\Delta t}{2}\right)}{2}}$$ **Equation 4.8**

The average kinetic energy per degree of freedom is:

$$\boldsymbol{\langle \frac{1}{2}mv^2 \rangle = \frac{1}{2}k_B T}$$ **Equation 4.9**

The system's instantaneous temperature can be calculated using:

$$\boldsymbol{T(t) = \frac{\sum_{i=1}^{N} m_i v_i^2(t)}{k_B N_f}}$$ **Equation 4.10**

where k_B is the Boltzman constant and N_f is the number of degrees of freedom of the system.

Experimentally the movement and interactions within a system are caused by forces acting on and between particles. The interactions are defined by a set of interatomic potentials. These potentials govern how each atom will interact with another and therefore the more accurate the potentials used the more accurate the simulation may be. This study will use three different types of potentials which represent different types of interactions within the system:

The Buckingham Potentials – This is known as a bond potential and governs the distances between bonded atoms and can be mathematically calculated using the equation:

$$\boldsymbol{U(r_{ij}) = A \exp\left(-\frac{r_{ij}}{\rho}\right) - \left(\frac{C}{r_{ij}^6}\right)} \qquad \textbf{Equation 4.11}$$

where A, ρ and C are potential parameters, r_{ij} is the separation of atoms and U is the potential. The equation contains both an attractive term $\left(-\frac{C}{r_{ij}^6}\right)$ and a repulsive term $A \exp\left(-\frac{r_{ij}}{\rho}\right)$. These potentials were obtained from literature. [5]

The Coulomb potential – This governs interactions between a pair of atoms I and j due to their respective charges, it can be mathematically represented using the equation: [6]

$$\boldsymbol{U = \frac{q_i q_j}{4\pi\varepsilon_0 r_{ij}}} \qquad \textbf{Equation 4.12}$$

The Three body potential – This governs the bond angle between three atoms and it can be mathematically calculated using the screened harmonic equation:

$$\boldsymbol{U(\theta_{jik}) = \frac{k}{2}(\theta_{jik} - \theta_0)^2 exp\left[-\left(\frac{r_{ij}}{\rho_1} + \frac{r_{ik}}{\rho_2}\right)\right]} \qquad \textbf{Equation 4.13}$$

Where $\theta_{ijk}$is the angle between atoms i, j and k, θ_0 is the equilibrium angle, and k is a spring constant. Again these potentials were obtained from literature. [7]

Table 4.1: charges and Buckingham potential parameters

i-j	q_i(e)	A_{ij} (eV)	P_{ij} (Å)	C_{ij} (eVÅ^{-6})
Li-O	0.6	41051.94	0.1561	0.00
Si-O	2.4	13702.00	0.1938	54.68
P-O	3.0	26655.47	0.18197	86.86
O-O	-1.2	1844.00	0.3436	192.58
Fe-O	1.8	19952.00	0.1825	4.66
Nb-O	3.0	11448.00	0.2280	95.19

Table 4.2: three body potential parameters

i-j-k	K	Θ_0	r_{ij}	r_{jk}
P-O-P	3.0	135.58	40.0	40.0
O-P-O	3.5	109.47	40.0	40.0

4.2 Creating A Glass Model Using DLPoly

The programme used to run the MD simulations in this study was DL_Poly_2. [3] For DL_POLY_2 to run a simulation, information must be input in the form of three input files named CONFIG, CONTROL and FIELD. Examples of these files can be found in the appendix. The CONFIG file contains information such as the models' box dimensions, samples density and atom labels including their positions (and may also include their velocities and forces). Densities for the models in this study were obtained from the pycnometry measurements in chapter 2 ($50Li_2O$-$50P_2O_5$ model), from SciGlass [8] ($33Li_2O$-SiO_2 model) and from estimating the density ($37.5Li_2O$-$20Fe_2O_3$-$5Nb_2O_5$-$37.5P_2O_5$ model) The initial CONFIG file was produced by running an executable named 'Mdconfig2'. Atoms were given random positions within a cubic box (see table 4.1). The CONTROL file contains the information about the system variables and what type of simulation to run, for example the time steps, desired temperature, equilibration and how often HISTORY

outputs are written. The FIELD file contains information about the interatomic potentials that govern interactions between particles (see tables 4.1 and 4.2).

As previously stated the temperature of the system is controlled. To do this DL_POLY_2 couples the system with a heat bath, which scales the atoms velocities every 5 steps in order to match the desired temperature. This study used a Berensden NVT algorithm, timesteps of 1 fs were used and all bath stages were run over 40000 time-steps. There are 6 stages in each full simulation. The initial stage is run at a temperature of 6000K this is to ensure that the samples structure is random as it allows the atoms to diffuse within the box. Next the temperature is reduced firstly to 4000K then to 2000K and finally to a temperature slightly above the melting temperature so that the system resembles a liquid. In this study the temperatures used for this stage ($33Li_2O$-$67SiO_2$ 1550K, $50Li_2O$-$50P_2O_5$ 1223K and $37.5Li_2O$-$20Fe_2O_3$-$5Nb_2O_5$-$37.5P_2O_5$ 1473K) match those used when making the glasses experimentally as this is what the simulation is attempting to replicate. Next is the quenching stage, again this scales the velocities so that the systems temperature is reduced at a rate of 10^{13}K/s down to a temperature of 300K. The final stage is to run a simulation at 300K so that the system is a solid. It is from this final stage which information for analysis of the sample can be taken. For conductivity measurements above 300K the final stage is repeated using the desired temperatures.

Table 4.3: composition, size and melt temperatures

Composition	Number of atoms	Box length (Å)	T_{melt} (K)
$33Li_2O – 67SiO_2$	3000	32.839	1550
$50Li_2O$-$50P_2O_5$	3000	33.130	1223
$37.5Li_2O$-$20Fe_2O_3$-$5Nb_2O_5$-$37.5P_2O_5$	3060	33.780	1473

4.3 Analysing the Structure of a Glass Model

DL_POLY_2 generates five output data files: OUTPUT, REVCON, STATIS, REVIVE and HISTORY. The OUTPUT file contains data such as rolling averages of energy, temperature, volume and pressure. The REVCON file contains data on the particles new coordinates. The HISTORY file contains information on atomic coordinates in a time ordered sequence as specified in the CONTROL file. Executables and analysis programs used to produce useful data are as follows (* denotes software codes developed within research group):

- xanal_02* to calculate radial distribution function and coordination numbers.
- xhst_hsc-gm2* to analyse connectivity via Q^n distribution.
- mdprep* to calculate diffusivity and hence conductivity.
- dlpxyz-50k* and ISAACS [9] for imaging and to calculate x-ray and neutron diffraction.

4.3.1 Nearest Neighbour Distances and Coordination Numbers

Glasses have no long range periodic atomic arrangement. [10] Instead distribution functions are used to describe the glass' structure. When looking at a glass structure, it can be seen that they often have a preferred atomic arrangement, for example silicon and oxygen tend to form SiO_4 tetrahedra. Similarly phosphorus and oxygen also tend to form a PO_4 tetrahedra. An example of a SiO_4 tetrahedron is depicted in figure 4.1 below.

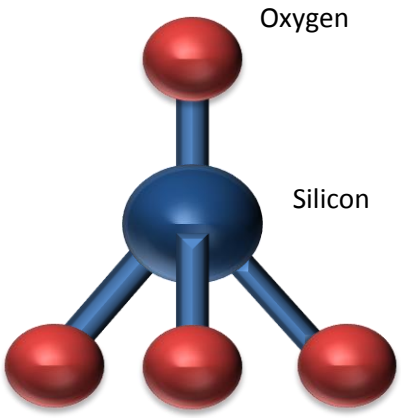

Figure 4.1: graphical representation of a SiO_4 tetrahedra

The radial distribution function (RDF) T_{ij}® tells us the number of neighbouring atoms at distances of $r \to r + dr$ from a specific atom, the formula can be written as:

$$\boldsymbol{T_{ij}(r) = 4\pi r \rho_j g(r)} \qquad \textbf{Equation 4.14}$$

where g(r) is the pair distribution function, and ρ_j is the density for atoms j. An example of a RDF plot is shown in figure 4.2 below.

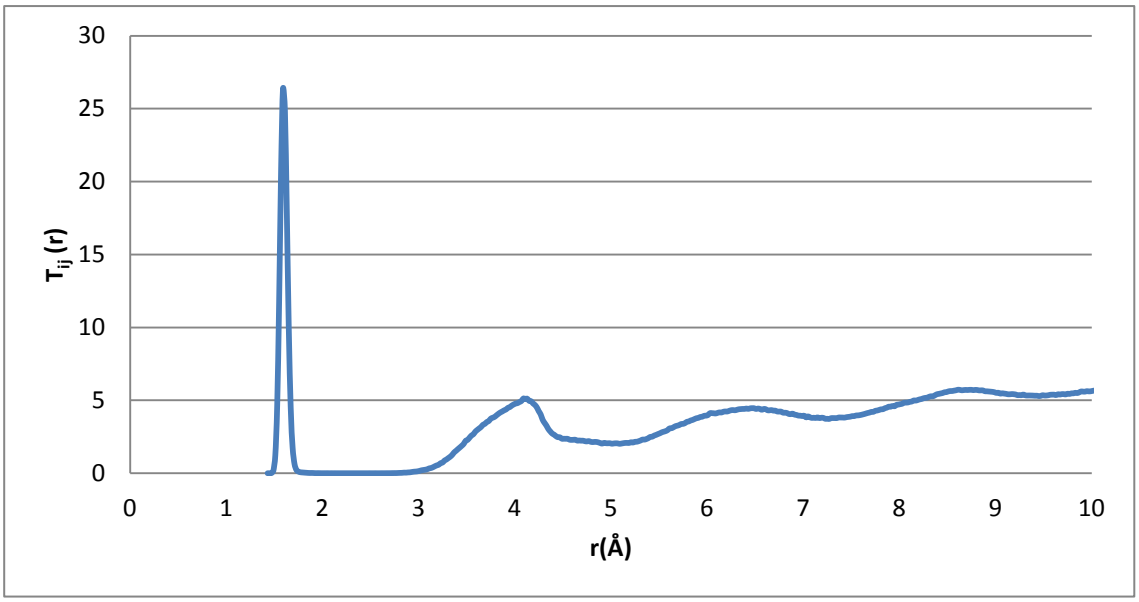

Figure 4.2: Radial Distribution Function of Si-O

When the RDF is plotted it can be seen to contain several peaks. The first peak indicates the distance r between an atom and its nearest neighbour. It can also be seen that whilst the first nearest neighbour peak is sharp other peaks are less well defined as, (due to the nature of amorphous materials). The next nearest neighbours are not always at the same distances from each other, so this can be thought of as a probability that the next nearest neighbour is located at the distance r. When the RDF is integrated:

$$\boldsymbol{N_{ij}(r_1) = \int_0^{r_1} r T_{ij}(r)\, dr} \qquad \textbf{Equation 4.15}$$

It gives the cumulative coordination number N_{ij}. This number indicates to how many other atoms j a specific atom i is surrounded by. For example in the silicon tetrahedron depicted above, the coordination number of silicon would be 4. Graphically the coordination number is found using the N_{ij} graph at specific cut off distances as shown in figure 4.3 below. From this graph at a cut off distance of ≈2Å it is clear that the Si-O coordination number is 4.0 which is as expected due to its tendency to form a tetrahedron.

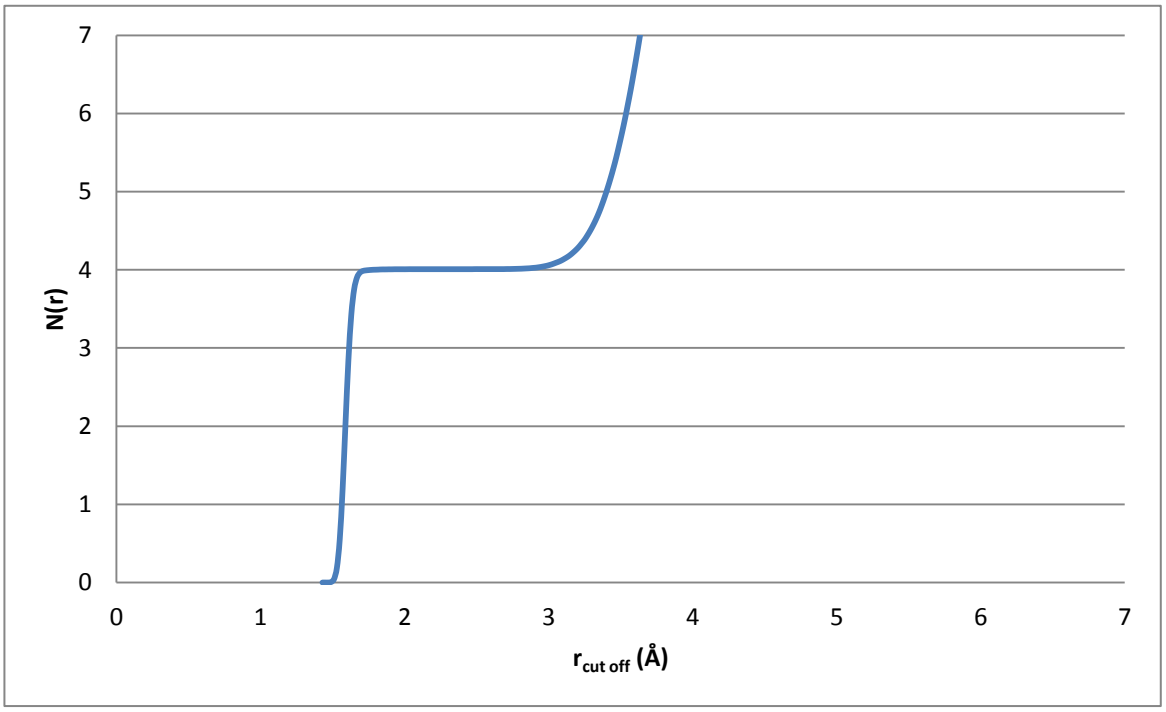

Figure 4.3: Coordination number for Si-O

4.3.2 X-ray and Neutron Diffraction

As previously mentioned X-ray scattering can give important structural information about a sample. Another technique often used for the characterisation of samples is neutron scattering. Both of these types of scattering can be calculated from the MD models and compared to published experimental data. [11] [12] [13] [14] [15]

ISAACS, the piece of software used to calculate the diffraction patterns for the models, uses the radial distribution function $T_{ij}(r)$ as in equation 4.14. This can then be used to calculate the interference function i(Q) which is measured in a diffraction experiment:

$$\boldsymbol{Qi(Q) = \int \sum_{ij} \frac{\omega_{ij}}{c_j} \left(T_{ij}(r) - 4\pi r \rho_j \right) \sin(Qr)\, dr} \qquad \textbf{Equation 4.16}$$

where ω_{ij} are weighting factors to calculate the scattering powers for atoms i and j. These weighting factors are calculated for neutron scattering as follows:

$$\boldsymbol{\omega_{ij} = \frac{(2-\delta_{ij}) c_i c_j b_i b_j}{[\bar{b}]^2}} \qquad \textbf{Equation 4.17}$$

where c_i and c_j are concentrations of atoms i and j respectively and b_i and b_j are the neutron scattering lengths for their respective atom types. For X-ray scattering:

$$\boldsymbol{\omega_{ij} = \frac{(2-\delta_{ij}) c_i c_j Z_i Z_j}{[\bar{Z}]^2}} \qquad \textbf{Equation 4.18}$$

where Z_i and Z_j are the atomic numbers for atoms i and j.

4.3.3 Glass Network Connectivity

Connectivity is of importance as it can be compared to experimental NMR data to see how the model structure compares to the real glass. As previously discussed the Q^n number is how many other structure units (for example SiO_4 tetrahedra) one structure unit is connected to. In the case of the phosphate and silicate glasses used in this experiment n is the count of bridging oxygen atoms per phosphorus or silicon respectively. An example is lithium metaphosphate, which has an O:P ratio of 3 which corresponds to a Q^n value where n=2. There is also a close relation between coordination numbers and and Q^n values. For example in a lithium metaphosphate sample where the Q^n is known to be Q^2 the P-P coordination number is also expected to be 2. Other compositions contain a mixture of Q^n values depending largely on the O:P ratio (as previously mentioned in chapter 3). In MD simulations there is often a variation in Q^n values so it is the average Q^n that is used to describe connectivity.

4.3.4 Conductivity via Diffusivity

Conductivity is a central quantity to this project and it can be estimated through diffusivity which in turn is calculated via mean squared displacement (MSD). MSD is a measurement of a particles random movement. MSD can be expressed mathematically using the following equation:

$$\langle r^2 \rangle = 6Dt + c \qquad \textbf{Equation 4.19}$$

Where D is the diffusion coefficient, t is time and c is a constant. The particles movement is affected by variables such as temperature. To observe this affect the final stage of the simulation was repeated at various temperatures increasing from 300K. An example of an MSD plot is shown in figure 4.4 below.

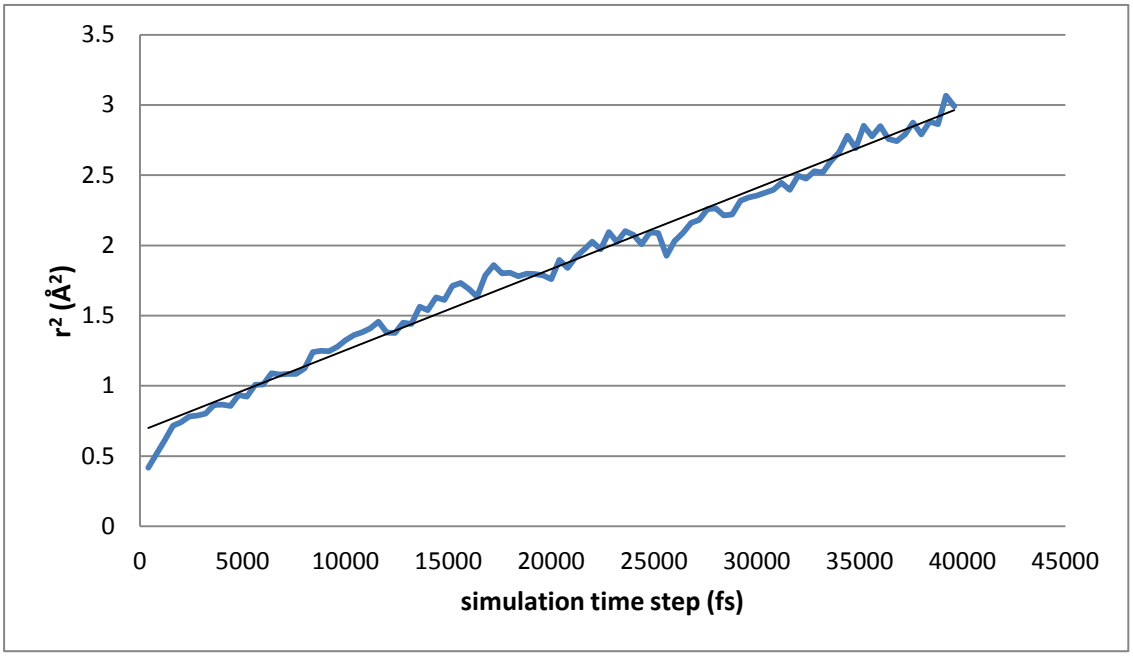

Figure 4.4: Example MSD of Lithium ions ($50Li_2O$-$50P_2O_5$ glass at 600K)

The diffusion coefficient is then calculated as the gradient of the graph and converting this into m^2s^{-1}. From this conductivity can be calculated using the Nernst-Einstein equation:

$$\boldsymbol{D^{\sigma} = \frac{\sigma k_B T}{N q^2}} \qquad \textbf{Equation 4.20}$$

this is then rearranged to:

$$\boldsymbol{\sigma = \frac{D^{\sigma} N q^2}{k_B T}} \qquad \textbf{Equation 4.21}$$

where σ is the conductivity, D^{σ} is the charge diffusion coefficient, N is the charge density, k_B is the Boltzmann constant, T is temperature and q is the charge. D (from equation 20) and D^{σ} are different diffusion coefficients, and this is discussed in more detail on page 19. As previously mentioned in chapted 3 the activation energies E_a are also calculated from the gradient of the conductivity graphs. Due to statistical fluctuations in the conductivity values from MD modelling the standard deviation in E_a values have been calculated using the following equation: [16]

$$\boldsymbol{S_m = \frac{S n^{\frac{1}{2}}}{\left[n \sum x_i^2 - (\sum x_i)^2\right]^{\frac{1}{2}}}} \qquad \textbf{Equation 4.22}$$

Where n is the number of conductivity points, and S is the standard deviation given by:

$$\boldsymbol{S = \left[\frac{1}{n-2} \sum (y_i - m x_i - c)^2\right]^{\frac{1}{2}}} \qquad \textbf{Equation 4.23}$$

4.4 MD Model of $33Li_2O$-$67SiO_2$ Glass

4.4.1 Nearest Neighbour Distance, Coordination Number and Connectivity

In Figure 4.5 below the SiO_4 tetrahedra are represented in blue with lithium showing as isolated green spheres. The nearest neighbour distances and coordination numbers have been calculated and T_{ij} are shown in table 4.4 below.

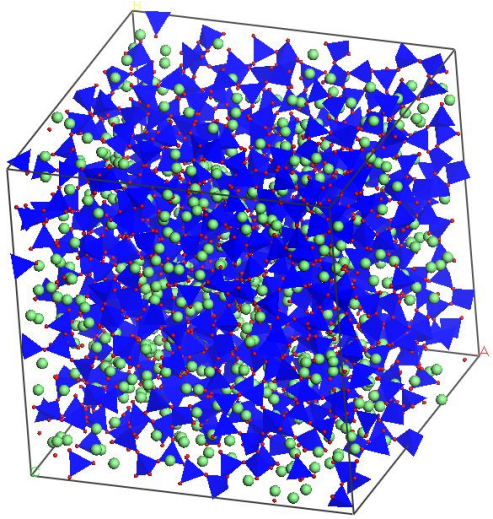

Figure 4.5: Image of $33Li_2O$-$67SiO_2$ glass model

Table 4.4: nearest neighbour distances and coordination numbers for $33Li_2O$-$67SiO_2$ glass model

Neighbour Type	Si-O	Li-O	O-O	Si-Si	Si-Li	Li-Li
Neighbour Distance (Å)	1.59	1.95	2.59	3.13	3.15	2.53
Coordination number N_{ij}	4.00	3.62	4.88	3.03	4.98	5.87
r_{cutoff} (Å)	2.00	2.61	2.85	3.40	4.00	4.15

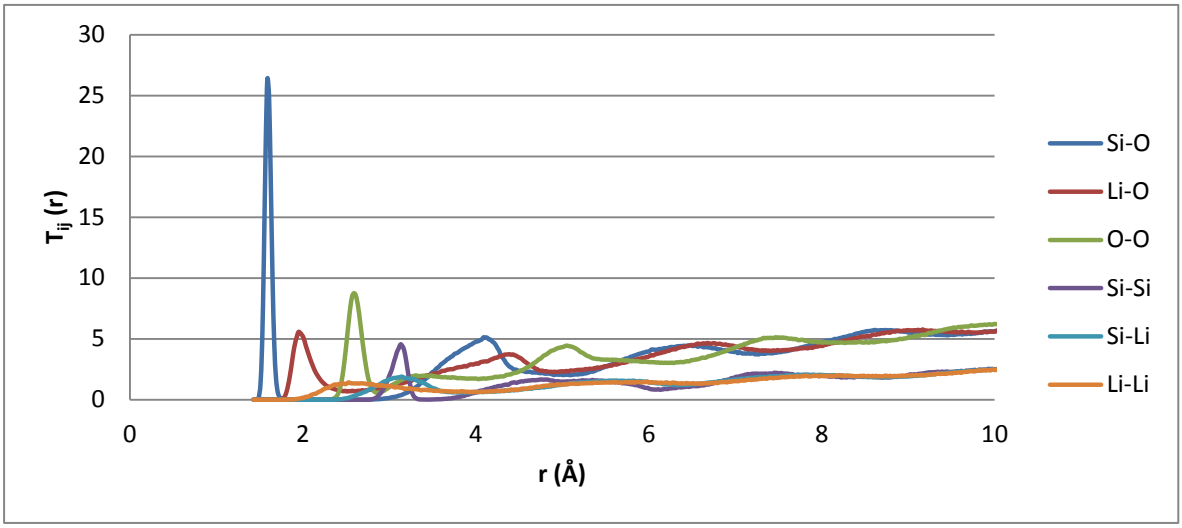

Figure 4.6: graphical representation of nearest neighbour distances for $33Li_2O$-$67SiO_2$ glass model

As expected Si-O has a coordination of 4.00 due to SiO_4 tetrahedra. It can be seen that the nearest neighbour distances for Si-O are 1.59Å. It can also be seen from the Si-Si distances that the distance between each neighbouring SiO_4 tetrahedra is 3.13Å. For Si-Si the coordination number is 3.03 suggesting that, on average, each SiO_4 tetrahedron is connected to three other SiO_4 tetrahedra. This will be examined again with the Q^n analysis.

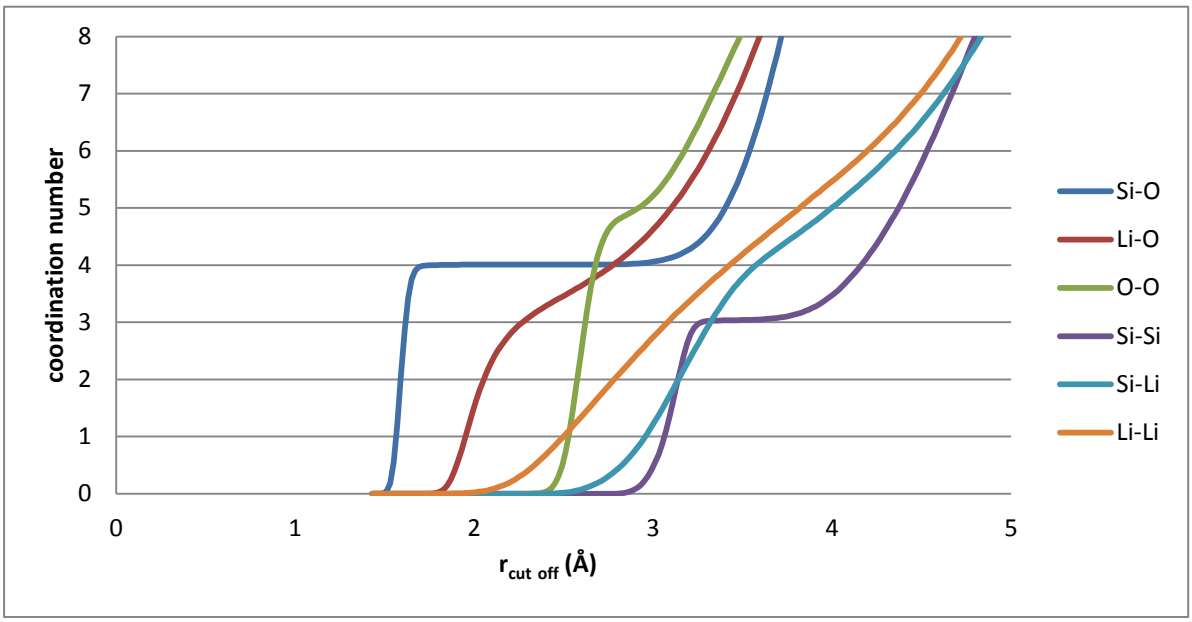

Figure 4.7 :A graphical representation of coordination numbers and cut off distances for $33Li_2O$-$67SiO_2$ model

Figure 4.7 above shows that some coordination numbers have well defined values (Si-O for example) others have poorly defined values. This suggests that while some elements such as network formers (Si) form well defined local structures (such as SiO_4 tetrahedra), other elements such as network modifiers (Li) coordination's have a range of possible coordinations. This is expected particularly in amorphous materials.

Below is table 4.5 showing the Q^n connectivity of the model created which will be compared to expected values for its composition. The table shows that there is a wide spread in the Q^n values which is common in MD model simulations. However, the average value for connectivity is 3.03 which is as expected values and matches the Si-Si coordination number as previously mentioned

Table 4.5: A table to show Q^n analysis of $33Li_2O$-$67SiO_2$ glass model

Q^n	0	1	2	3	4
%	0.448	3.582	20.013	44.455	31.055

4.4.2 X-ray and Neutron Diffraction

Figure 4.8 and 4.9 are graphs comparing X-ray and Neutron diffraction data calculated from the glass models in this study and published experimental results. Comparing the graphs of x-ray diffraction above it can be seen that whilst the results are not identical the main features are shared. Peaks are in similar locations and of similar intensity and broadness. This is a good indication that the model of the glass is reasonable and has a similar structure to a real $33Li_2O$-$67SiO_2$ glass.

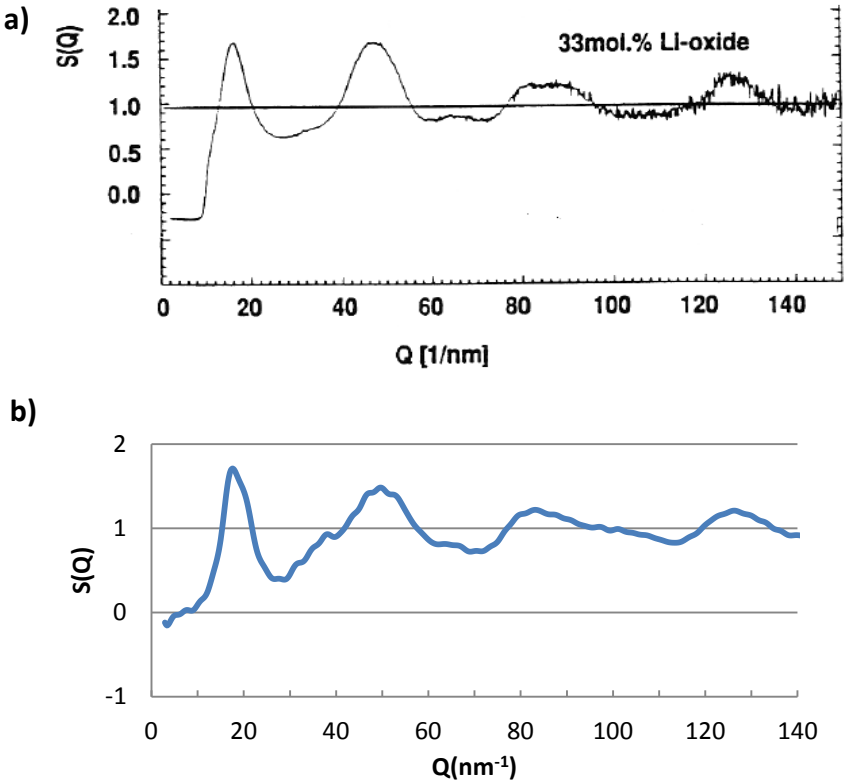

Figure 4.8: X-ray diffraction data comparison between a) experimental [13] and b) modelling (this study)

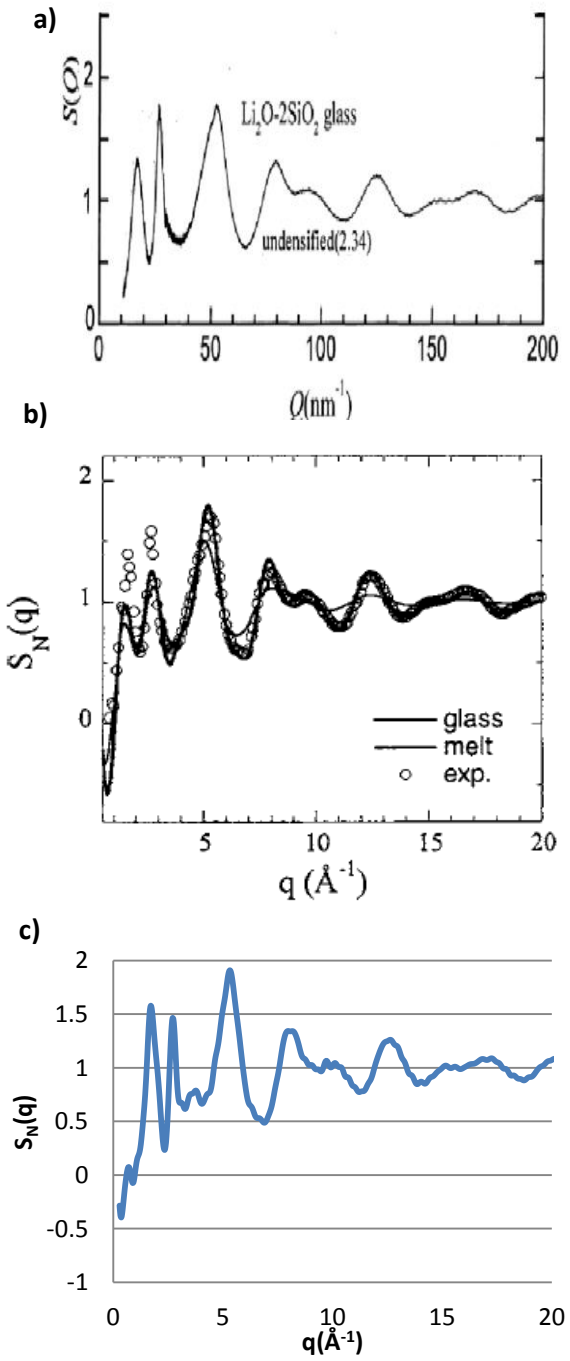

Figure 4.9:Neutron diffraction data comparison between experimental a) [12] b) [11] and c) modelling (this study)

Again comparing the neutron diffraction graphs above it can be seen that all graphs share a resemblance in peak location, intensity and broadness. However the results from this study have a feature (extra 'bump') found between the 2nd and 3rd peaks which is absent from the experimental data. Nevertheless the good likeness between the modelling and experimental results is an indication that the model is reasonable.

4.4.3 Conductivity

Below is table 4.6 and figure 4.10 showing the conductivity values obtained for the silicate glass model calculated from the particle diffusion coefficient D.

Table 4.6: conductivity values for $33Li_2O$-$67SiO_2$ glass model

1000K/T	$Log_{10}(\sigma)$
3.333	-2.437
2.857	-2.411
2.500	-2.085
2.222	-1.957
2.000	-1.878
1.818	-1.567
1.667	-1.409
1.429	-1.121
1.250	-0.968

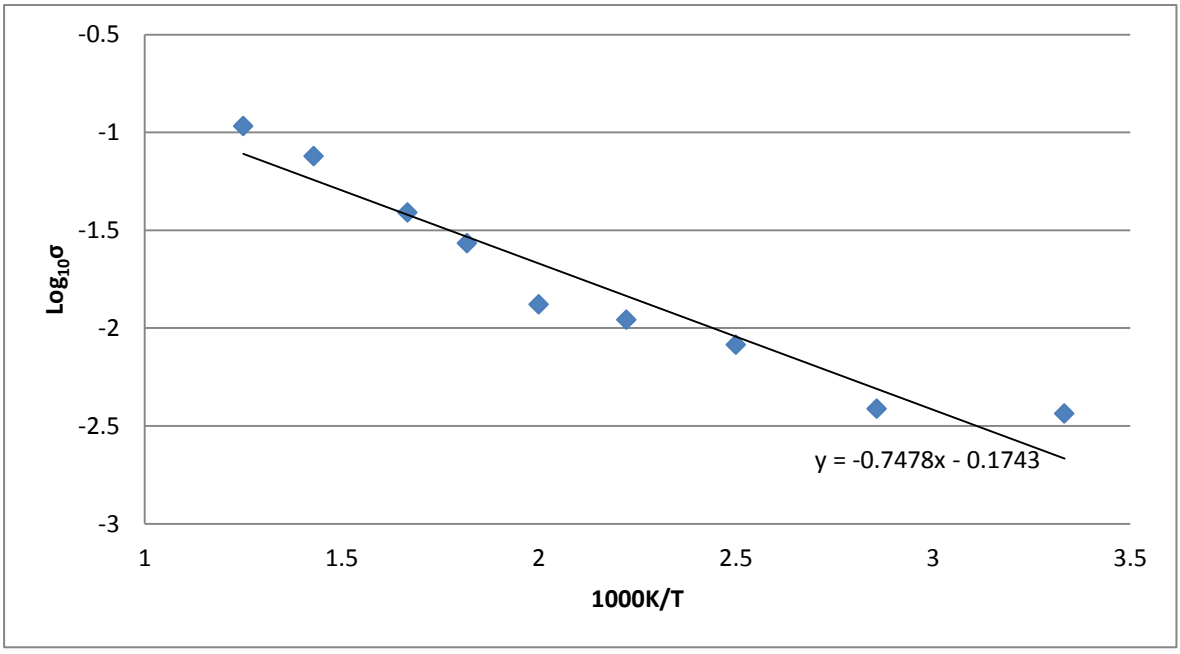

Figure 4.10: Temperature dependant conductivity plots for $33Li_2O$-$67SiO_2$ glass model

The results show that an increased temperature corresponds to an increased conductivity value which is expected. However, the values obtained from the model are several orders of magnitude (≈6 orders at room temperature) higher than values obtained experimentally. This phenomenon is often observed when modelling conductivity. [17] One reason for this is the miscalculation of mobile ion density n. In this method of modelling it is assumed that all lithium ions are equally mobile and can contribute to conductivity (as the strong electrolyte model previously mentioned suggests). However, in reality not all ions are mobile and therefore some ions do not contribute to conductivity (as the weak electrolyte model previously mentioned suggests). [18] This results in an overestimation of the conductivity in a model. There are other methods to calculate the conductivity from molecular dynamics which give more satisfactory results such as the "non-equilibrium" method, [17] however, altering the modelling code to use this method was not within the scope of this project and so the method based on diffusivity was used. Another reason for higher conductivity values is that the program calculated the particle diffusion coefficient D and the Nernst-Einstein equation uses the charge diffusion coefficient D^{σ}. Typically D is lower than D^{σ}. The ratio between D and D^{σ} is known as the Haven ratio (discussed in chapter 1) which for phosphate glasses is typically 0.3 – 0.6. [18] The graph also shows fluctuations in conductivity values rather than a strong linear relationship as would be expected. A possible explanation for this is that the model is relatively small and the simulation over a short amount of time. This means that over the short period of time in which the simulation is run only a small fraction of ions might have moved and this can cause statistical fluctuations in conductivity values. A simple way to test this would be to increase model size and rerun the simulation over a longer period of time and recalculate the conductivity. From the gradient of the graph E_a was calculated to be 14.32 $kJmol^{-1}$ ±19.6% which is significantly lower than the experimental value of 53.98 $kJmol^{-1}$ obtained in chapter 3. This is expected due to the significantly higher conductivities in the model compared to the real glass. Errors were calculated using equations 4.23 and 4.24 and are large due to the large statistical fluctuations in model conductivity results.

4.5 MD Model of $50Li_2O$-$50P_2O_5$ Glass

4.5.1 Nearest Neighbour Distance, Coordination Number and Connectivity

In figure 4.11 above the PO_4 tetrahedra are represented in pink with lithium showing as isolated green spheres. The nearest neighbour distances and coordination numbers have been calculated and tabulated along with a graphical representation shown below.

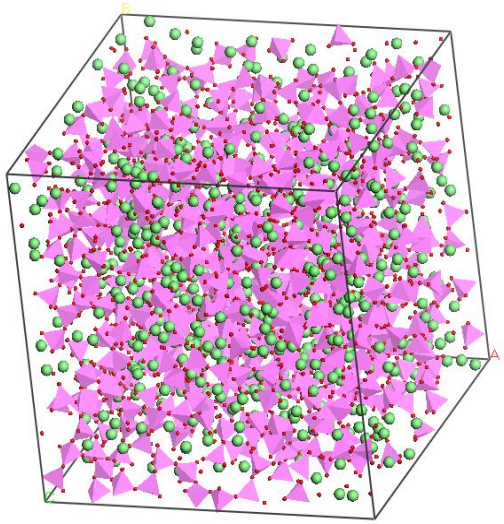

Figure 4.11: image of $50Li_2O$-$50P_2O_5$ glass model

Table 4.7: nearest neighbour distances and coordination numbers for $50Li_2O$-$50P_2O_5$ glass model

Neighbour Type	P-O	Li-O	O-O	P-P	P-Li	Li-Li
Neighbour Distance (Å)	1.45	1.99	2.43	2.95	3.21	2.63
Coordination number N_{ij}	4.00	3.67	4.02	2.00	4.00	3.61
r_{cutoff} (Å)	2.00	2.60	2.65	3.25	3.75	3.81

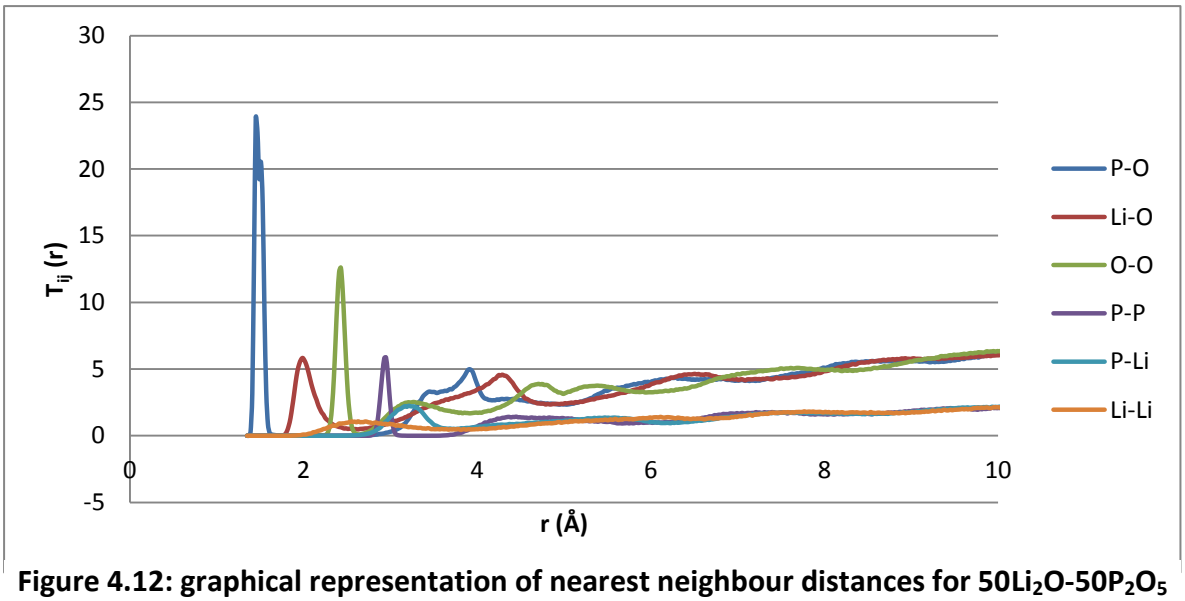

Figure 4.12: graphical representation of nearest neighbour distances for $50Li_2O$-$50P_2O_5$ model

Results show that the P-O coordination number is 4.00 which is as expected due to the formation of PO_4 tetrahedra. Table 4.7 and figure 4.12 shows that the bond lengths between phosphorus and each of the four oxygen atoms in the PO_4 tetrahedra is 1.45Å. The P-P neighbour distance of 2.95Å represents the distance between phosphorus in neighbouring tetrahedra.

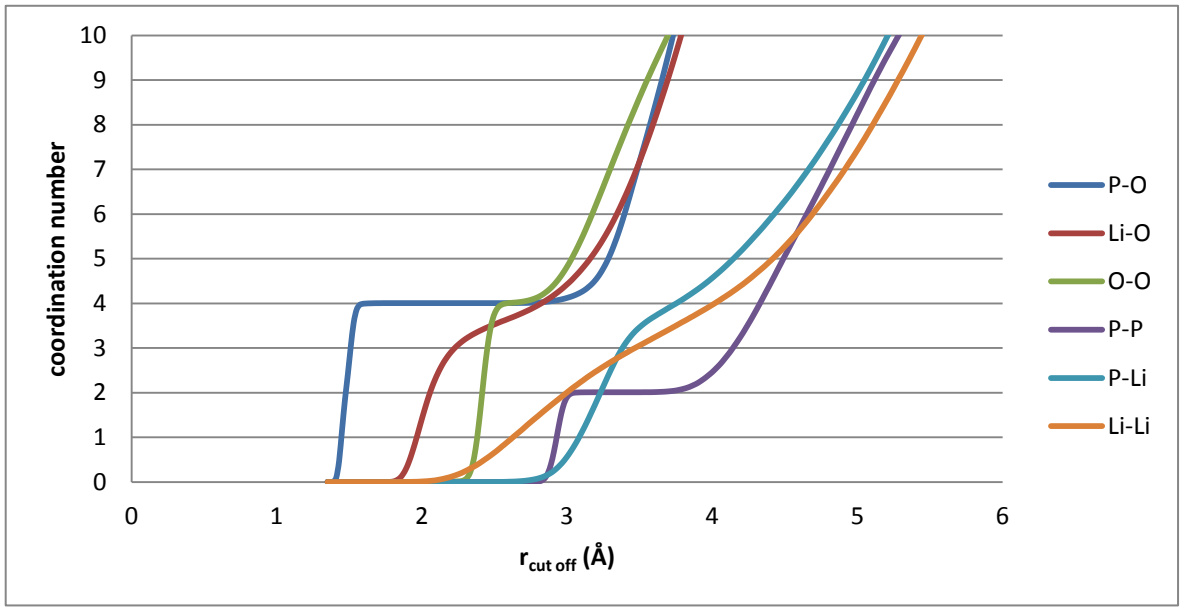

Figure 4.13: A graphical representation of coordination numbers and cut off distances for $50Li_2O$-$50P_2O_5$ model

Figure 4.13 above shows the coordination numbers for the lithium metaphosphate model. Again it shows that whilst some coordination numbers such as P-O and P-P have very well defined values others have poorly defined values. The P-P coordination number is 2 which to be expected as previously discussed in the characterisation chapter. For a lithium metaphosphate glass the connectivity of PO_4 tetrahedra is 2, again this will be confirmed in the Q^n analysis of this model.

Table 4.8: A table to show Qn analysis of $50Li_2O$-$50P_2O$ glass model

Q^n	0	1	2	3	4
%	1.333	20.333	56	20.667	1.667

Table 4.8 shows that there is a wide spread of connectivity values in the model which would not be expected experimentally in a metaphosphate glass. As previously discussed $50Li_2O$-$50P_2O_5$ glass is expected to contain 100% Q^2 connectivity, and the experimental NMR data found in chapter 2 shows the 50% sample contained 99.59% Q^2. This phenomena of a broad distribution of Q^n values in models of phosphate glasses has been previously observed in literature. [19] [20] The best that can be expected is that the model has an average Q^2 connectivity as this model does.

4.5.2 X-ray and Neutron Diffraction

Figure 4.14 below shows a comparison between x-ray diffraction calculated from the model in this study and published experimental results. Comparing the x-ray diffraction it can be seen that all main features are shared. Peaks are in similar locations and have similar intensities. However, it can also be seen that the second peak from the model is less defined than in S. Beaufils 2003 experimental data. Despite this, due to similarities in the graphs, it can be seen as a reasonable

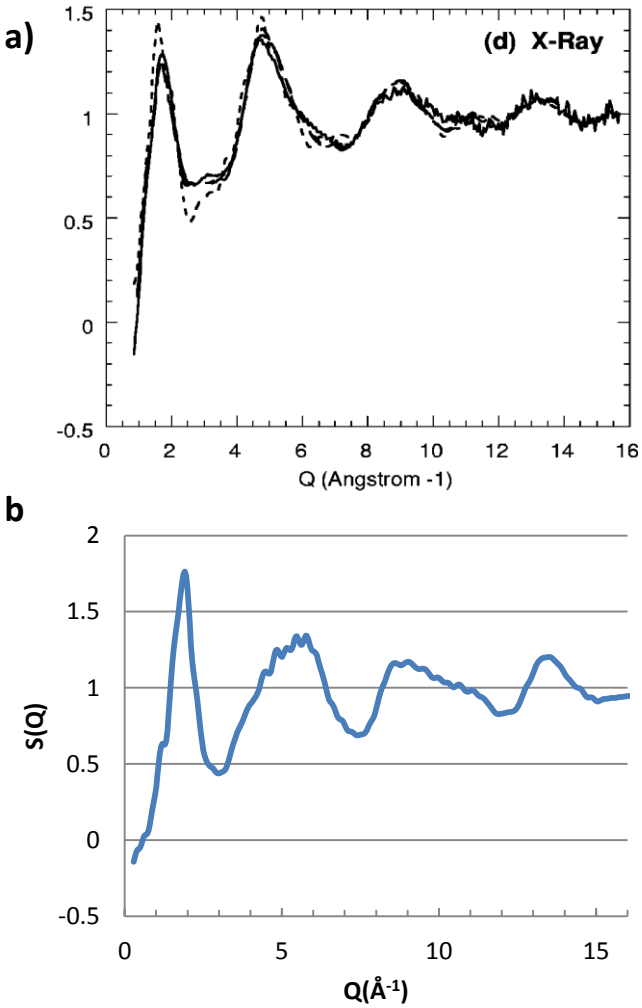

Figure 4.14: X-ray diffraction data comparison between a) experimental [14] and b) modelling (this study)

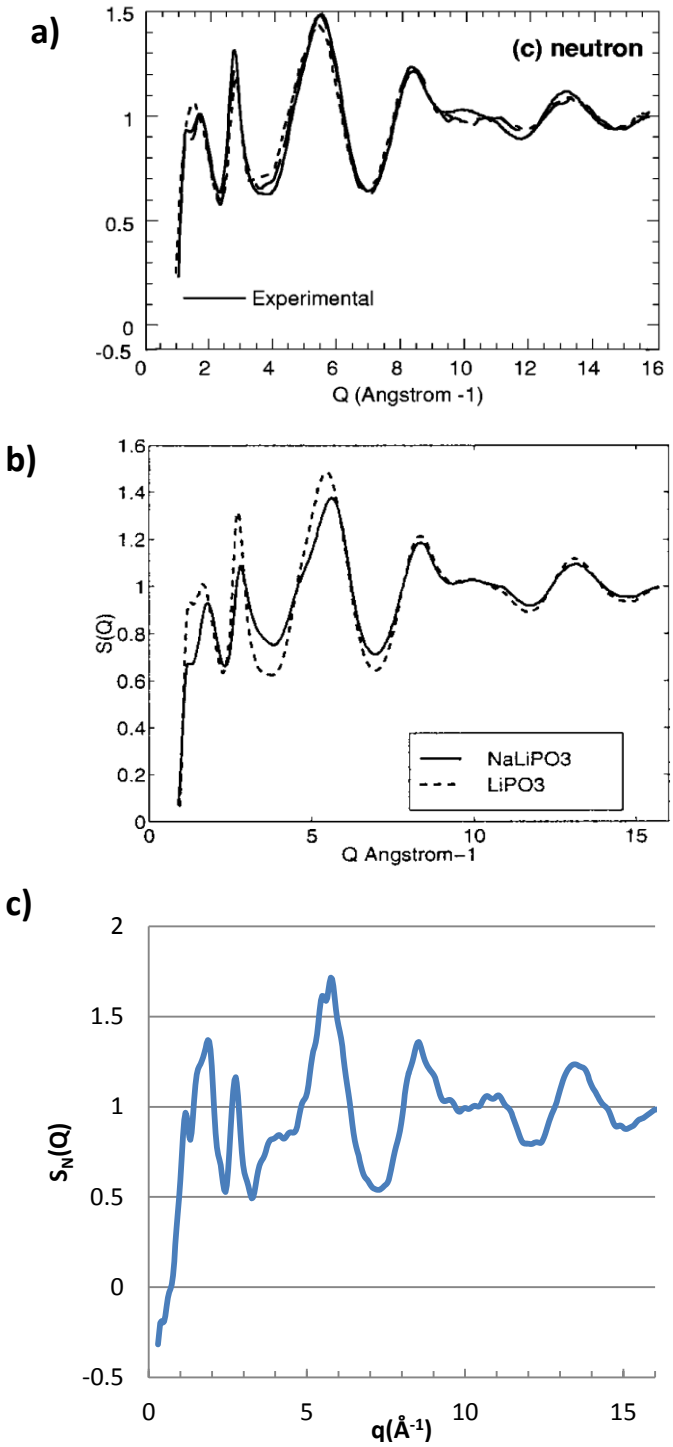

Figure 4.15:Neutron diffraction data comparison between experimental a) [14] b) [15]and c) modelling (this study)

Figure 4.15 shows a comparison between the Neutron diffraction patterns from this study and published experimental data. Again, comparing the neutron diffraction graphs above, it can be seen that all graphs share all major features (peak location, intensities and broadness). However, the results from the model seem to have an extra feature in the

form of a 'bump' in between the 2nd and 3rd peaks. Due to the good resemblance between the diffraction pattern from the model and experiment the models structure can again be thought of as reasonable.

4.5.3 Conductivity

Table 4.9 and figure 4.16 show the conductivity values for the phosphate glass model calculated from the diffusion coefficient D. The data below again shows that an increased temperature corresponds to an increased conductivity which is as expected. The 900K point has been included (red plot) in the graph to show the increase in conductivity past T_g which does not follow the Arrhenius equation. It also shows fluctuations in conductivity rather than a strong linear relationship, the reasoning behind this is put down to the relatively small model and simulation running time. Conductivity values are orders of magnitude higher than experiment results and possible reasons for this were discussed for the $33Li_2O$-$67SiO_2$ model above. The value of E_a was calculated from the gradient of the graph to be 10.70 $kJmol^{-1}$ ±15.2%. This gives the lithium metaphosphate a lower activation than the lithium disilicate glass which was not found experimentally in chapter 3. Again the activation energy is significantly smaller in the model than the real glass.

Table 4.9: conductivity values for $50Li_2O$-$50P_2O_5$ glass model

1000K/T	$Log_{10}(\sigma)$
3.333	-2.709
3.077	-2.567
2.353	-2.198
2.500	-2.473
2.222	-2.125
1.667	-1.752
1.111	-0.990

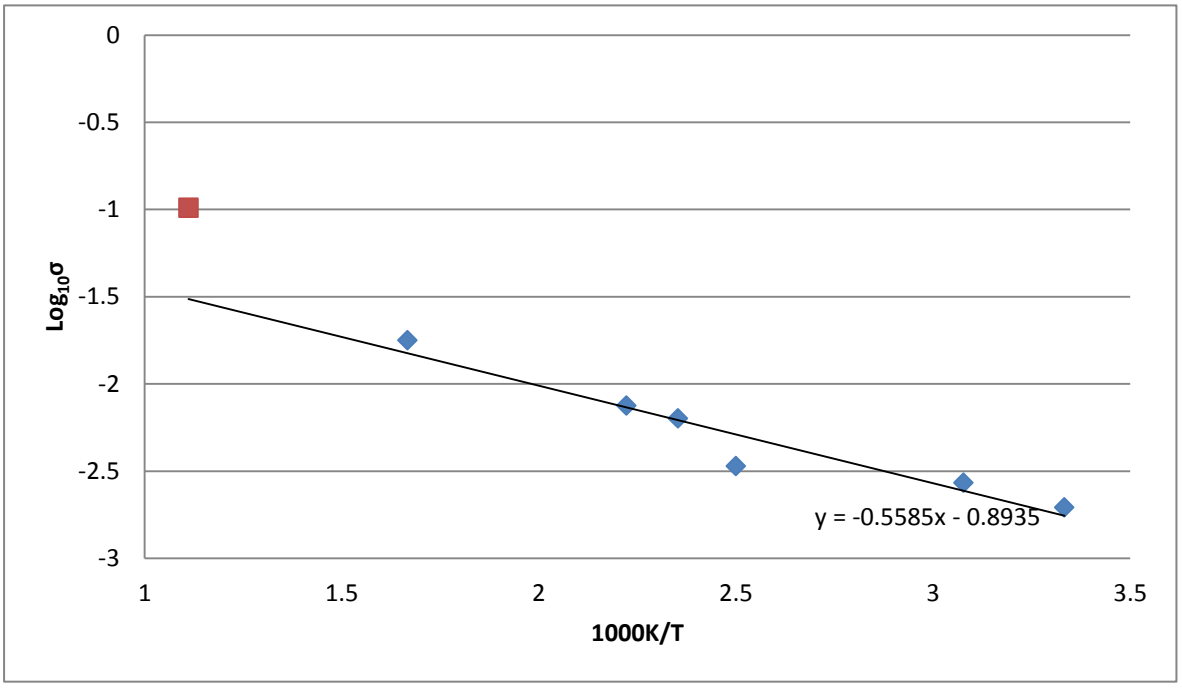

Figure 4.16: Temperature dependant conductivity plots for $50Li_2O$-$50P_2O_5$ glass model

The simulations to calculate conductivity in the $50Li_2O$-$50P_2O_5$ model were repeated using 400000 timesteps in an attempt to reduce the statistical error associated with short simulations. Table 4.10 and figure 4.17 below show the results. It can be seen that the longer simulations give reduced conductivity estimates, which are marginally closer to experimental results. However, the fluctuations in conductivity and lack of a strong linear correlation remain. E_a was recalculated to 11.53 $kJmol^{-1}$ ±27.81% whilst the slight increase in activation energy slightly reduces the disagreement with experimental result the standard deviation has not decreased, so there remains uncertainty in this estimate.

Table 4.10: conductivity values for $50Li_2O$-$50P_2O_5$ glass model (extended run time)

1000K/T	$Log_{10}(\sigma)$
3.333	-2.862
3.077	-2.912
2.353	-2.657
2.500	-2.669
2.222	-2.419
1.667	-1.821

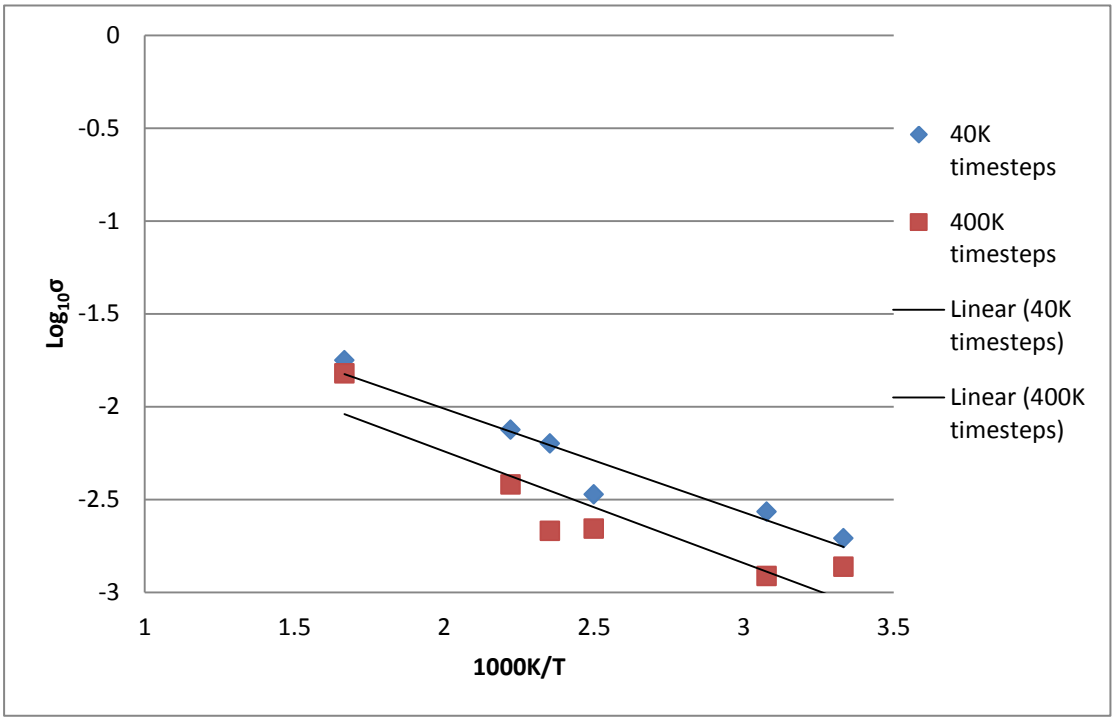

Figure 4.17: Temperature dependant conductivity plots for $50Li_2O$-$50P_2O_5$ glass model (extended run time)

4.6 MD Model of $37.5Li_2O$-$20Fe_2O_3$-$5Nb_2O_5$-$37.5P_2O_5$ Glass

4.6.1 Nearest Neighbour Distance, Coordination Number and Connectivity

In figure 4.18 below the PO_4 tetrahedra are represented in pink, FeO_4 tetrahedra in yellow, niobium polyhedra in dark green and lithium showing as isolated green spheres. The nearest neighbour distances and coordination numbers have been calculated and tabulated along with T_{ij} (r) shown below. The results for nearest neighbours among Li, P and O and other nearest neighbour types have been separated so a direct comparison can be made to the lithium metaphosphate glass model previously presented.

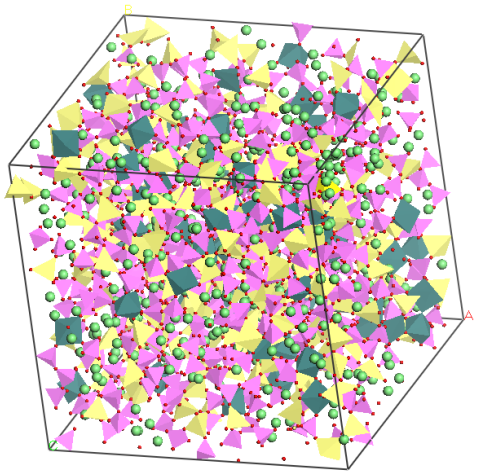

Figure 4.18: image of $37.5Li_2O$-$20Fe_2O_3$-$5Nb_2O_5$-$37.5P_2O_5$ glass model

Table 4.11: nearest neighbour distances and coordination numbers for $37.5Li_2O$-$20Fe_2O_3$-$5Nb_2O_5$-$37.5P_2O_5$ glass model

Neighbour Type	P-O	Li-O	O-O	P-P	P-Li	Li-Li
Neighbour Distance (Å)	1.47	1.95	2.41	2.93	3.13	2.49
Coordination number N_{ij}	3.87	3.47	3.08	0.66	2.93	2.84
r_{cutoff} (Å)	2.00	2.60	2.63	3.23	3.71	3.89

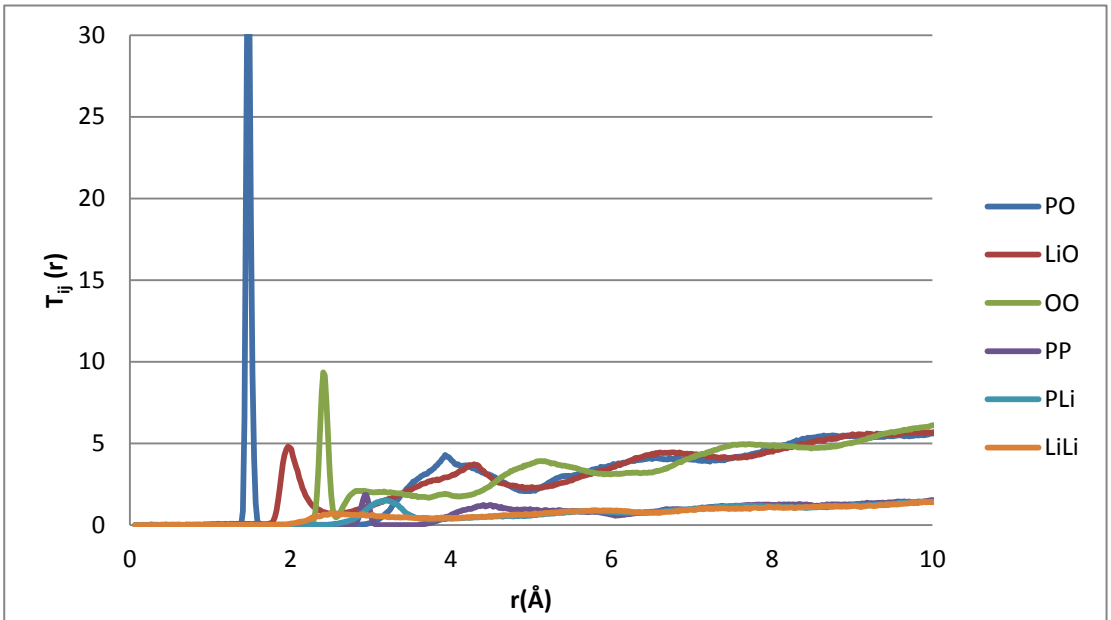

Figure 4.19: graphical representation of nearest neighbour distances for L-P-O in $37.5Li_2O$-$20Fe_2O_3$-$5Nb_2O_5$-$37.5P_2O_5$ model

Table 4.11 and figure 4.19 above shows that the nearest neighbour distances for P-O is 1.47Å, this means that the size of the PO_4 tetrahedra is similar to that in the $50Li_2O$-$50P_2O_5$ model (1.45Å) which is to be expected. The P-P neighbour distance of 2.93Å is also close to that of the $50Li_2O$-$50P_2O_5$ model (2.95Å). Next figure 4.20 shows the coordination numbers for these neighbour types.

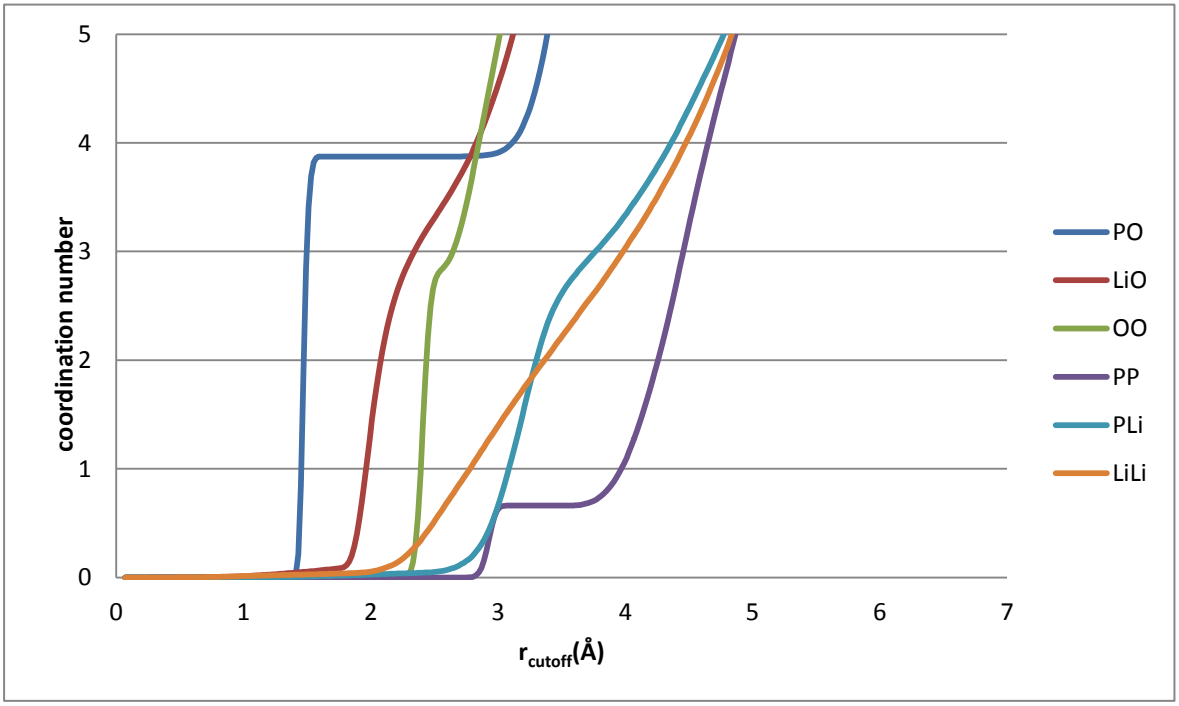

Figure 4.20: graphical representation of coordination numbers and cut off distances for L-P-O in $37.5Li_2O$-$20Fe_2O_3$-$5Nb_2O_5$-$37.5P_2O_5$ model

When looking at coordination numbers distinct differences between this model and the metaphosphate model appear. The P-O coordination number is 3.87 instead of the 4 that would be expected due to the formation of PO_4 tetrahedra. This indicates that the model is not an accurate representation of the physical glass. This may be down to the addition of other elements Fe and Nb, making this a more complex model. Some alterations were made in an attempt to improve the model, including altering box size (a reduction of around 7% total volume) and changing the phosphorus repulsion interatomic potential parameter A (by ±5%) to alter binding. When simulations were repeated the changes seemed to have no effect on P-O coordination numbers and therefore the original model has been used in this study's analysis as a "first attempt" model. Improvement on this model is still necessary for future work. Another difference is that the P-P coordination number is 0.66 which is much less than 2 seen in the lithium metaphosphate. This shows the connectivity of the phosphate glass network has been reduced as discussed later.

The coordination numbers for Fe-O and Nb-O are 4.31 and 5.83 respectively. Unlike phosphorus which should always have a coordination number of 4, iron and niobium are ions which are capable of having a range of coordination numbers in different materials.

Table 4.12: The remaining nearest neighbour distances and coordination numbers for $37.5Li_2O$-$20Fe_2O_3$-$5Nb_2O_5$-$37.5P_2O_5$ glass model

Neighbour Type	Fe-O	Nb-O	Fe-Fe	Li-Fe	Li-Nb	P-Fe	P-Nb	Nb-Nb
Neighbour Distance (Å)	1.89	1.95	3.51	3.09	3.33	3.31	3.39	3.77
Coordination number N_{ij}	4.31	5.83	0.99	1.32	0.27	1.74	0.50	0.66
r_{cutoff} (Å)	2.63	2.25	3.91	3.83	3.79	3.61	3.67	4.23

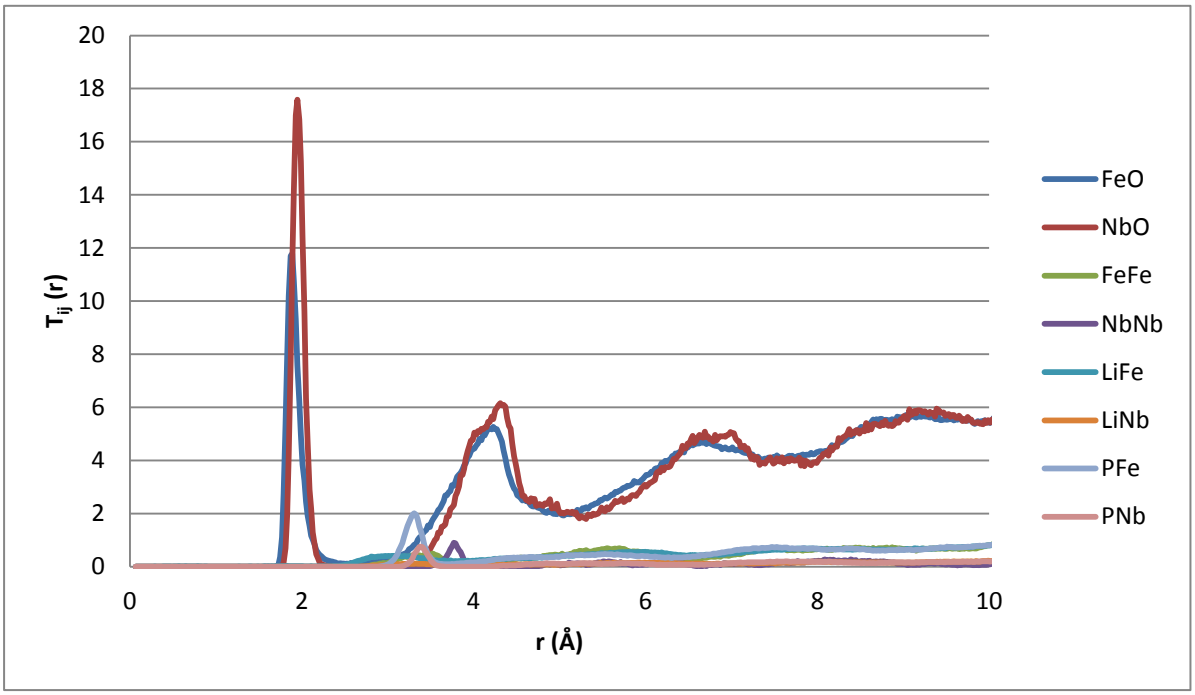

Figure 4.21: graphical representation of the remaining nearest neighbour distances in $37.5Li_2O$-$20Fe_2O_3$-$5Nb_2O_5$-$37.5P_2O_5$ model

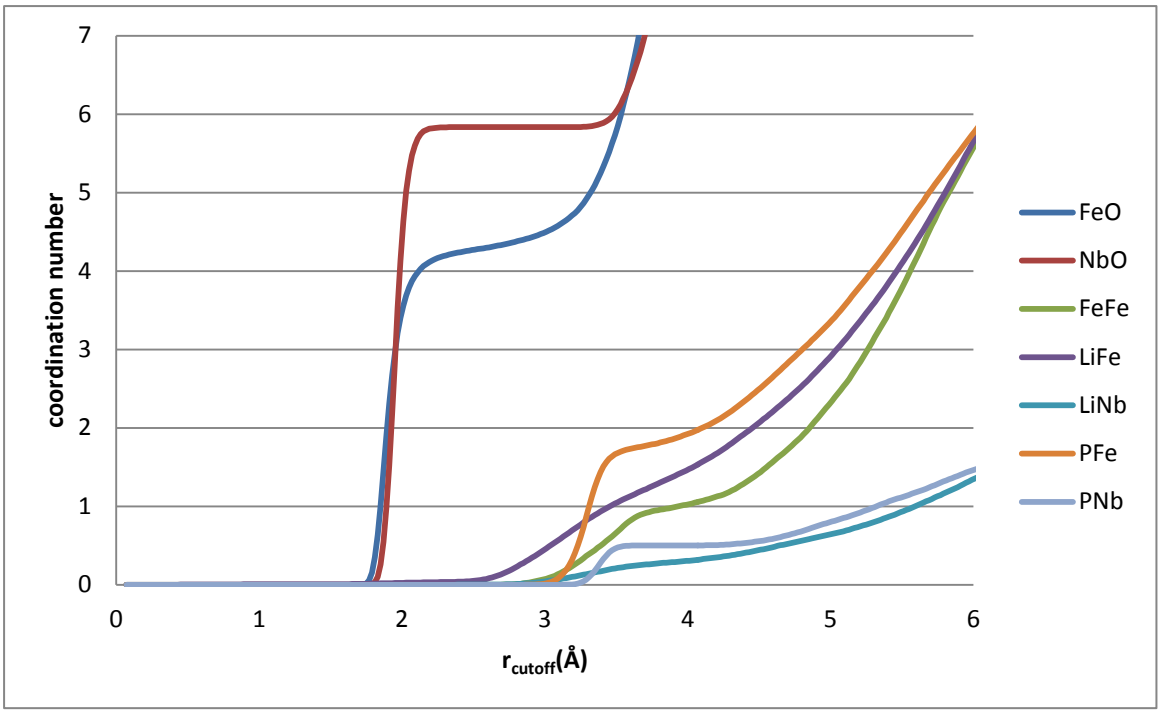

Figure 4.22: graphical representation of the remaining coordination numbers and cut off distances in $37.5Li_2O$-$20Fe_2O_3$-$5Nb_2O_5$-$37.5P_2O_5$ model

The next step would be to confirm the Q^n connectivity of the model, however, this model had 3060 atoms and the precompiled programme software used for this analysis has a built in limit of 3000 atoms and therefore this could not be done. However, the expected connectivity Q^n can be calculated using the O:P ratio of the model where a ratio of 4.0 or greater means n=0. For the model composition: $37.5Li_2O$-$20Fe_2O_3$-$5Nb_2O_5$-$37.5P_2O_5$ the O:P ratio is 4.467 and this ratio corresponds to a connectivity of n=0. It can be seen in table 4.12 above that the P-P coordination is 0.662 not 0. This occurs due to having less P in the model and having Fe which was not present in the lithium metaphosphate model. Since Fe has a coordination of approximately 4 we can consider Fe as a network former and then the O:(P+Fe) ratio = 2.91 which corresponds to a connectivity mixture of Q^2 and Q^3. When adding the P-P and P-Fe coordination numbers, 0.66 and 1.74 respectively we get a value of 2.4 which corresponds to a mixture of Q^2 and Q^3.

4.6.2 Conductivity

Below is table 4.13 and figure 4.23 showing the conductivity values for the $37.5Li_2O$-$20Fe_2O_3$-$5Nb_2O_5$-$37.5P_2O_5$ glass model. The data from table 4.13 and figure 4.23 shows that whilst a general trend of increased temperature corresponding to an increase in conductivity is observed there are two points (450K and 550K) in which conductivity decreases. This again is likely due to a statistical factor caused by having a small sample and being run over a short period of time. However, when comparing the conductivity results of all three models it can be seen that the $33Li_2O$-$67SiO_2$ model and the $50Li_2O$-$50P_2O_5$ model have similar conductivity values, whilst the $37.5Li_2O$-$20Fe_2O_3$-$5Nb_2O_5$-$37.5P_2O_5$ model has lower conductivity values. This pattern was also observed in this study's experimental results, suggesting that whilst the absolute conductivity values for a glass are not accurately calculated via this modelling method, it may be used as an indicator of whether a glass would have higher or lower conductivity values compared to another sample. E_a for this model was calculated to be 9.6822 $kJmol^{-1}$ ±15.1% which is again significantly lower than the experimental value of 64.86 $kJmol^{-1}$. However, when comparing the numerical order in which the three samples activation energies are found it can be seen that the $37.5Li_2O$-$20Fe_2O_3$-$5Nb_2O_5$-$37.5P_2O_5$ model has the lowest whilst

the Li silicate has the highest. This is in the opposite order to the activation energies found experimentally. Reasons for this may be due to the large uncertainties in the E_a calculations.

Table 4.13: conductivity values for $37.5Li_2O$-$20Fe_2O_3$-$5Nb_2O_5$-$37.5P_2O_5$ glass model

1000K/T	$Log_{10}(\sigma)$
3.333	-2.807
2.857	-2.486
2.500	-2.191
2.222	-2.218
2.000	-2.046
1.818	-2.155
1.667	-1.819

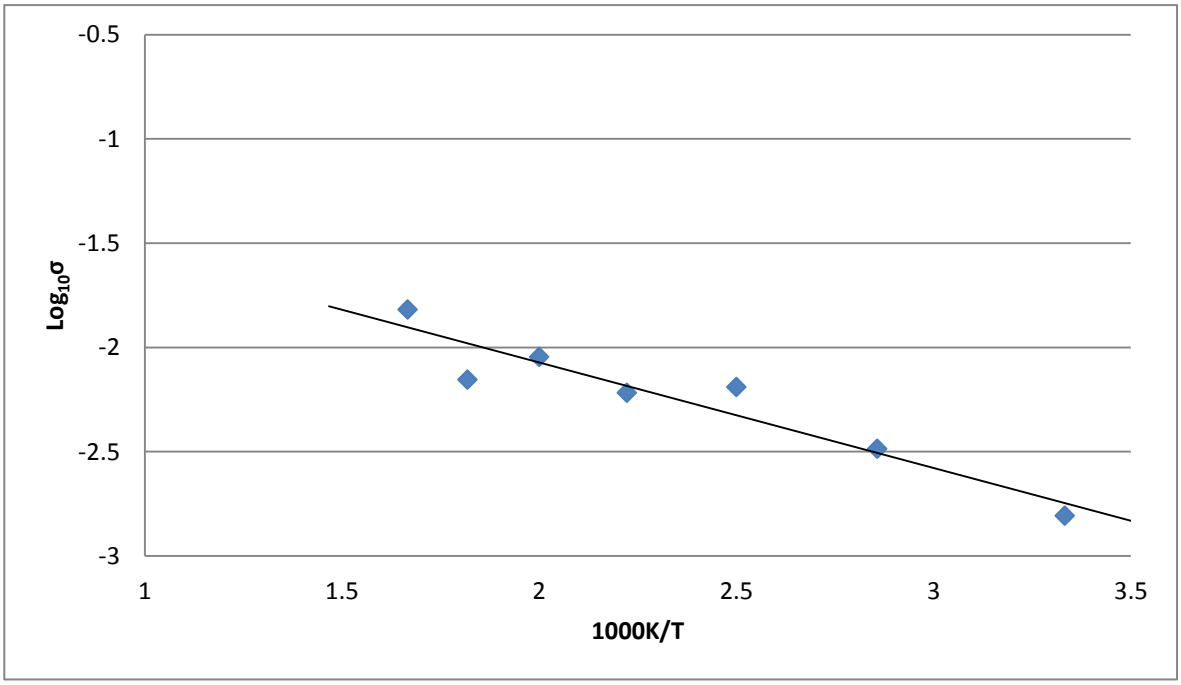

Figure 4.23: Temperature dependant conductivity plots for $37.5Li_2O$-$20Fe_2O_3$-$5Nb_2O_5$-$37.5P_2O_5$ glass model

[1] D. Frenkel and B. Smit, Understanding Molecular Simulation: From Algorithms to Applications, Academic Press, 2002.

[2] C. Saluena, “Molecular dynamics algorithm enforcing energy conservation for microcanonical cimulations,” *Physical Review,* vol. 89, no. 5, pp. 1539-3755, 2014.

[3] W. Smith and T. Forester, “DL_POLY_2.0: A general-purpose parallel molecular dynamics simulation package,” *Journal of Molecular Graphics,* vol. 14, pp. 136-141, 1996.

[4] W. Smith, T. Forester and I. Todorov, The DL_POLY_2 User Manual, STFC Daresbury Laboratory, 2008.

[5] D. Teter, *private communication,* 2004.

[6] A. Leach, Molecular Modelling: Principles and Applications, Harlow: Peason Education Limited, 1996.

[7] E. B. Clark, R. N. Mead and G. Mountjoy, “A molecular dynamics model of the atomic structure of Tb metaphosphate glass (Tb2O3)0.25(P2O5)0.75,” *Journal of Physics: Condensed Matter,* vol. 18, pp. 6815-6826, 2006.

[8] G. El Damrawi, “Dependence of properties on structural units in Li2O-Al2O3-SiO2 glasses,” *Physics and Chemistry of glasses,* vol. 42, no. 2, pp. 116-120, 2001.

[9] S. L. Roux and V. Petkov, “ISAACS - interactive structure analysis of amorphous and crystalline systems,” *Journal of Applied Crystallography,* vol. 43, pp. 181-185, 2010.

[10] S. Elliott, Physics of Amorphous Materials second edition, Longman Scientific and Technical, 1990.

[11] J. Du and L. R. Corrales, “Structure, dynamics, and electronic properties of lithium disilicate melt and glass,” *The Journal of Chemical Physics,* vol. 125, p. 114702, 2006.

[12] N. Kitamura, K. Fukumi, H. Mizoguchi, M. Makihara, A. Higuchi, N. Ohno and T. Fukunaga, “High pressure densification of lithium silicate glasses,” *Journal of Non-Crystalline Solids,* vol. 274, pp. 244-248, 2000.

[13] H. Uhlig, M. Hoffmann, H. Lamparter, F. Aldinger, R. Bellissent and S. Steeb, “Short-rang and Medium-range Order in Lithium Silicate Glasses, Part 1: Diffraction Experiments and Results,” *Journal of American Ceramics Society,* vol. 79, pp. 2833-38, 1996.

[14] S. Beaufils, L. Cormier, M. Bionducci, C. Ecolivet, G. Calas, A. L. Sauze and R. Marchand, “Medium-range order in alkali metaphosphate glasses and melts investigated by reverse monte carlo simulations and diffraction analysis,” *Physical Review,* vol. 67, pp. 104201-7, 2003.

[15] S. Beaufils, M. Bionducci, C. Ecolivet, R. Marchand and A. L. Sauze, “First diffraction peak in alkali metaphosphate glasses,” *Solid state communications,* vol. 116, pp. 687-690, 2000.

[16] L. Kirkup, Experimental Methods: an introduction to the analysis and presentation of data, Sydney: John Wiley and Sons, 1994.

[17] P. Mustarelli, C. Tomasi, M. Garcia and A. Magistris, “A NMR, conductivity and molecular dynamics study of Agl-Ag2O-B2O3 glasses,” *Physics and Chemistry of Glasses,* vol. 47, no. 4, pp. 484-488, 2006.

[18] J. Dyre, P. Maass, B. Roling and D. Sidebottom, “Fundamental questions relating to ion conduction in disordered solids,” *Reports on Progress in Physics,* vol. 72, p. 046501, 2009.

[19] B. Al-Hasni and G. Mountjoy, “Structural investigation of iron phosphate glasses using molecular dynamics simulation,” *Journal of Non-Crystalline Solids,* vol. 357, no. 15, pp. 2775-2779, 2011.

[20] G. Mountjoy, B. Al-Hasni and C. Storey, “Structural organisation in oxide glasses from molecular dynamics modelling,” *Journal of Non-Crystalline Solids,* vol. 357, no. 14, pp. 2522-2529, 2010.

Chapter 5: Conclusions and Future Work

5.1 Conclusions

The aim of this study was to synthesise, characterise, test and model three types of glasses one of which is novel and a possible candidate for a solid electrolyte in all solid-state lithium ion batteries. Samples were successfully synthesised using the conventional melt quenching technique. They were characterised using multiple techniques where the DSC analysis was used so the samples could be determined as glasses.

Conductivity values were obtained using impedance spectroscopy for the lithium disilicate, lithium metaphosphate and $37.5Li_2O$-$20Fe_2O_3$-$5Nb_2O_5$-$37.5P_2O_5$ glasses. It was found that the lithium disilicate and the lithium metaphosphate glasses had similar conductivities throughout the temperature range 300K-525K and compared well with published data. In the previous literature [1] the similar conductivities of lithium disilicate and lithium metaphosphate glasses was explained as being due to similar content of NBOs. However, this does not seem correct because lithium metaphosphate glass has two NBOs per P or per Li, whereas lithium disilicate glass has one NBO per Si or per Li. What is similar between these is the Li content, i.e. one Li per network former. The $37.5Li_2O$-$20Fe_2O_3$-$5Nb_2O_5$-$37.5P_2O_5$ glass has the same ratio of Li to P as the lithium metaphosphate glass but has a lower Li content due to the presence of Fe.

The room temperature $37.5Li_2O$-$20Fe_2O_3$-$5Nb_2O_5$-$37.5P_2O_5$ glass conductivity result of 9.895×10^{-10} Scm^{-1} (which is believed to be a first report for this) is lower than both the lithium disilicate and the lithium phosphate glasses. When comparing the conductivity values of the glasses in this study against other candidates for solid electrolytes [2] [3] it can be stated that the glasses tested in this study would not be suitable as electrolytes in solid state lithium ion batteries due to relatively low conductivities throughout the temperature range 300K-525K. In particular, the conductivity of the $37.5Li_2O$-$20Fe_2O_3$-$5Nb_2O_5$-$37.5P_2O_5$ glass is much lower than that of the ceramic [2] and glass-ceramic [3] forms of this compound.

Lithium disilicate and lithium metaphosphate glasses were successfully modelled using MD. A comparison to experimental literature results for x-ray and neutron diffraction

showed them to be acceptable models. The $37.5Li_2O$-$20Fe_2O_3$-$5Nb_2O_5$-$37.5P_2O_5$ model cannot be thought of as an accurate model due to the P-O coordination of 3.87 instead of 4 as expected. It has however, been studied as a first attempt model. Conductivity values for all models were estimated via MSD and then compared to experimental values. It was found that conductivities in the models are greatly overestimated compared to the real glasses, due to the overestimation of the diffusion coefficient. However, the MD modelling conductivity results showed lithium disilicate and lithium metaphosphate glasses to have similar conductivities and the $37.5Li_2O$-$20Fe_2O_3$-$5Nb_2O_5$-$37.5P_2O_5$ glass to have lower conductivity which is also observed for the real glasses. Hence MD modelling may yet prove useful as a tool to predict the relative conductivity of related glasses.

5.2 Future Work

There are vaious avenues in which this work can be taken further, as discussed here.

The lithium disilicate glass had a similar conductivity to the lithium metaphosphate despite having a lower lithium content. Other lithium silicate compositions with higher lithium content could be worth investigating as possible solid electrolyte materials.

The $37.5Li_2O$-$20Fe_2O_3$-$5Nb_2O_5$-$37.5P_2O_5$ glass has lower conductivity than the ceramic material [2] which itself had a lower conductivity than the glass-ceramic material. [3] Further investigation would be useful to understand why a glass-ceramic shows better performance than either the glass or ceramic alone.

Improvements need to be made on the $37.5Li_2O$-$20Fe_2O_3$-$5Nb_2O_5$-$37.5P_2O_5$ model, in particular to fix the incorrect P-O coordination number.

Larger lithium disilicate and lithium metaphosphate glass models should be made and longer simulations run in an attempt to reduce statistical fluctuations in diffusivity and hence conductivity estimates.

Also the use of the non-equilibrium method in MD simulations [4] should be considered as a potentially superior method to estimate conductivity from MD models.

[1] S. Martin and C. Angell, “Dc and ac Conductivity in Wide Composition range Li2O-P2O5 glasses,” *Journal of Non-Crystalline Solids,* vol. 83, pp. 185-207, 1986.

[2] A. Ivanov-Schitz, A. Nistuk and N. Chaban, “Li3Fe2(PO4)3 solid electrolyte prepared by ultrasonic spray pyrolosis,” *Solid State Ionics,* vol. 139, pp. 153-157, 2001.

[3] K. Nagamine, K.Hirose, T. Honma and T. Komatsu, “Lithium ion conductive glass-ceramics with Li3Fe2(PO4)3 and YAG laser-induced local crystallization in lithium iron phosphate glasses,” *Solid State Ionics,* vol. 179, p. 508, 2008.

[4] P. Mustarelli, C. Tomasi, M. Garcia and A. Magistris, “A NMR, conductivity and molecular dynamics study of Agl-Ag2O-B2O3 glasses,” *Physics and Chemistry of Glasses,* vol. 47, no. 4, pp. 484-488, 2006.

Appendix A

A.1 DSC and TGA Results

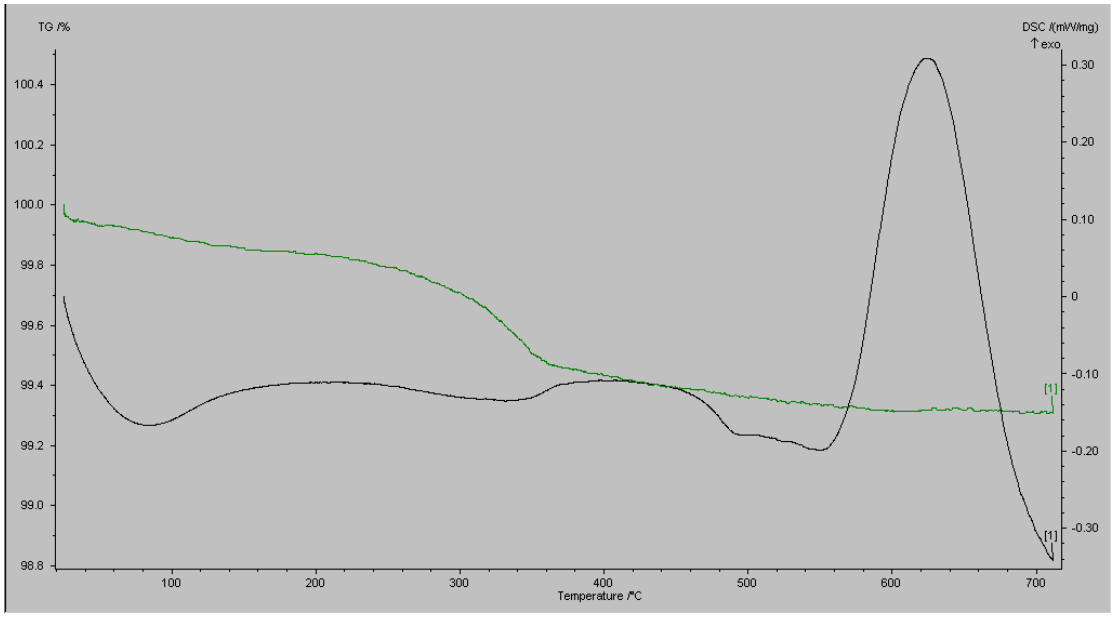

Figure A.1: DSC and TGA for $33.3Li_2O$-$66.7SiO_2$ glass

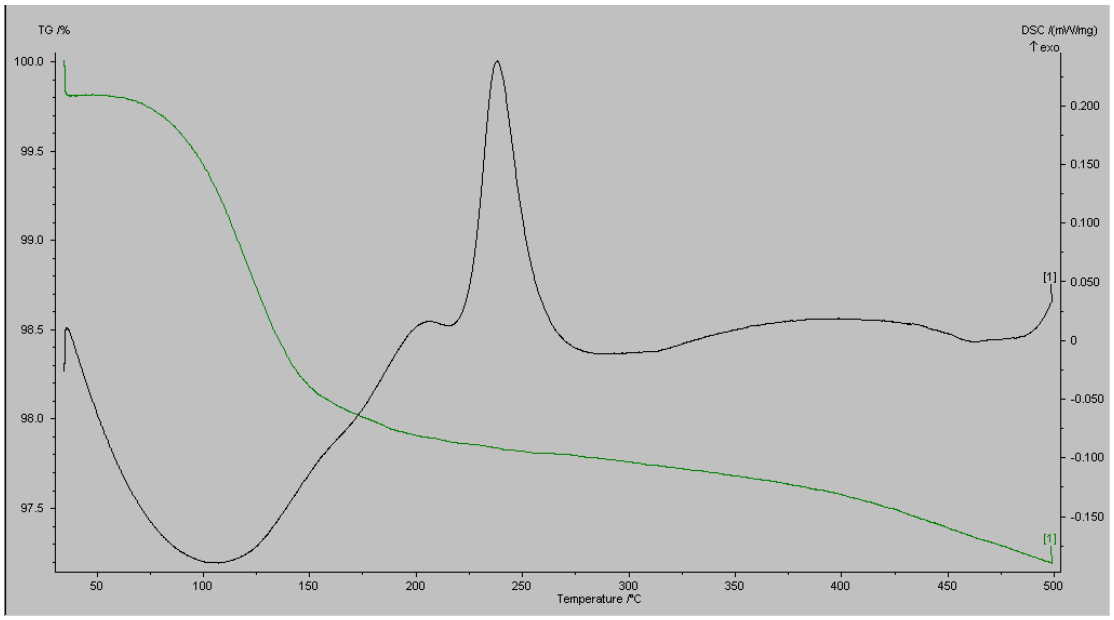

Figure A.2: DSC and TGA for $36.8Li_2O$-$63.2P_2O_5$ glass

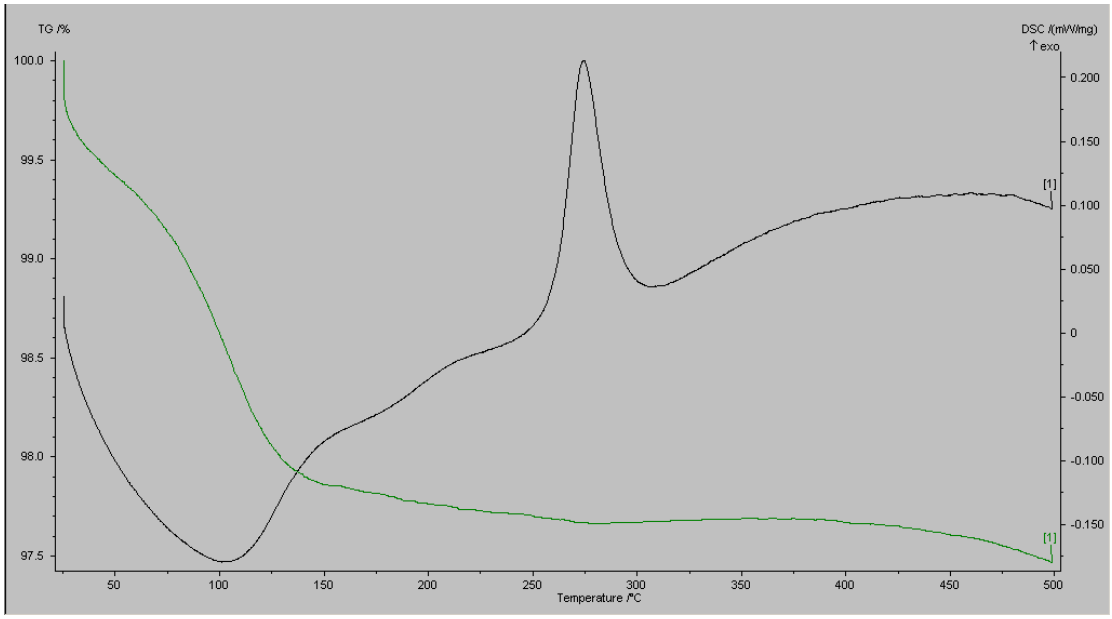

Figure A.3: DSC and TGA for $40Li_2O$-$60P_2O_5$ glass

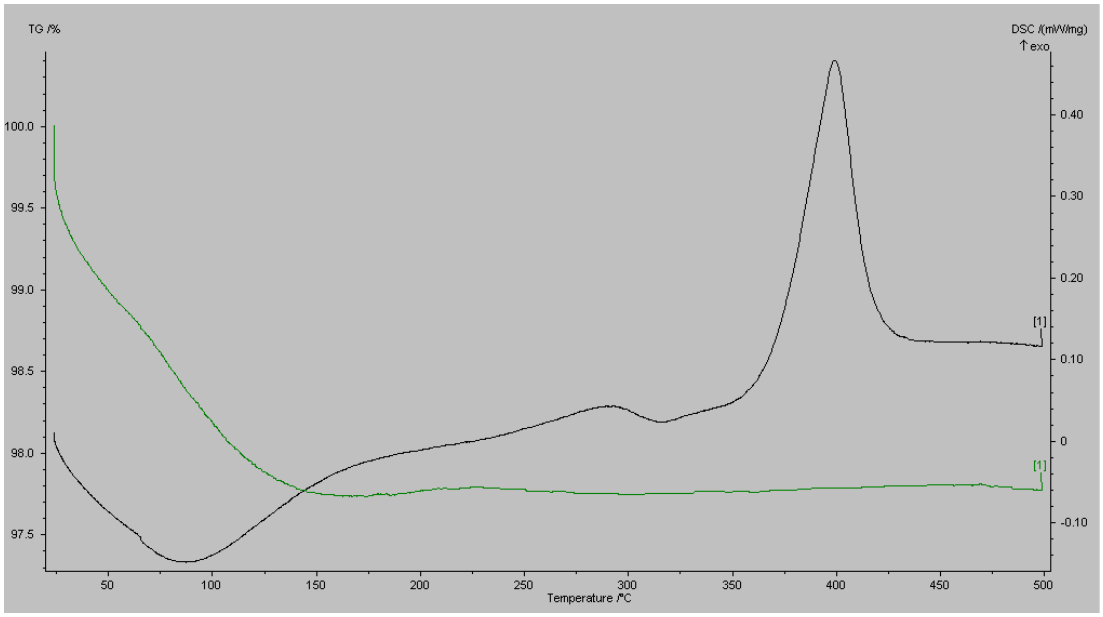

Figure A.4: DSC and TGA for $45Li_2O$-$55P_2O_5$ glass

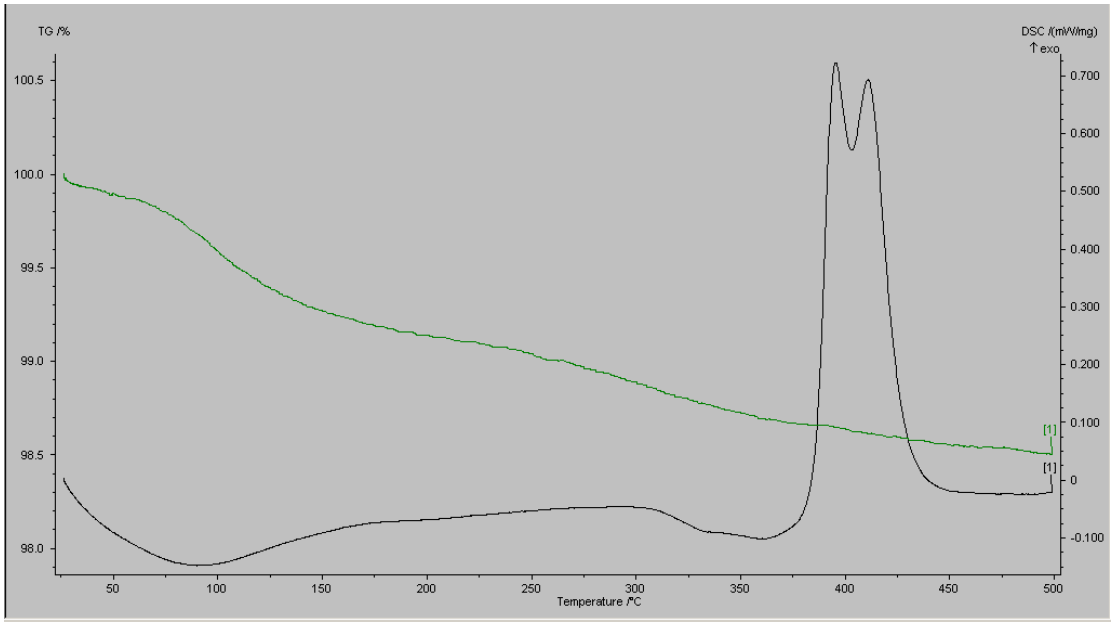

Figure A.5: DSC and TGA for $55Li_2O$-$45P_2O_5$ glass

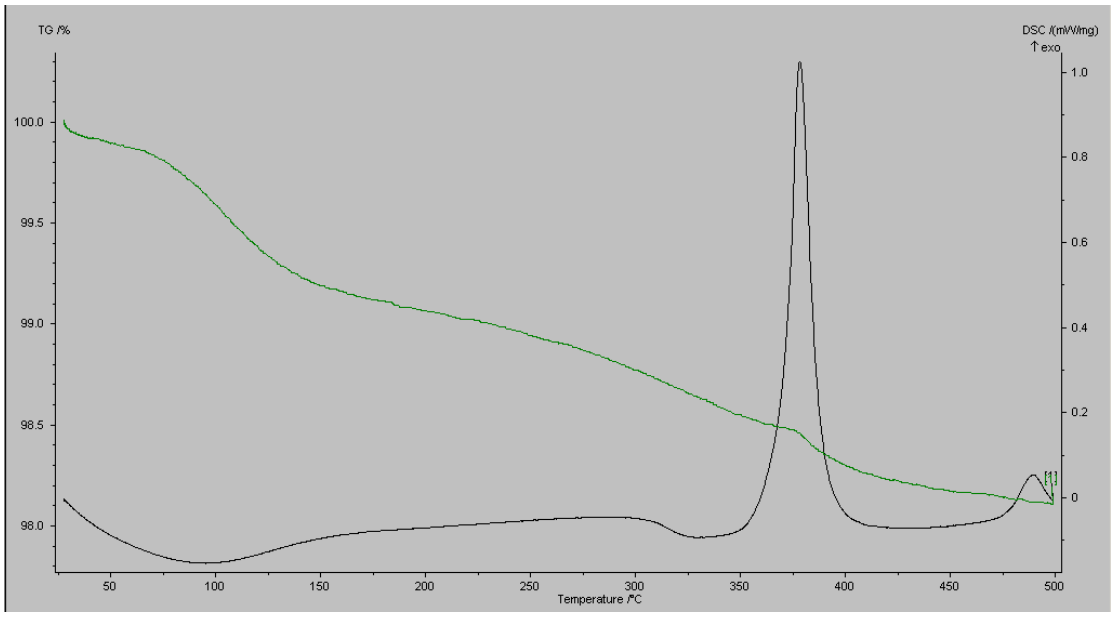

Figure A.6: DSC and TGA for $60Li_2O$-$40P_2O_5$ glass

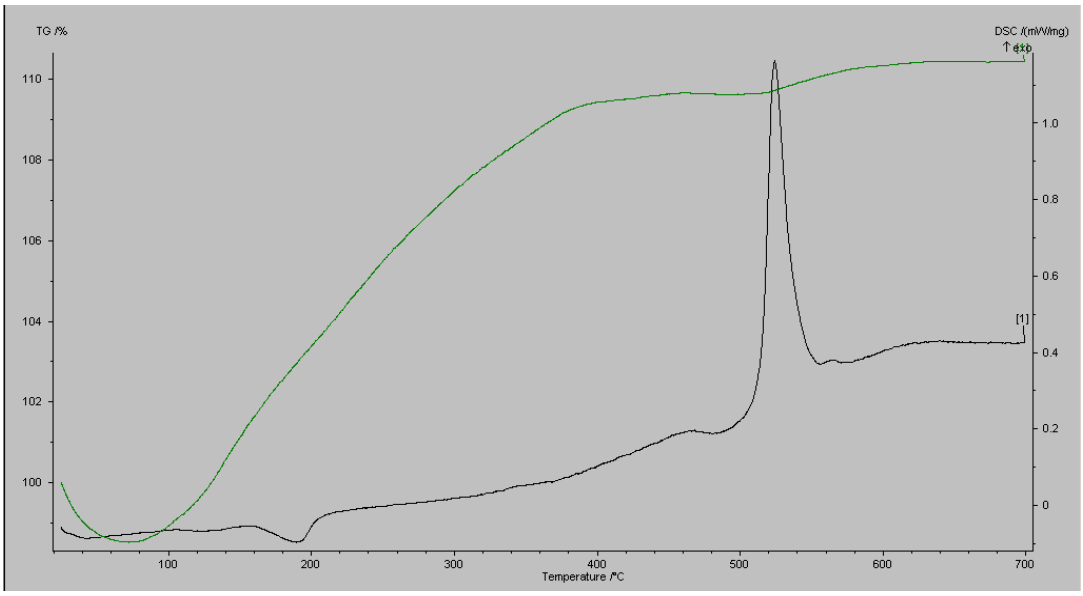

Figure A.5: DSC and TGA for $37.5Li_2O$-$20Fe_2O_3$-$5Nb_2O_5$-$37.5P_2O_5$ glass

A.2 NMR Results

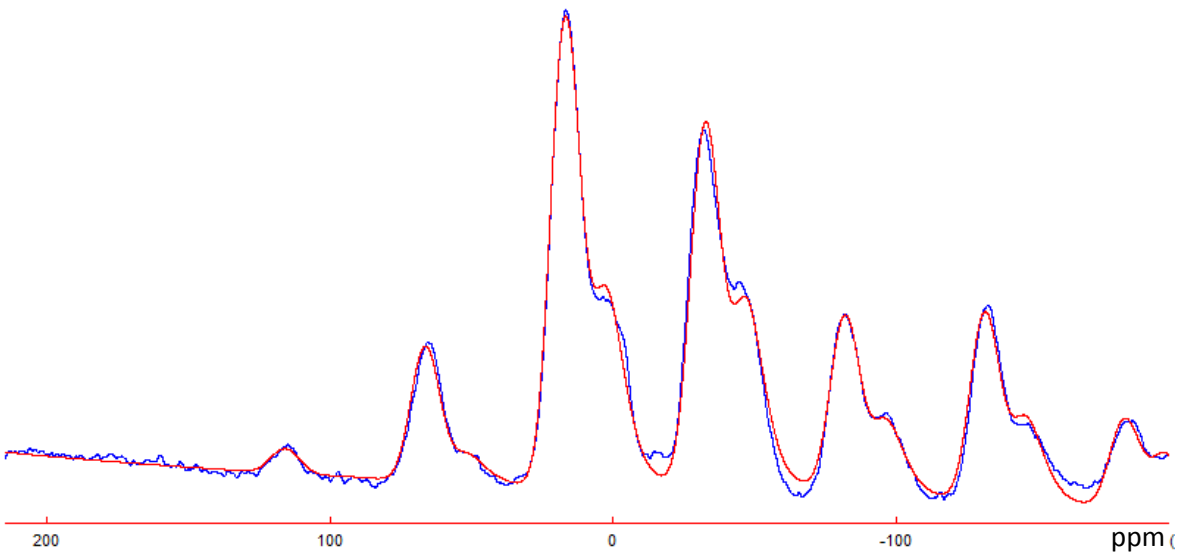

Figure A.6: ^{31}P MAS-NMR spectrum and DMfit for $36.8Li_2O$-$63.2P_2O_5$ glass

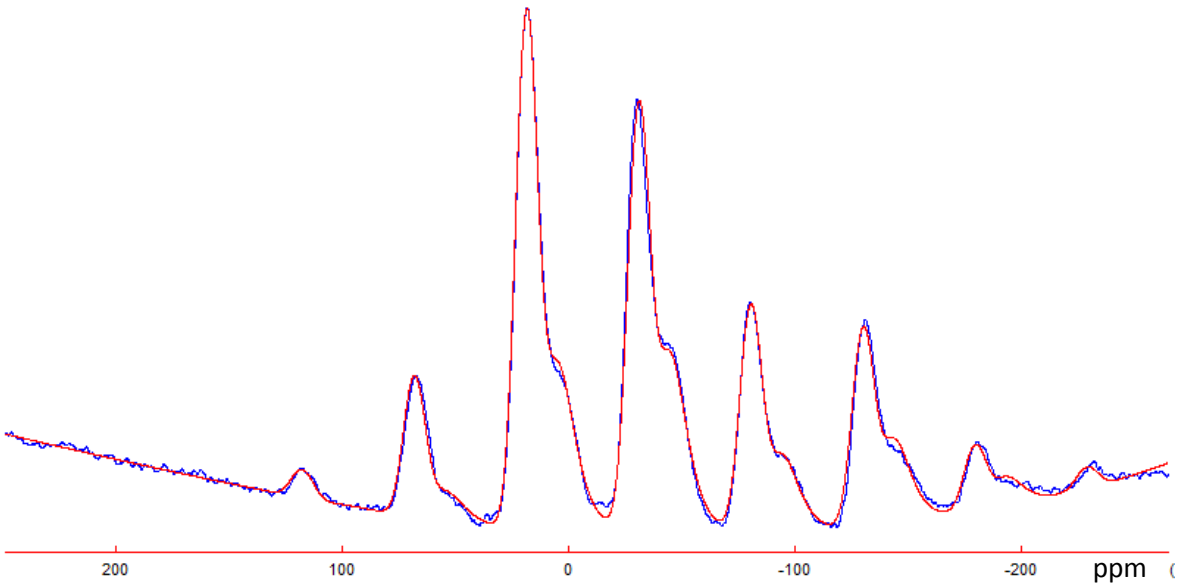

Figure A.7: ^{31}P MAS-NMR spectrum and DMfit for $40Li_2O$-$60P_2O_5$ glass

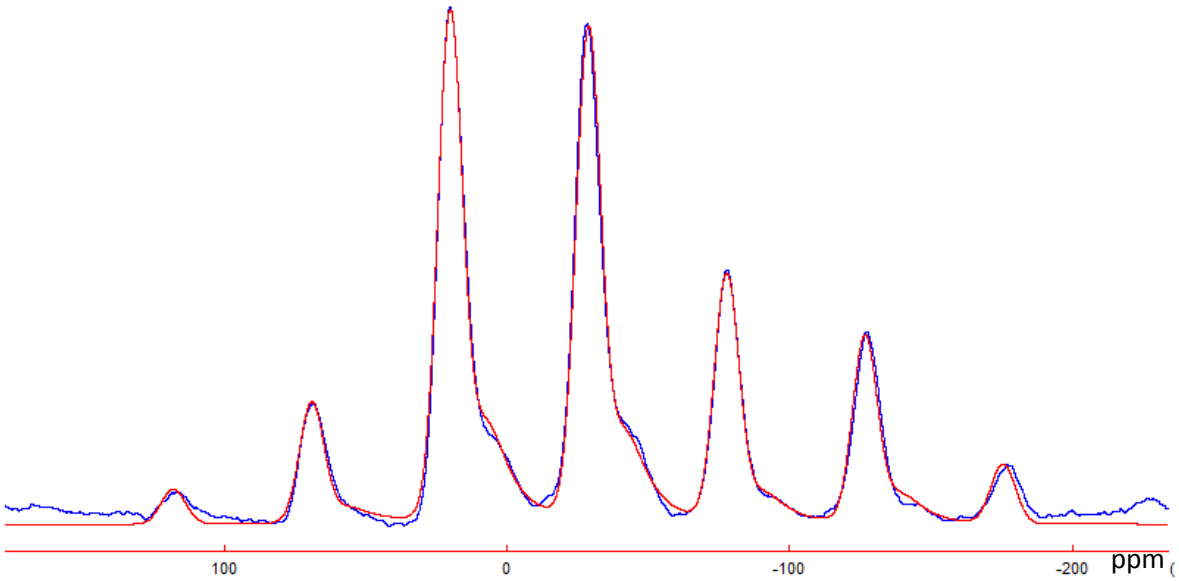

Figure A.8: ^{31}P MAS-NMR spectrum and DMfit for $45Li_2O$-$55P_2O_5$ glass

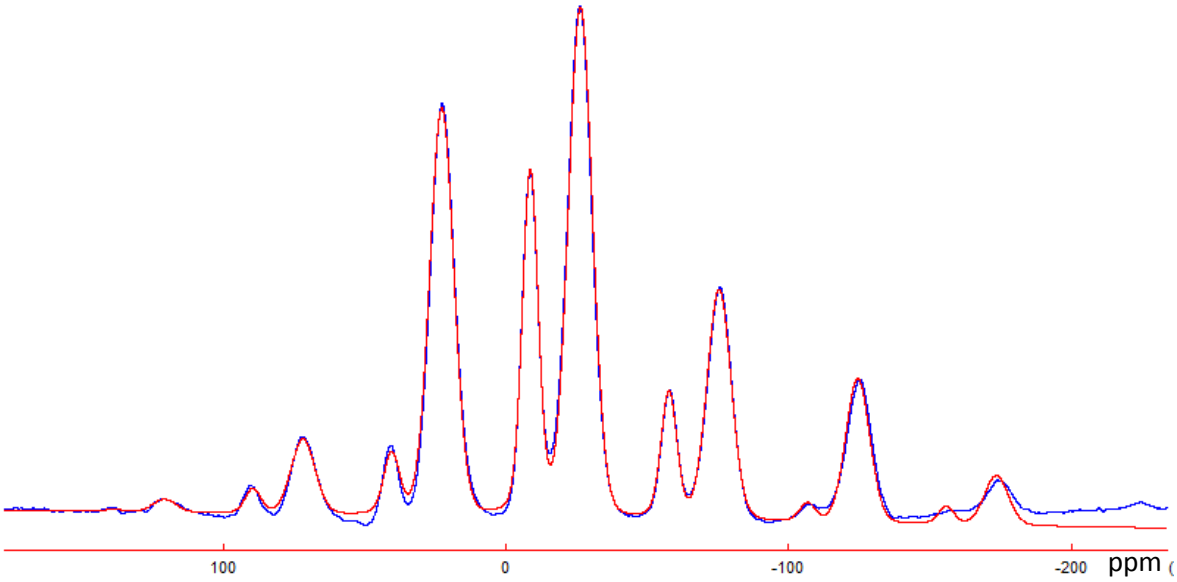

Figure A.9: ^{31}P MAS-NMR spectrum and DMfit for $55Li_2O$-$45P_2O_5$ glass

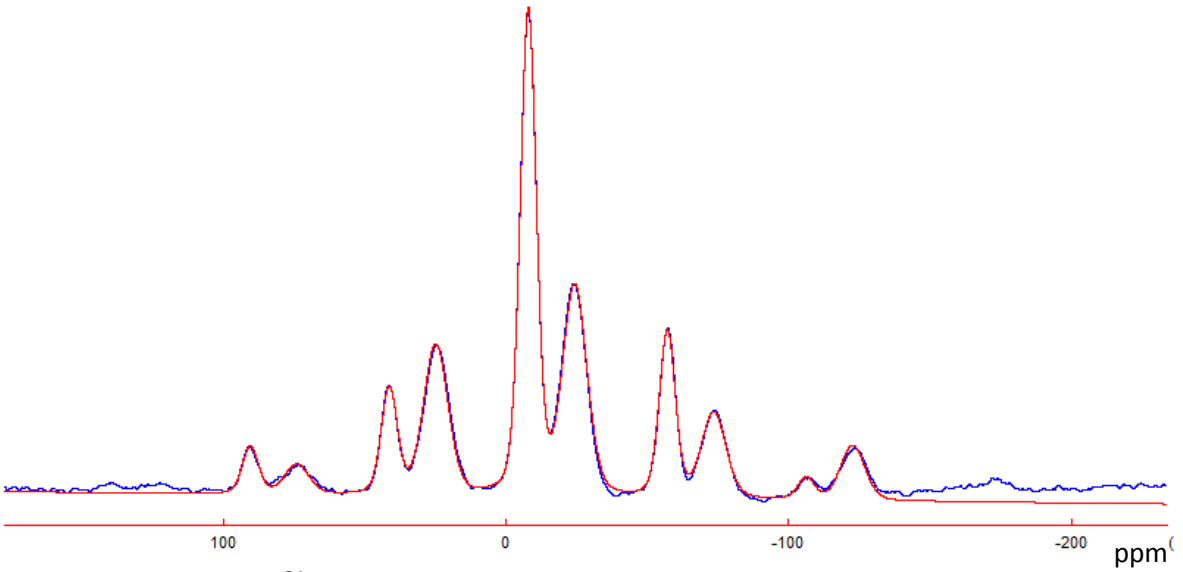

Figure A.10: ^{31}P MAS-NMR spectrum and DMfit for $60Li_2O$-$40P_2O_5$ glass

A.3 Impedance Spectroscopy Results

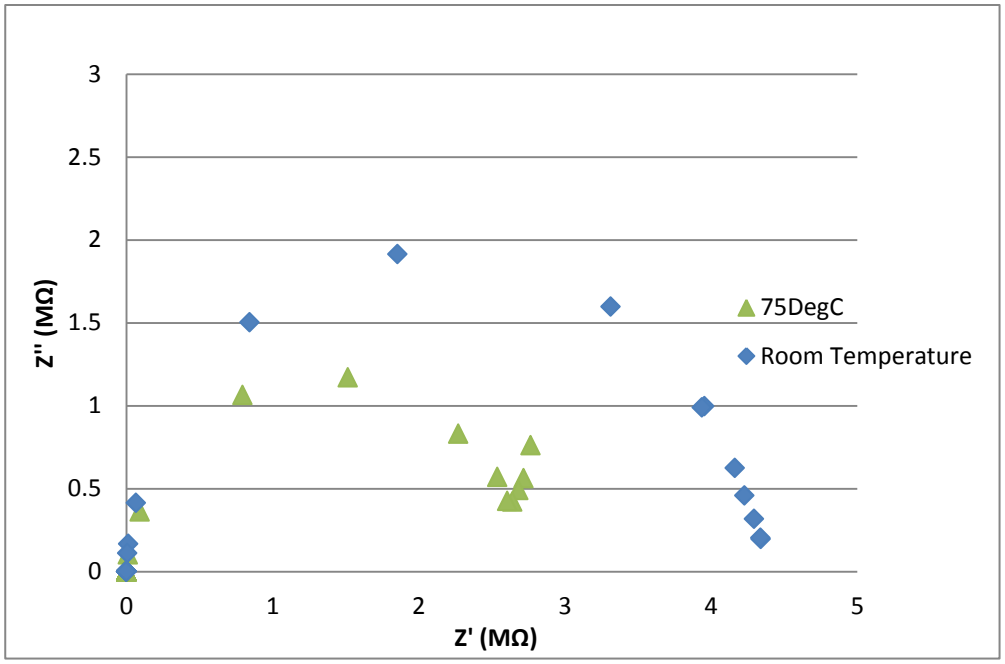

Figure A.11:Impedance measurements for $33.3Li_2O$-$66.7SiO_2$ glass

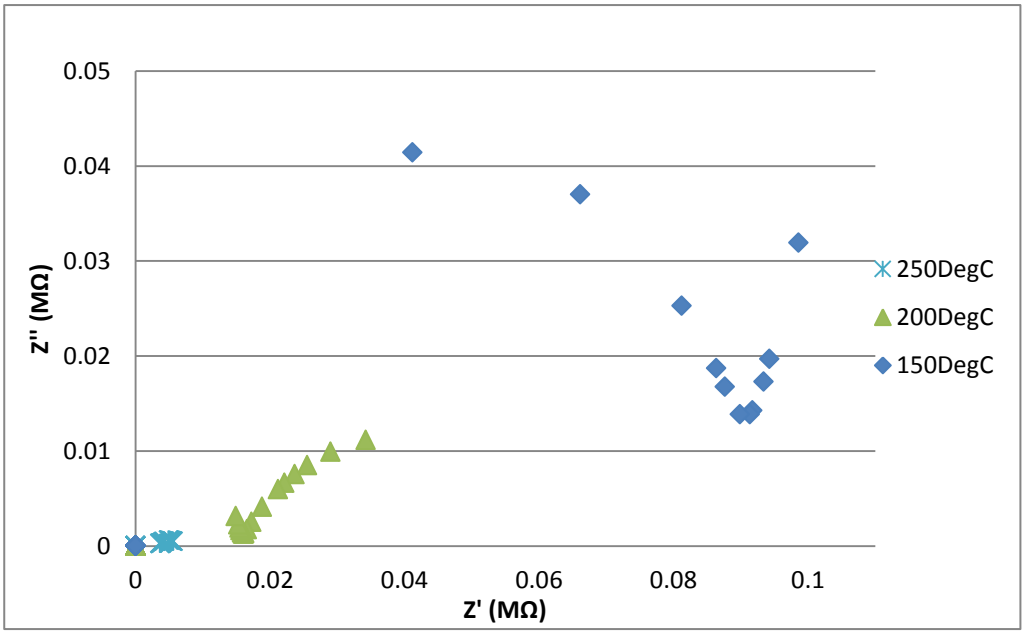

Figure A.12: Impedance measurements for $33.3Li_2O$-$66.7SiO_2$ glass

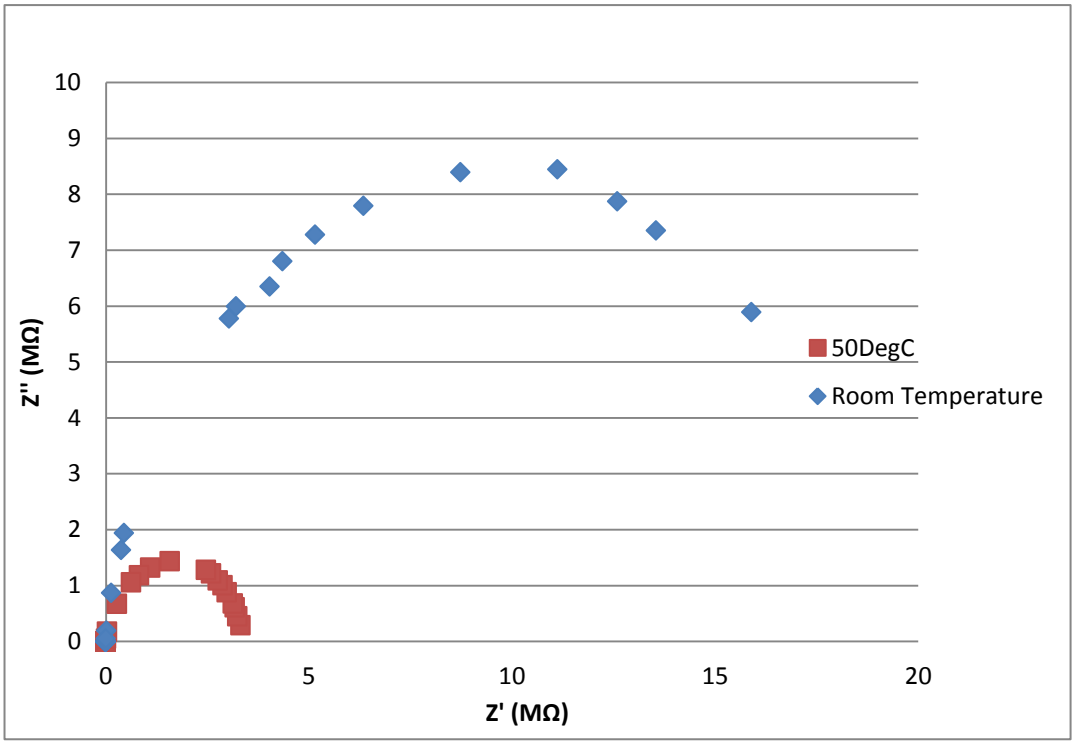

Figure A.13: Impedance measurements for $50Li_2O$-$50P_2O_5$ glass

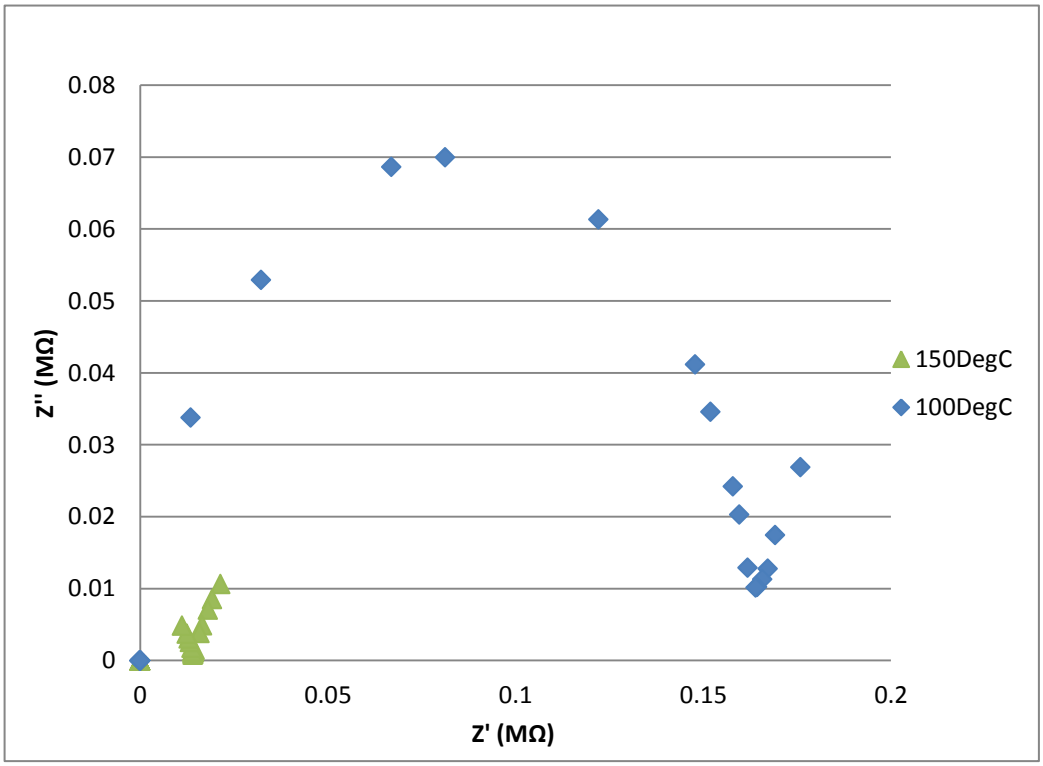

Figure A.14: Impedance measurements for $50Li_2O$-$50P_2O_5$ glass

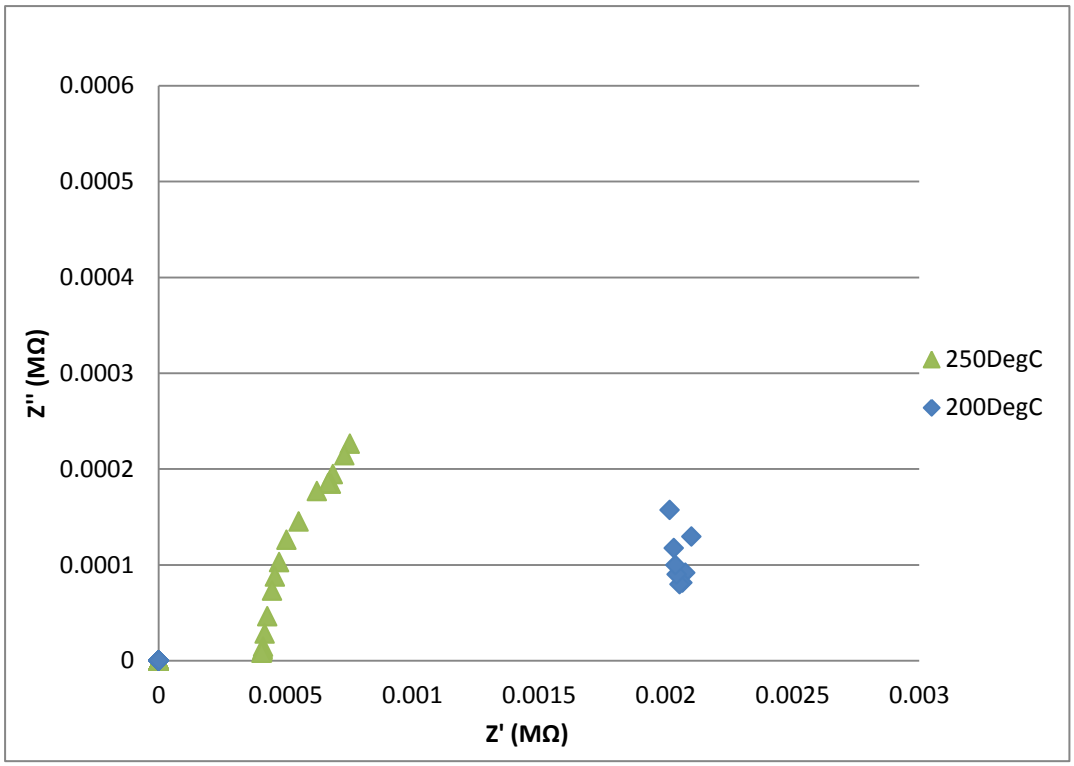

Figure A.15: Impedance measurements for $50Li_2O$-$50P_2O_5$ glass

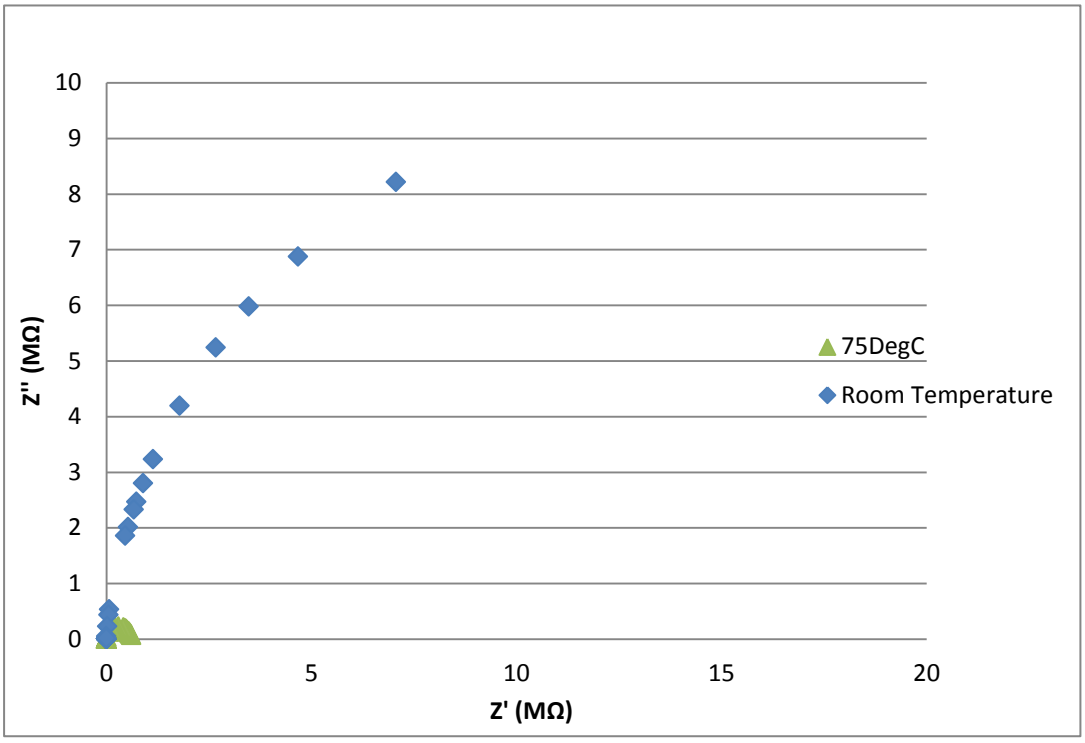

Figure A.16: Impedance measurements for $37.5Li_2O$-$20Fe_2O_3$-$5Nb_2O_5$-$37.5P_2O_5$ glass

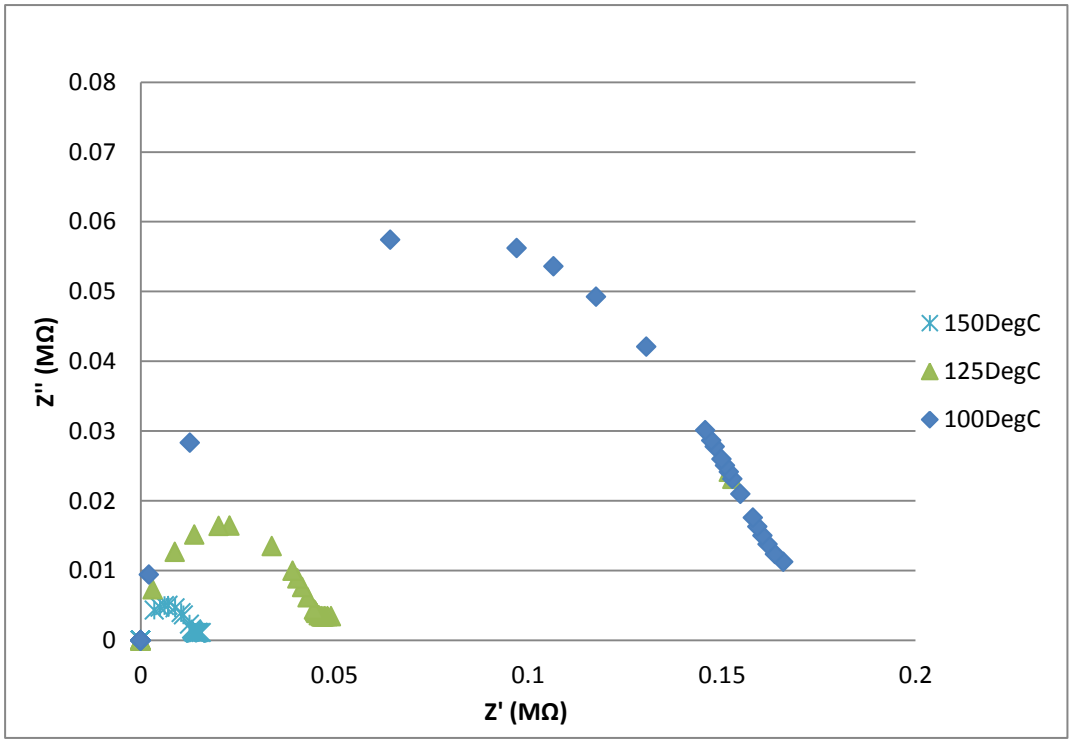

Figure A.17: Impedance measurements for $37.5Li_2O$-$20Fe_2O_3$-$5Nb_2O_5$-$37.5P_2O_5$ glass

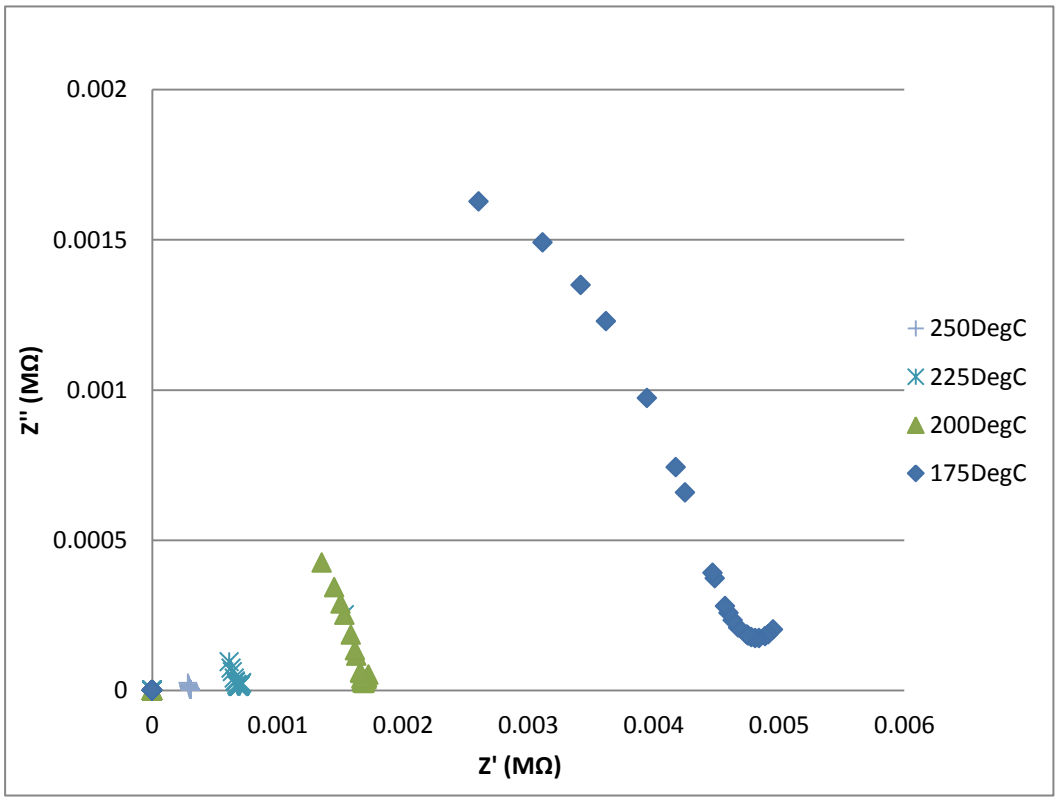

Figure A.18: Impedance measurements for $37.5Li_2O$-$20Fe_2O_3$-$5Nb_2O_5$-$37.5P_2O_5$ glass

A.4 Example DLPoly input Files

Config File

```
CONFIG: 50Li2OP2O5          [  3000atoms 2.3540g/cm3 ]
         2         1     46150    0.1000000000E-02
     33.129714965800      0.000000000000      0.000000000000
      0.000000000000     33.129714965800      0.000000000000
      0.000000000000      0.000000000000     33.129714965800
P5+              1
    0.3658039659        -9.075115187         2.160318977
  -2.95268567947       2.66424315825      0.155052452199
  -3135.55003747      -14754.8725249       8292.58187966
P5+              2
     13.47961775         8.077968724        -3.701078182
   3.99326921485       2.65218577018       3.34192979170
   8509.13992894      -31189.9354291      -10309.3178590
P5+              3
   -0.9288214757         16.50791478        -2.827026560
  -3.59641126973      -2.46921048517      -2.21520702798
   449.128576646      -2136.08201293      -16391.2255364
P5+              4
     3.152595159        -6.947249794         11.02571907
   3.04318625388     0.666055771194E-01    2.24449308574
   4112.03473674       10100.0060936       7968.32271910
P5+              5
    -11.00798876         15.57002118         10.33544502
  -4.49142402337      0.228459964252     -0.221908153405
   16644.5380840      -16486.7265101      -19459.0452229
P5+              6
    -12.42695578        0.4092452624        -13.06907557
   2.01118996686       2.53869008030     -0.189887237260
  -4368.23899398      -4224.63433135      -13809.2345378
P5+              7
     8.249117452        -9.716536361         16.40419738
   2.95619710001      -3.00108339697      0.723496471288
   4539.93121223      -6571.38748592      -7952.44224413
P5+              8
    -16.08650884        -12.09336441        -5.031244703
  0.782202984522      0.370182086723       1.03203297829
  -5946.79613584       15644.0155048       9153.05604689
P5+              9
     1.724394383        -12.38733013        -9.977665341
   1.27944950781       6.54517129419      -4.70543913110
  -16909.3936110      -22277.1191654      -14262.1771607
```

Control File

```
CONTROL: at T k
temperature                          300.0
pressure                              0.00
ensemble nvt ber therm                 2.0
steps                                40000
equilibration                        40000
multiple  step                           5
scale                                    5
print                                 1000
stack                                 1000
stats                                 1000
rdf                                   1000
timestep                             .0010
primary cutoff                         8.0
cutoff                                11.0
delr width                             1.0
rvdw cutoff                            5.0
ewald precision                       1d-5
print rdf
job time                         621000000
close time                             100
cap                                   8000
trajectory write HISTORY from 400 every 400 key 0
finish
```

Field File

```
DL_POLY
UNITS eV
MOLECULES 3
phosphorus
nummols 600
atoms 1
P5+          30.97        3.0
finish
lithium
NUMMOLS 600
ATOMS 1
Li1+          6.941       0.6
finish
oxygen
nummols 1800
atoms 1
O2-          16.00       -1.2
finish
VDW 3
P5+      O2-    buck     26655.47    0.18197      86.86      0.0
1.2
Li1+     O2-    buck     41051.94    0.1561        0.00      0.0
1.2
O2-      O2-    buck      1844.00    0.3436      192.58      0.0
1.7
TBP 2
P5+     O2-     P5+     shrm    3.0      135.58     40.0        40.0
2.0
O2-     P5+     O2-     shrm    3.5      109.47     40.0        40.0
2.0
CLOSE
```

A.5 MD Results for Diffusivity

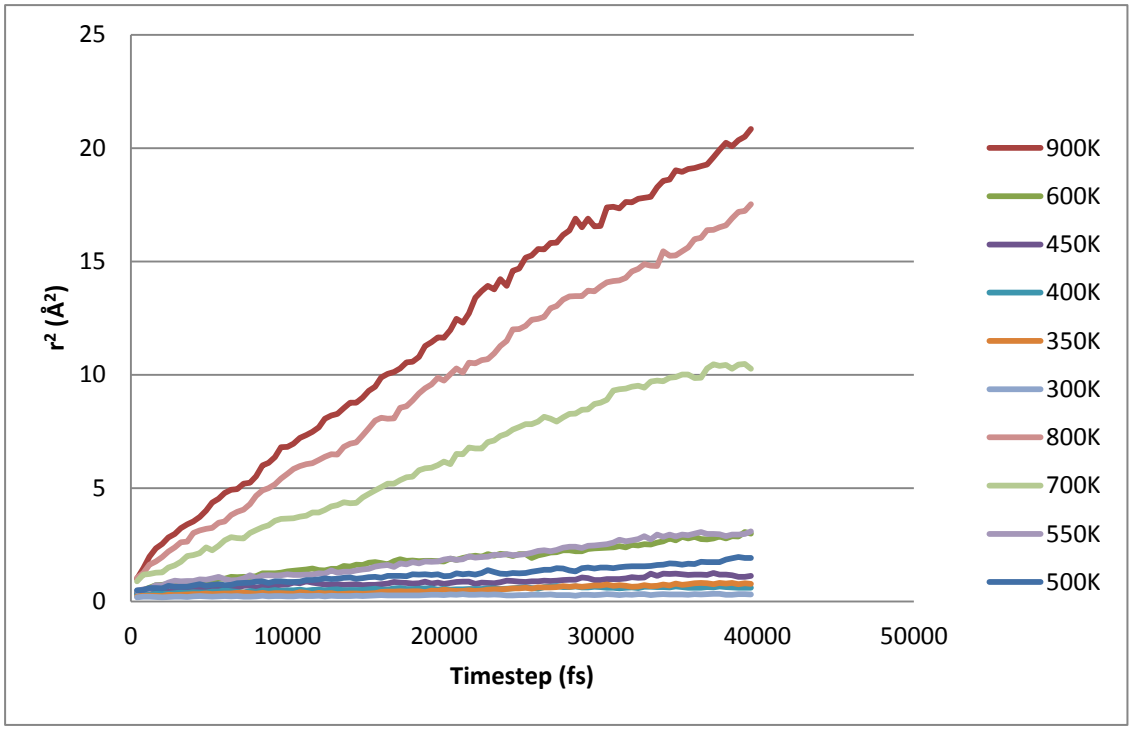

Figure A.19: MSD for $33Li_2O$-$67SiO_2$ glass model

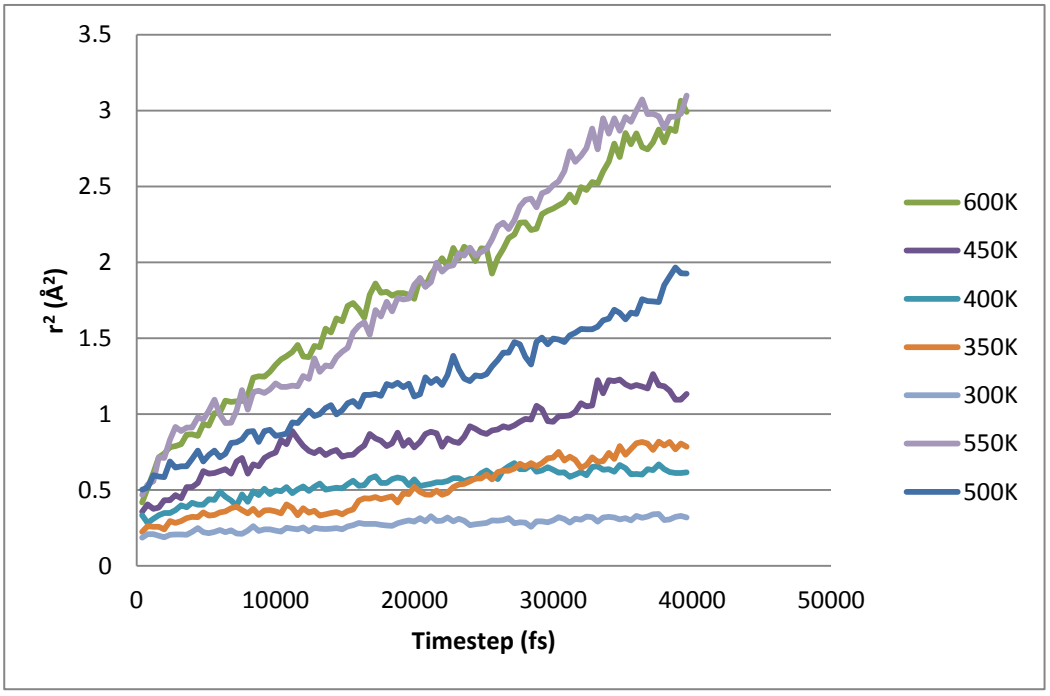

Figure A.20 MSD for $33Li_2O$-$67SiO_2$ glass model (scaled to 600K to observe lower temperatures)

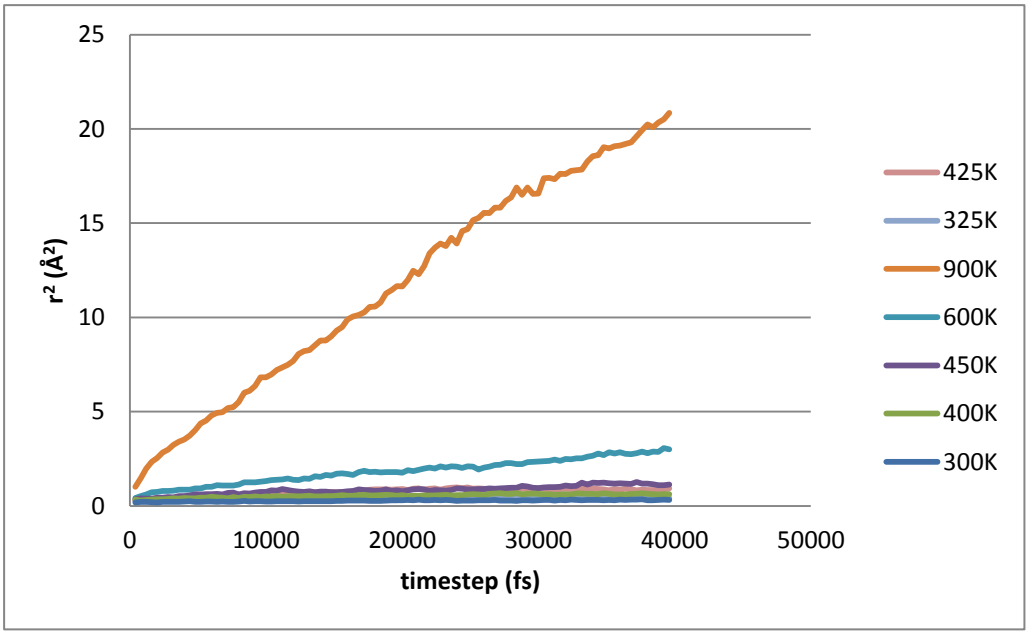

Figure A.21 MSD for $50Li_2O$-$50P_2O_5$ glass model

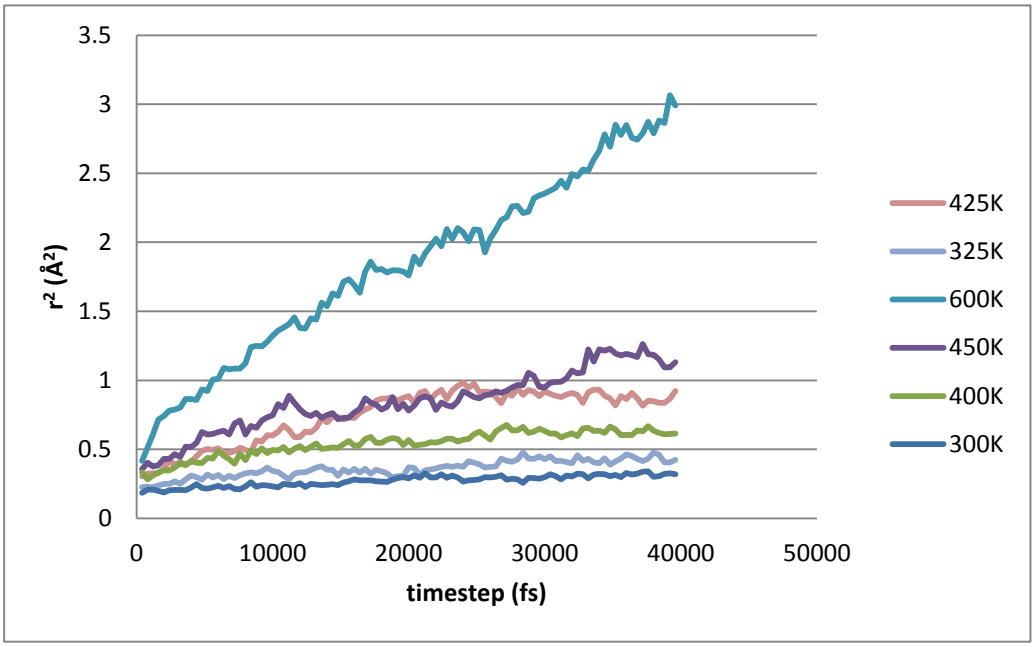

Figure A.22 MSD for $50Li_2O$-$50P_2O_5$ glass model (scaled to 600K to observe lower temperatures)

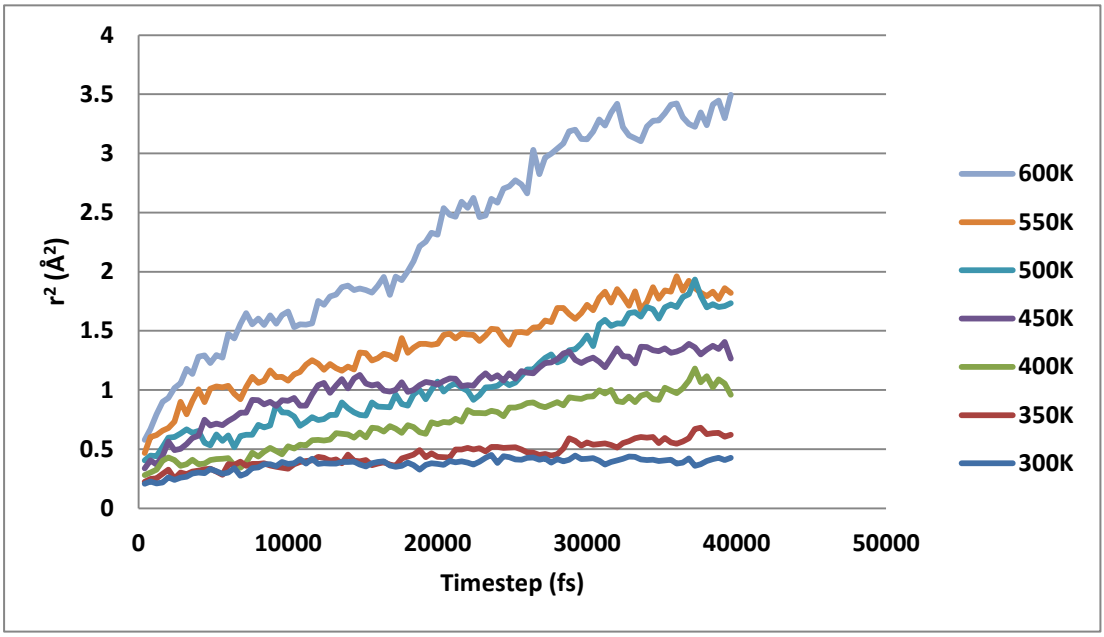

Figure A.23 MSD for $37.5Li_2O$-$20Fe_2O_3$-$5Nb_2O_5$-$37.5P_2O_5$ glass model

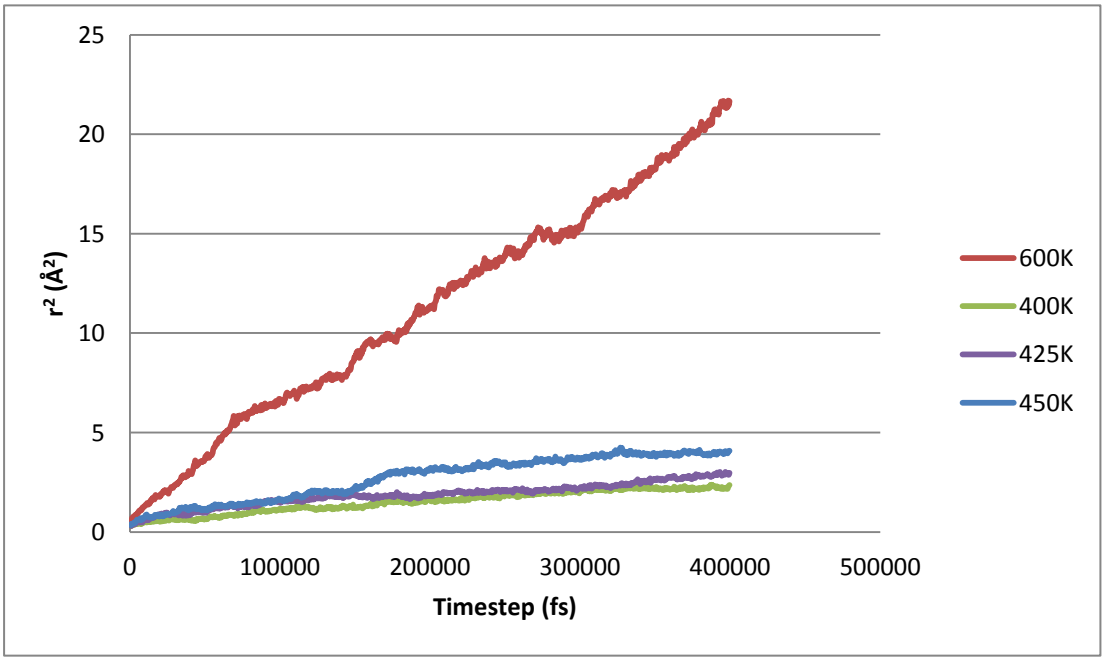

Figure A.24: MSD for $37.5Li_2O$-$20Fe_2O_3$-$5Nb_2O_5$-$37.5P_2O_5$ glass model (400000 timesteps)

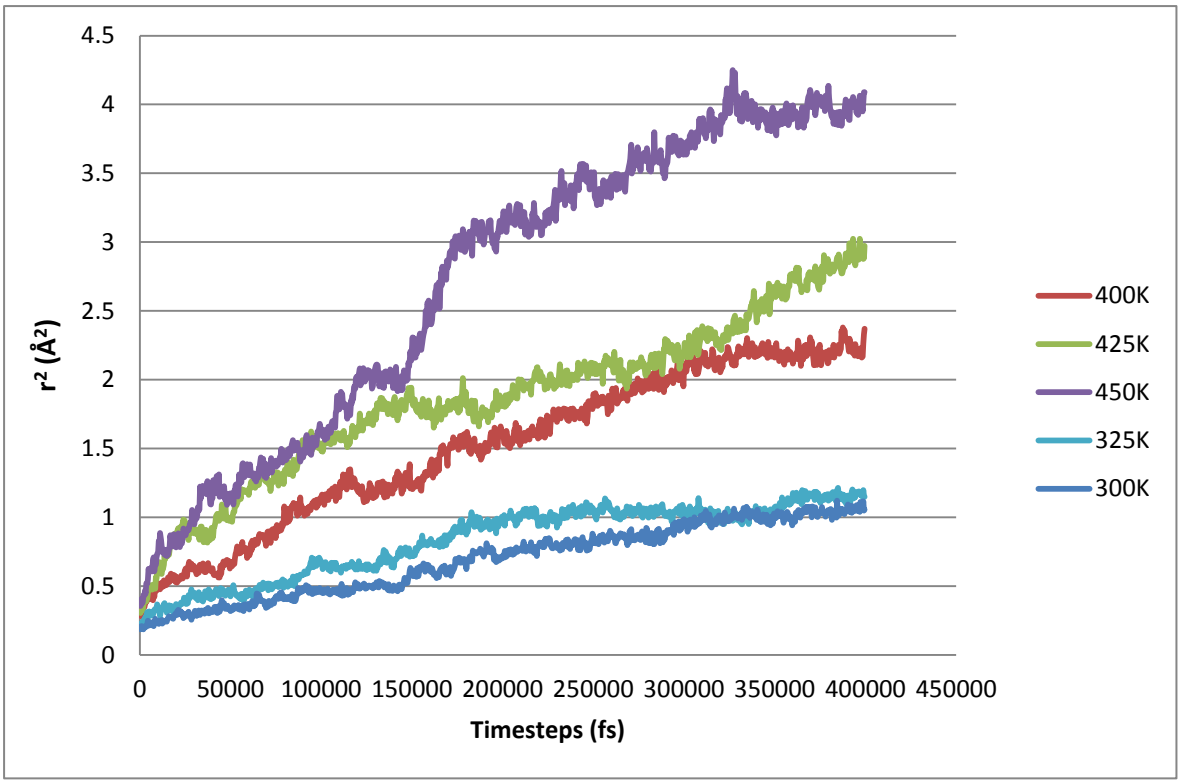

Figure A.25: MSD for $37.5Li_2O$-$20Fe_2O_3$-$5Nb_2O_5$-$37.5P_2O_5$ glass model (400000 timesteps) (scaled to 450K to observe lower temperatures)